Spring 2013

# Computational Analysis to Enhance Laminar Flow Convective Heat Transfer Rate in an Enclosure Using Aerosol Nanofluids

Andrew Hudson

# COMPUTATIONAL ANALYSIS TO ENHANCE LAMINAR FLOW CONVECTIVE HEAT TRANSFER RATE IN AN ENCLOSURE USING AEROSOL NANOFLUIDS

by

ANDREW HUDSON

(Under the Direction of Mosfequr Rahman)

## ABSTRACT

The current research intends to provide a starting point to effectively model aerosol heat transfer in a narrow, enclosed body. This research can lead to future modeling of nano fluids including their heat transfer characteristics and erosion effects on the walls of an enclosure.

The model was developed using ICEM CFD for the mesh and FLUENT for the fluid flow modeling. Six different aspect ratio enclosures were developed to study the effects of varying aspect ratio. The natural convection of air was developed first to establish the appropriateness of the models being used. A mesh check was performed using one of the natural convection cases to ensure the mesh was appropriate. The forced convection of air was then developed. The velocity vector, isotherm, surface heat flux, and surface nusselt number were recorded for future comparison to models. The models for nanoparticle natural convection were then activated to ensure the distribution of particles was as expected.

This research proved that nanoparticle tracking can be accomplished with a computer model instead of using the traditional volume ratio method. The effects of aspect ratio on the surface heat flux as well as surface nusselt number were recorded for both natural and forced convection of air.

The development of the appropriate model for particle tracking is started and proven to be valid. The natural convection and forced convection of air has been solved for future comparison to natural and forced convection.

INDEX WORDS: Nanoparticles, Aerosol, Heat transfer, Forced convection, Nano fluid, Georgia Southern University, Master of Science in Applied Engineering

# COMPUTATIONAL ANALYSIS TO ENHANCE LAMINAR FLOW CONVECTIVE HEAT TRANSFER RATE IN AN ENCLOSURE USING AEROSOL NANOFLUIDS

by

ANDREW HUDSON

B.S., Georgia Southern University, 2011

A Thesis Submitted to the Graduate Faculty of Georgia Southern University in

Partial Fulfillment of the Requirements for the Degree

MASTER OF SCIENCE

STATESBORO, GEORGIA

2013

# COMPUTATIONAL ANALYSIS TO ENHANCE LAMINAR FLOW CONVECTIVE HEAT TRANSFER RATE IN AN ENCLOSURE USING AEROSOL NANOFLUIDS

by

ANDREW HUDSON

Major Professor: Mosfequr Rahman

Committee: Gustavo Molina

Cheng Zhang

Electronic Version Approval:

May 2013

## Contents



## List of Figures

# Chapter 1. Introduction

As modern electronic devices are continually miniaturized, the cooling of these devices becomes more difficult. The difficulty in cooling these devices arises from the trend towards thinness and the close packaging of components. This trend reduces the amount of space available for cooling air flow, while the close packaging of the components increases the heat density within the device. Both of these characteristics lead to increased temperatures in devices. This increase in temperature causes the failure rate of the devices to increase making it necessary to find ways to provide more cooling. This situation was explained in "Growing power densities are making thermal consideration a first-class citizen in the design and deployment of next-generation servers and data centers." (Choi, Kim, Sivasubramaniam, Srebric, Wang and Lee 2008, 1129-1142).

In the case of modern production computers forced air cooling is the most popular method since it is economic and simple to implement. To implement an air cooling system vents are placed at various locations around the device, and a fan is placed at one or more of these vents. The fan moves ambient air through the device allowing the air to absorb heat from the components. The air is then expelled from the device taking the heat with it. This results in the device being kept at a lower temperature.

Most modern computers that cannot be adequately cooled using forced air cooling use a forced liquid cooling system. This consists of a closed loop system that uses specialized heat sinks on each component of the computer that requires cooling. These heat sinks have fluid cavities attached to them and tubing connects to these cavities. A pump pushes liquid from a reservoir tank into these heat sinks, then the liquid flows to another heat exchanger that expels the heat from the liquid to the atmosphere. The seals that keep the liquid separated from the electronic components must be absolutely perfect or this system can destroy the computer. A potential system that could be developed involves using characteristics of both forced liquid cooling and forced air cooling. If the heat transfer of the air could be increased using an additive the system could be cooled more effectively. This system would require that the device contains a closed cooling loop similar to the forced liquid system described above. It has the potential to only require seals on the exterior surfaces of the device allowing the cooling air stream to affect the entire device unlike air cooling. This system would also have less catastrophic consequences if a leak develops.

Current research proposes that by including nanoparticles in a cooling airflow the heat transfer of the air flow will increase. A nanoparticle can be defined as particles of various materials that have at least

one dimension between 1 and 100 nm (Sundar and Sharma 2008, 121- 129). For the purposes of this research only man made nanoparticles used to increase the heat transfer of base fluids will be considered. By including the nanoparticles in the air stream, an air based is created. It has been shown during various studies that adding a small volume fraction of metal or metal oxide powders to fluids increase the thermal conductivities of the particle-fluid mixture over those of the base fluid (Wang, Xu and Choi 1999, 474-480). This increase in thermal conductivity will lead to the mixture absorbing more heat from the components as well as achieving the transfer faster.

The idea of using nanoparticles to increase the heat transfer of a base fluid has been explored since 1993 (Masuda, Ebata, Teramae and Hishinuma 1993, 227-233). The basic idea of increasing the heat transfer of a fluid by introducing particles of metal has been used for more than 100 years (Trisaksri and Wongwises 2005, 512-523). In the past the particles used have been on the scale of millimeter or micrometer. These particles have problems with sedimentation, erosion, and large pressure drop in the system (Trisaksri and Wongwises 2005, 512-523). The use of nanoparticles can achieve increases in heat transfer without as severe problems arising.

For the purposes of this study a simplified model was used to evaluate the increase in heat transfer of air when nanoparticles are included in the flow. This research states that if the introduction of nanoparticles into a cooling air stream is incurred, then an optimal amount of nanoparticles can increase the heat transfer from the surrounding area.

Previous research has been performed on liquid based nano fluids for cooling purposes. Recently natural convection of gas based nano fluids has been performed as well. There has been little to no work done in the field of forced convection of aerosol nanoparticle systems. Forced convection has greater potential for cooling than natural convection making it a topic worthy of researching.

This research can lead to a more thorough understanding of heat transfer. This will allow future researchers and engineers to have more tools available for future products and designs.

## Chapter 2. Literature Review

According to the researcher's knowledge the earliest published work that specifically mentioned use of nano particles in suspension to increase heat transfer was in 1993. This research used ultra-fine particles of $Al_2O_3$, $SiO_2$, and $TiO_2$ with particle sizes that varied from 12 to 27nm depending on the material. These particles were suspended in water. This research utilized a hot wire experiment and measured the viscosity of the various solutions containing the ultra-fine particles at weight fractions from 2.3 to 16 percent. The thermal conductivity was found to increase for the solutions containing $Al_2O_3$ and $TiO_2$ ultra-fine particles as the concentrations increased. Viscosity was also found to increase with the addition of these ultra-fine particles. (Masuda, Ebata, Teramae and Hishinuma 1993, 227-233).

The first mention of the term was made in a technical report published in 1995 titled "Enhancing thermal conductivity of fluids with nanoparticles." The authors of this paper coined the term and defined them as "heat transfer fluids which contain metallic particles with average particle sizes of about 10 nanometers" (Choi and Eastman 1995). Choi and Eastman also stated that the increased surface area of nanoparticles will allow significantly higher heat transfer capabilities when compared to conventional micrometer-sized particles (Choi and Eastman 1995).

In the past decade and a half there has been a dramatic increase in research in the field of nano fluids. There have been theoretical models developed starting with Choi and Eastman. They observed that using an equation developed by Hamilton and Crosser equation they found good agreement when compared to previous experimental results (Choi and Eastman 1995).

As the research on nanoparticles for heat transfer has progressed through time the understanding of them has increased. This increase in understanding has allowed researchers to produce better results. In 1999, Wang, Xu, and Choi have studied the effect of adding nanoparticles to distilled water, vacuum pump fluid, ethylene glycol and engine oil. They used nanoparticles of $Al_2O_3$ and CuO. When the researchers attempted to compare the results that they found with the results from previous researchers the numbers did not match. They found that while they were using the same materials they were not using the same method for mixing of the fluid. The particles they were using also had different diameters when compared to the previous research. Based on these findings they stated that as the diameter of the particles decreases, the thermal conductivity of the resulting fluid increased. They also stated that the method of mixing the also had an effect on the final fluids properties. (Wang, Xu and Choi 1999, 474- 480)

In 2008 Kulkarni, Namburu, Bargar, and Gas studied the effect of $SiO_2$ as nano size particles had when mixed into an ethylene glycol mixture. They used nanoparticles with diameters of 20 nm, 50 nm, and 100 nm. They observed the changes in the viscosity, convective heat transfer, and pressure loss. They found that as particle size increases the heat transfer coefficient increases at a fixed Reynolds number. Viscosity was dependent on particle concentration where higher particle concentrations lead to high viscosity values. Pressure loss was found to increase with respect to concentration. There was no appreciable change in pressure loss when the particle diameter was varied. Overall, they found that many of these characteristics are tied together and affect each other. (Kulkarni, Namburu, Bargar and Das 2008, 1027-1035)

In 2010 Mosavian, Heris, Etemad, and Esfahany compared three different nanoparticles in water. They used $Al_2O_3$, CuO, and Cu to find that metallic particles have a higher heat transfer than oxide particles do. They also found that as the concentration of nanoparticles was increased the heat transfer to the fluid increased. There was an optimal level of nanoparticles for each of the particles. They also found that the experimental values of heat transfer were higher than was found by modeling the system as a single phase heat transfer correlation. (Mosavian, Heris, Etemad and Esfahany 2010, 2611-2619)

There are numerous methods available to make nanoparticles. Choi and Eastman mention gas-phase condensation where the base material is evaporated, then rapidly condensed in an inert low pressure environment. They also mention a method of production where a solution of the base material is made, then sprayed through a nozzle. The resulting spray is then rapidly air dried. (Choi and Eastman 1995)

The mechanisms that act on nanoparticles in fluids are very complex and varied. Some of the mechanisms that take place include Brownian motion and thermophoresis motion (Mädler and Friedlander 2007, 301-342). Brownian motion is the random motion of the nanoparticles in a base fluid that results from the collisions that occur between the nanoparticles and the base particles (Buongiorno 2006, 240-250). This motion is based on the random motion that all particles have because of their internal energy. The nanoparticles are constantly colliding with other nanoparticles as well as the particles of the base fluid. Thermophoresis is a motion that is caused by temperature gradient in the base fluid. This motion makes the particles move down the temperature gradient. This means that the particles will move from an area of higher temperature to an area of lower temperature. (Buongiorno 2006, 240-250). Both of these mechanisms cause the nanoparticles to move within the base fluid. This motion of the nanoparticles has a large effect on how they are able to transfer heat effectively. The nanoparticles are able to absorb heat from an area of high temperature and carry the energy to an area of lower temperature where it will be released. One other factor that affects the motion of the nanoparticles is the motion of the base fluid.

It has been demonstrated that nanoparticles contained in aerosol solutions have a strong tendency to follow the air stream that contains them. It has also been shown that during CFD simulations the nanoparticles have more motion when the Brownian and Thermophoresis forces are accounted for (Akbar, Rahman and Ghiaasiaan 2009, 747-761). Thermophoresis was found to have the greatest effect on the deposition location of the nanoparticles leading to the particles gathering at the cold wall of the enclosure (Akbar, Rahman and Ghiaasiaan 2009, 747-761).

Two heat transfer mechanisms commonly researched are natural convection and forced convection. Natural convection is a mechanism that moves fluids away from areas of high temperature towards areas of low temperature. This occurs because the fluid touching the high temperature area is gaining energy and becoming less dense, this makes that part of the fluid move upward in the body of fluid. As the higher temperature fluid moves up the lower temperature, therefore more dense, fluid from the top moves down under the force of gravity to take its place. Forced convection is a mechanism that induces movement of a fluid by the application of an external force. Examples of the devices used to apply the external force are a fan or pump. Typically forced convection is used to increase heat transfer of a system when natural convection does not provide adequate heat transfer.

In 2009 Akbar, Rahman and Ghiaasiaan studied particle transport in an enclosure using a nanoparticle and air mixture. The computer simulation performed used an enclosure that was heated from one side and the movement of the particles was recorded. The various mechanisms of particle motion were turned on and off during the testing scenario to determine how strong each acts on the particles (Akbar, Rahman and Ghiaasiaan 2009, 747-761).

As has been shown many studies have been done on heat transfer using a liquid base. The study of using nanoparticles in suspension of air has previously been very lightly researched. The natural flow convection has been studied while the forced convection has not been previously explored.

# Chapter 3. Method

For the purposes of this research, computer simulation was performed to develop a method to find the heat transfer characteristics of nano fluids. Various aspect ratio enclosures were used to determine the characteristics of the fluid. In this research work various enclosures with natural convection of air, forced convection of air, and natural convection of air with nano particles simulations were performed.

To perform all these numerical simulations, ICEM CFD was used to develop the geometry and mesh properties of the model. ANSYS-FLUENT was then used to simulate the effects of temperature and flow on the appropriate models. All simulations were performed for a 2D enclosure with the bottom of the enclosure held at a temperature of 350°K while the roof was held at a temperature of 300°K. Two side walls were considered adiabatic during the natural convection experiments. During the forced convection numerical experiments, the left wall was considered to be a velocity inlet velocity and the right wall was considered a vent outlet. All of the forced convection simulations were performed with an inlet Reynolds number of 50 to ensure the laminar flow regime. During the simulation process air velocity vector, air isotherm, surface heat flux, and surface Nusselt number are calculated.

To perform the simulations of this numerical experimentation multiple steps were performed. The first step is to use FLUENT to develop skills in the program. This was accomplished by creating the 1-1 aspect ratio natural convection simulation and comparing these results with the previous research results. The first situation was solved for the natural convection of air in a closed narrow enclosure as shown in Figure 1.

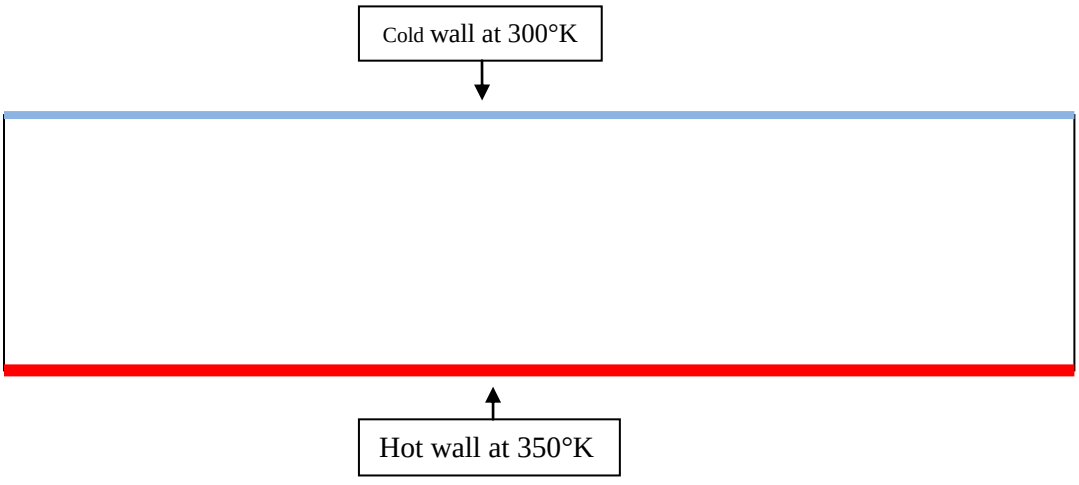


**Figure 1. Natural convection of air experimental setup**

Once the natural convection of air had been completed the simulation was performed for the forced convection of air in the narrow enclosure. This involved opening the enclosure, and introducing the forced air flow necessary for forced convection to take place. This setup is illustrated in Figure 2.

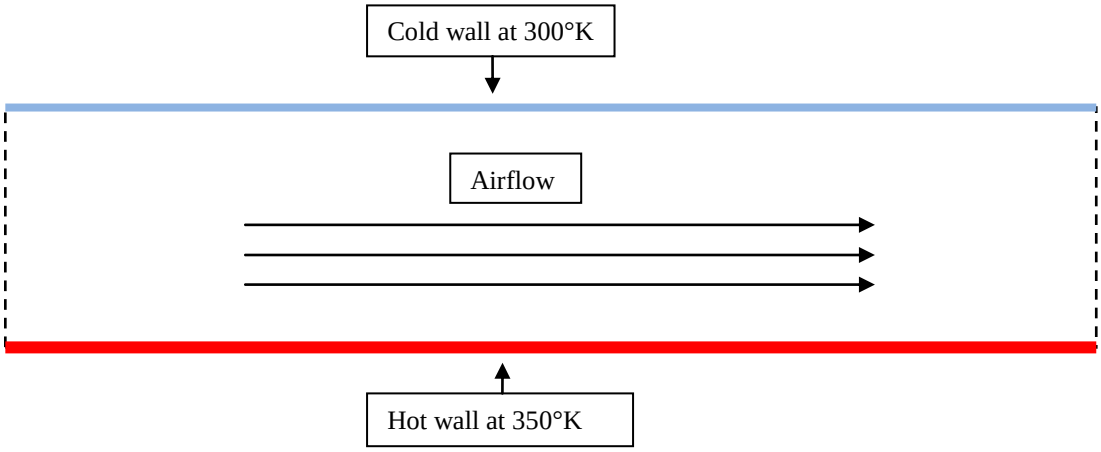


**Figure 2. Forced convection of air experimental setup**

Once the air only simulation was performed, the nanoparticles were introduced into the system to simulate the nanoparticles suspended in air.

## Governing Equations

The governing equations used include conservation of mass, conservation of momentum, and conservation of energy.

$$\frac{\partial p}{\partial t} + \nabla * (p\vec{v}) = S_m \tag{1}$$

$$\frac{\partial}{\partial t}(p\vec{v}) + \nabla * (p\vec{v}\vec{v}) = -\nabla p + \nabla * (\bar{\bar{\tau}}) + p\vec{g} + \vec{F} \tag{2}$$

$$\frac{\partial}{\partial t}(\rho E) + \nabla * \left(\vec{v}(\rho E + p)\right) = -\nabla * \left(\sum_j h_j J_j\right) + S_h \tag{3}$$

The vector form of the particle momentum equation [Chen, and McLaughlin 1995, 1129 – 1142, Elghobashi, Truesdell 1992, 655 – 700, Ounis, Ahmadi, and McLaughlin 1991, 235 – 250, and Thakurt, Chen, McLaughlin, and Kontomaris 1998, 4167 – 4182] can be expressed as:

$$\rho_P V_P \frac{d\vec{U}_P}{dt} = -f\left(\vec{U}_P - \vec{U}_G\right) + \left(\rho_P - \rho_G\right) V_P \vec{g} + \vec{F}_B + \vec{F}_{TP} \tag{4}$$

where

$$f = \frac{3\pi\mu_G d_P}{C} \tag{5}$$

The Brownian dispersion effect is represented by the inclusion of the random Brownian force term $\vec{F}_B$, whose Cartesian components are found from:

$$F_{B,i} = G_i \left( \frac{6\pi\mu d_P \kappa T_G}{C\,\Delta t} \right)^{\frac{1}{2}} \tag{6}$$

where $\Delta t$ is the time step in the numerical particle motion calculations, and $G_i$ ($i$ = 1, 2, 3) are three independent Gaussian random numbers (for the three coordinates) with zero means and unit variances.

The particle thermophoresis force is obtained from the semi-empirical expression of:

$$F_{TP,i} = -f \frac{C_T \nu}{T} \nabla T_{,i} \tag{7}$$

where,

$$C_T = \frac{2.34\left(k/k_p + 2.18\,Kn\right)C}{\left(1+3.42Kn\right)\left(1+2k/k_p + 4.36Kn\right)}$$

In Eq. (4), $\overrightarrow{U_G}$ represents the component of gas velocity at the particle's location. The position of a particle should also be updated by integrating the following equation:

$$\frac{dx_j}{dt} = u_{P,j} \tag{8}$$

The ordinary differential equation set represented by Eqs. (4) and (8) were explicitly integrated over each time step according to:

$$u_{P,i}^{(t+\Delta t)} = \left(u_{g,i} + B/f\right)^{(t)} + \left[u_{P,i} - \left(u_{g,i} + B/f\right)\right]^{(t)} e^{-\frac{f}{A}\Delta t} \tag{9}$$

$$x_i^{(t+\Delta t)} = x_i^{(t)} + \left(u_{g,i} + B/f\right)\Delta t + \frac{A}{f}\left[u_{p,i} - \left(u_{g,i} + B/f\right)\right]^{(t)} \left(1 - e^{-\frac{f}{A}\Delta t}\right) \tag{10}$$

where:

$$A = \rho_P V_P \tag{11}$$

$$B = \left(\rho_P - \rho_G\right)V_P g_i + F_{B,i} + F_{TP,i} \tag{12}$$

## Mesh Setup

6 aspect ratio meshes setup were considered for this numerical research which includes 1×1, 2×1, 4×1, 6×1, 8×1, and 10×1 aspect ratios. The meshes were all created with length units of cm. The number of nodes on the left wall was maintained at 45 for all cases to ease comparison, and the top wall had 40 nodes per length unit. The spacing and ratio values were maintained at the same values through the simulations for ease of comparison. All of the values for mesh setup are shown in Table 1, Table 2, Table 3, Table 4, Table 5 and Table 6 respectively.

**Table 1: 1×1 Mesh Setup Values**

| Mesh Size | 1x1 | |
|---|---|---|
| | 1 | 1 |
| Blocking | Top | Left |
| Length (cm) | 1 | 1 |
| Nodes | 40 | 45 |
| Spacing 1/Ratio 1 | 0/2 | 0.01/1.15 |
| Spacing 2/Ratio 2 | 0/2 | 0.01/1.15 |

**Table 2: 2×1 Mesh Setup Values**

| Mesh Size | 2x1 | |
|---|---|---|
| | 2 | 1 |
| Blocking | Top | Left |
| Length (cm) | 2 | 1 |
| Nodes | 80 | 45 |
| Spacing 1/Ratio 1 | 0/2 | 0.01/1.15 |
| Spacing 2/Ratio 2 | 0/2 | 0.01/1.15 |

Table 3: 4×1 Mesh Setup Values

| Mesh Size | 4x1 | |
|---|---|---|
| | 4 | 1 |
| Blocking | Top | Left |
| Length (cm) | 4 | 1 |
| Nodes | 160 | 45 |
| Spacing 1/Ratio 1 | 0/2 | 0.01/1.15 |
| Spacing 2/Ratio 2 | 0/2 | 0.01/1.15 |

**Table 4: 6×1 Mesh Setup Values**

| Mesh Size | 6x1 | |
|---|---|---|
| | 6 | 1 |
| Blocking | Top | Left |
| Length (cm) | 6 | 1 |
| Nodes | 240 | 45 |
| Spacing 1/Ratio 1 | 0/2 | 0.01/1.15 |
| Spacing 2/Ratio 2 | 0/2 | 0.01/1.15 |

**Table 5: 8×1 Mesh Setup Values**

| Mesh Size | 8x1 | |
|---|---|---|
| | 8 | 1 |
| Blocking | Top | Left |
| Length (cm) | 8 | 1 |
| Nodes | 320 | 45 |
| Spacing 1/Ratio 1 | 0/2 | 0.01/1.15 |
| Spacing 2/Ratio 2 | 0/2 | 0.01/1.15 |

**Table 6: 10×1 Mesh Setup Values**

| Mesh Size | 10x1 | |
|---|---|---|
| | 10 | 1 |
| Blocking | Top | Left |
| Length (cm) | 10 | 1 |
| Nodes | 400 | 45 |
| Spacing 1/Ratio 1 | 0/2 | 0.01/1.15 |
| Spacing 2/Ratio 2 | 0/2 | 0.01/1.15 |

## Numerical Setup for Natural Convection of Air in the Enclosure

A pressure based steady time solver was used. The gravity was set to -9.81m/$s^2$. The energy model as well as the viscous laminar model was used. The materials were specified with air having a density specified by the ideal gas law, a specific heat of 10006.43 kg/m*s, a thermal conductivity of 0.242 w/m*°K, a viscosity of 1.7894e-05 kg/m*s, and molecular weight of 28.966 kg/kgmol. Aluminum was specified as having a density of 2719 kg/$m^3$, specific heat of 871 j/kg*°K, and thermal conductivity of 202.4 w/m*°k.

The boundary condition was set for the upper cold wall as a stationary wall with 300°K constant temperature. The lower hot wall was defined as a stationary wall with a constant temperature of 350°K.

The left and the right side walls were defined as stationary, adiabatic walls with zero heat flux. All four walls were defined as being made of aluminum.

The solution method used pressure-velocity coupling scheme defined as SIMPLE, the spatial discretization gradient was set to least square cell based, the pressure was set as standard, the density was set to second order upwind, momentum was set to second order upwind, and energy was set to second order upwind. The solution under relaxation factor for pressure was set to 0.3, density was set to 1, body forces was set to 1, momentum was set to 0.7, and energy was set to 1. The scaled residuals equation for continuity was set to 1e-06, x-velocity was set to 1e-06, y-velocity was set to 1e-06, and energy was set to 1e-06.

## Numerical Setup for Forced Convection of Air in the Enclosure

A pressure based steady time solver was used. The gravity was set to -9.81m/$s^2$. The energy model as well as the viscous laminar model was used. The materials were specified with air having a density specified by the ideal gas law, a specific heat of 10006.43 kg/m*s, a thermal conductivity of 0.242 w/m*°K, a viscosity of 1.7894e-05 kg/m*s, and molecular weight of 28.966 kg/kgmol. Aluminum was specified as having a density of 2719 kg/$m^3$, specific heat of 871 j/kg*°K, and thermal conductivity of 202.4 w/m*°k.

The upper cold wall was stationary with 300°K constant temperature. The lower hot wall was defined as a stationary with a constant temperature of 350°K. Both stationary walls were specified as being made of aluminum. The left side has inlet velocity with a magnitude of 0.037911 m/s, in the x direction and a constant temperature of 300°K. The right side is an outlet vent with atmospheric pressure, and the backflow direction specification method as normal to boundary.

The solution method of pressure-velocity coupling scheme was defined as SIMPLE, the spatial discretization gradient was set to least square cell based, the pressure was set as standard, the momentum was set to second order upwind, and energy was set to second order upwind. The solution under relaxation factor for pressure was set to 0.3, density was set to 1, body forces was set to 1, momentum was set to 0.7, and energy was set to 1. The scaled residuals equation for continuity was set to 1e-06, x-velocity was set to 1e-06, y-velocity was set to 1e-06, and energy was set to 1e-06.

## Numerical Setup for Natural Convection with Nanofluid in the Enclosure

A pressure based steady time solver was used. The gravity was set to -9.81m/$s^2$. The energy model as well as the viscous laminar model, radiation P1, and the discrete phase models were used. The discrete phase model was set to have interaction with the continuous phase, update DPM sources every

flow iteration, unsteady particle tracking, particle time step of 0.0005, and the number of time steps equals one. The maximum number of tracking steps was set to be 15000, the step length factor was set to be 5, and the drag model was set to be spherical. The particle radiation interaction and Brownian motion physical models were set. The injection was set to have 125 particle streams, inert particles, and linear particle distribution. The injected area was set as a line from the bottom left of the area to the top right of the area leaving a 0.25 cm gap from the walls. The initial velocity of the particles was set to be 0 m/s, with a diameter of 1e-09 m, temperature of 300°K, and the injection continued for 0.05 seconds per 1×1cm area being solved for. This resulted in 12,500 particles being present for the 1x1 case, 25,000 particles for the 2x1 case, 50,125 particles for the 4x1 case, 75,125 particles for the 6x1 case, 100,125 particles for the 8x1 case, and 125,125 particles for the 10x1 case.

The materials were specified with air having a density specified by the ideal gas law, a specific heat of 10006.43 kg/m*s, a thermal conductivity of 0.242 w/m*°K, a viscosity of 1.7894e-05 kg/m*s, molecular weight of 28.966 kg/kgmol, absorption coefficient of zero, scattering coefficient of zero, and the refractive index of 1.000293. Aluminum was specified as having a density of 2719 kg/$m^3$, specific heat of 871 j/kg*°K, and thermal conductivity of 202.4 w/m*°k. The copper for the particle was defined as having a density of 8978 kg/$m^3$, specific heat of 871 j/kg*°K, thermal conductivity of 387.6 w/m*°K, particle emissivity of 0.9, and particle scattering factor of 0.9.

The boundary condition was set for the upper cold wall as stationary, with 300°K constant temperature. The lower hot wall was defined as stationary with a constant temperature of 350°K. The left wall was stationary with zero heat flux. The right wall was also stationary with zero heat flux. All four walls were defined as being made of aluminum with the boundary condition type for the DPM being reflective.

The solution method of pressure-velocity coupling scheme was defined as SIMPLE, the spatial discretization gradient was set to least square cell based, the pressure was set as standard, the density was set to second order upwind, momentum was set to second order upwind, and energy was set to second order upwind. The solution under relaxation factor for pressure was set to be 0.3, density was set to be 1, body forces was set to be 1, momentum was set to be 0.7, and energy was set to be 1. The scaled residuals equation for continuity was set to be 1e-06, x-velocity was set to be 1e-06, y-velocity was set to be 1e-06, and energy was set to be 1e-06.

## Convergence Testing

To ensure convergence, the models were solved until the scaled residuals plots stabilized. A xy plot of the static temperatures at a horizontal centerline was then created. The solution was then run for an additional number of iterations, and the same xy plot was created. These two plots were then put together and compared. Once these two plots fell on the same line the solution was considered converged. All of the cases had scaled residuals of at least 1e-04 while some values were as low as 1e-07. The values found from the simulations are shown in Table 7.

**Table 7. Convergence Criteria**

| Scaled Residuals Nanofluid | | | | | |
|---|---|---|---|---|---|
| | Natural Convection Nanofluid | | | | |
| | Continuity | X-Velocity | Y-Velocity | Energy | P1 |
| 1-1 | 1.00E-05 | 1.00E-07 | 1.00E-07 | 1.00E-07 | 1.00E-07 |
| 2-1 | 1.00E-04 | 1.00E-07 | 1.00E-07 | 1.00E-07 | 1.00E-07 |
| 4-1 | 1.00E-04 | 1.00E-07 | 1.00E-07 | 1.00E-07 | 1.00E-07 |
| 6-1 | 1.00E-04 | 1.00E-07 | 1.00E-07 | 1.00E-07 | 1.00E-07 |
| 8-1 | 1.00E-04 | 1.00E-07 | 1.00E-07 | 1.00E-07 | 1.00E-07 |
| 10-1 | 1.00E-04 | 1.00E-07 | 1.00E-07 | 1.00E-07 | 1.00E-07 |

## Mesh Check

The mesh was modified with different combinations of nodes on the top and left side. The number of nodes for each refinement is shown in Table 8. The original mesh has 1800 areas, refinement 1 has 2750 areas, refinement 2 has 2250 areas, and refinement 3 has 1400 areas.

**Table 8. Mesh Refinement Values**

| | Original Mesh | | Refinement 1 | | Refinement 2 | | Refinement 3 | |
|---|---|---|---|---|---|---|---|---|
| | Top | Left | Top | Left | Top | Left | Top | Left |
| Length | 1 | 1 | 1 | 1 | 1 | 1 | 1 | 1 |
| Nodes | 40 | 45 | 50 | 55 | 45 | 50 | 35 | 40 |
| Spacing 1 | 0 | 0.01 | 0 | 0.01 | 0 | 0.01 | 0 | 0.01 |
| Ratio 1 | 2 | 1.15 | 2 | 1.15 | 2 | 1.15 | 2 | 1.15 |
| Spacing 2 | 0 | 0.01 | 0 | 0.01 | 0 | 0.01 | 0 | 0.01 |
| Ratio 2 | 2 | 1.15 | 2 | 1.15 | 2 | 1.15 | 2 | 1.15 |

# Chapter 4. Findings and Analysis

## Appropriate Mesh Generation

The first thing that was checked was the appropriateness of the mesh that was developed. This was accomplished by creating multiple meshes of the 1-1 area and simulating the natural convection of air. The results for the centerline temperatures for four different cases are shown in Figure 3

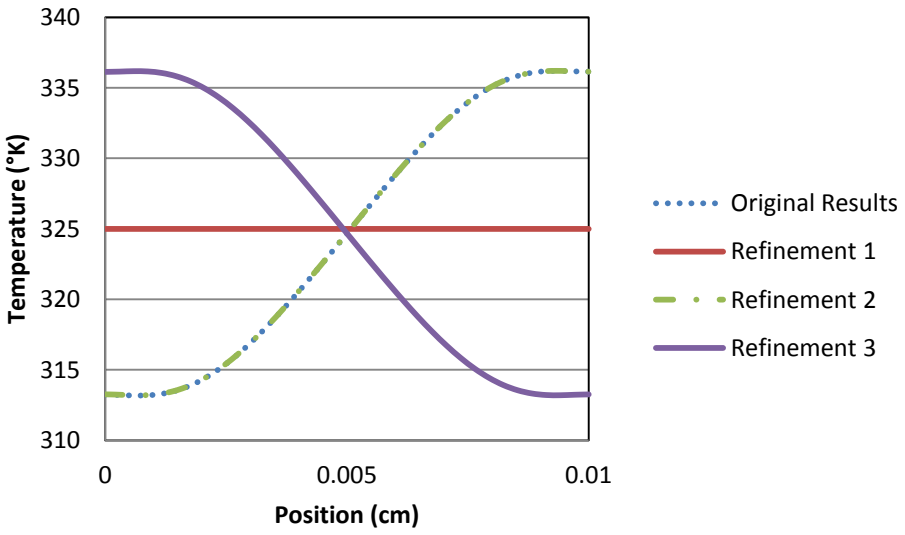


**Figure 3. 1-1 Mesh Check Temp Centerline**

Figure 3shows that refinement 1mesh had a constant centerline temperature, refinement 2 and the original meshes had the same centerline temperature; and refinement 3 mesh had the same temperatures as refinement 2 with the inversed positions. Refinement 1 represented adding 10 nodes to each wall of the area and resulted in no natural convection within the domain which believed to have been from computer being unable to solve the domain. Refinement 2 represents adding 5 nodes to each wall of the area resulting in the same centerline temperature. Refinement 3 represented taking 5 nodes away from each wall of the area and the centerline temperature was flipped with respect to the original.

## Velocity Vectors for Different Generated Meshes

The original mesh velocity vector is shown in Figure 4, the refinement 1 mesh velocity vector is shown in Figure 5, the refinement 2 mesh velocity vector is shown in Figure 6, and the refinement 3 velocity vector is shown in Figure 7. Velocity vector for Refinement 1 mesh does not follow the same trend as the original mesh velocity vector or any of the other setups as shown in Figure 5. Refinement 2

mesh has a very similar velocity vector when compared to the original mesh as shown in Figure 6 and Figure 4. Refinement 3 mesh has a less smooth velocity vector as well as flowing in the opposite direction when compared to the original mesh as shown in Figure 7 and Figure 4.

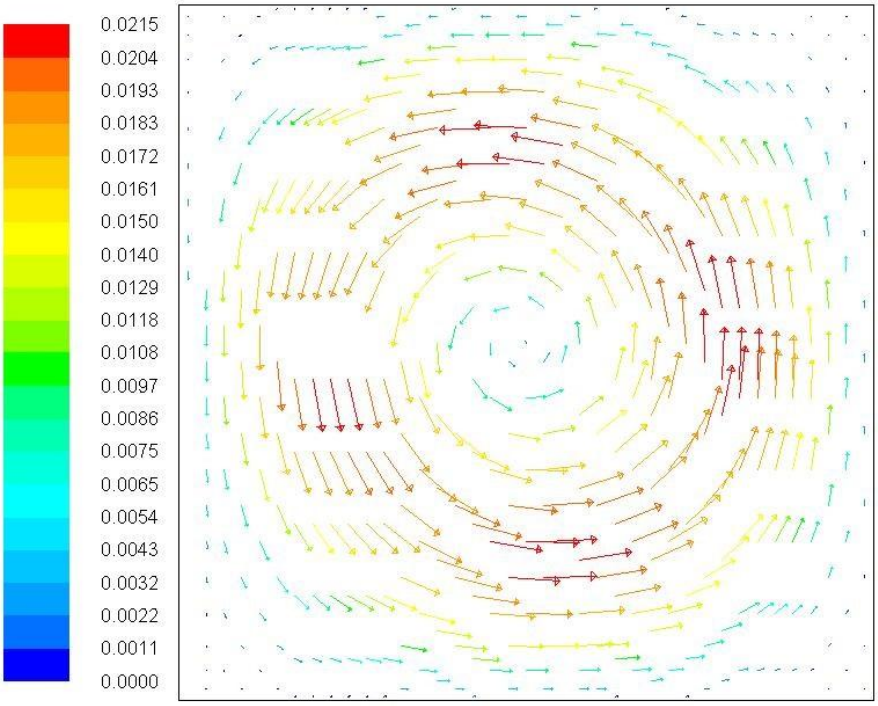


**Figure 4. Original Mesh Velocity Vector**

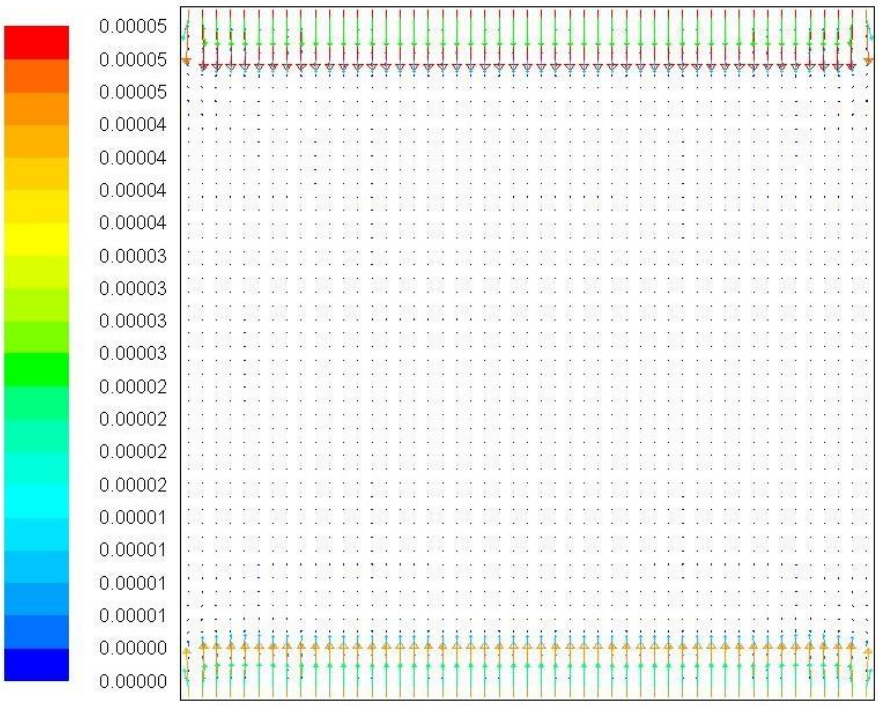


**Figure 5. Refinement 1 Mesh Velocity Vector**

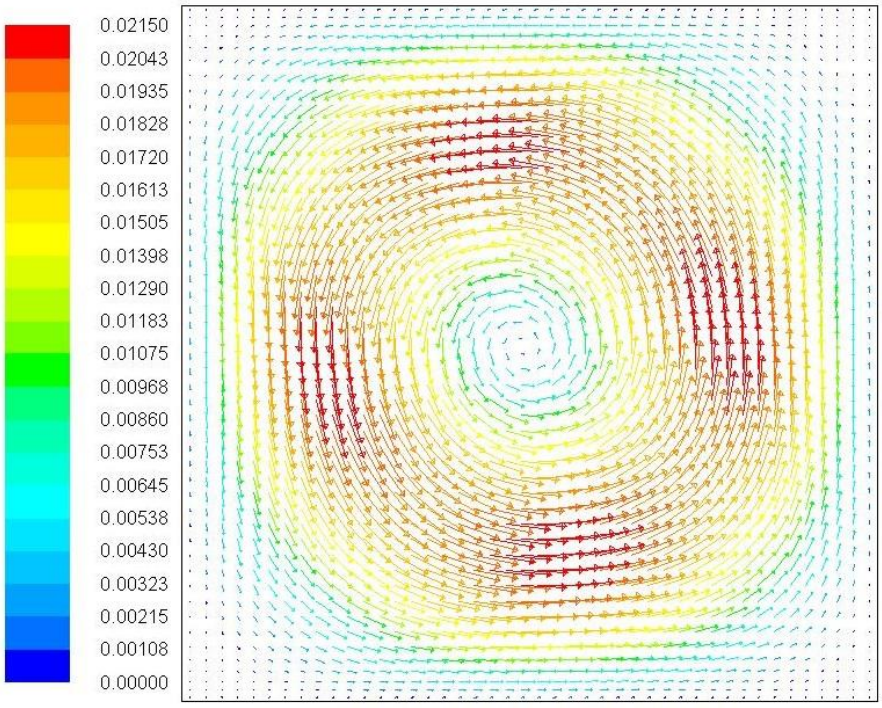


**Figure 6. Refinement 2 Mesh Velocity Vector**

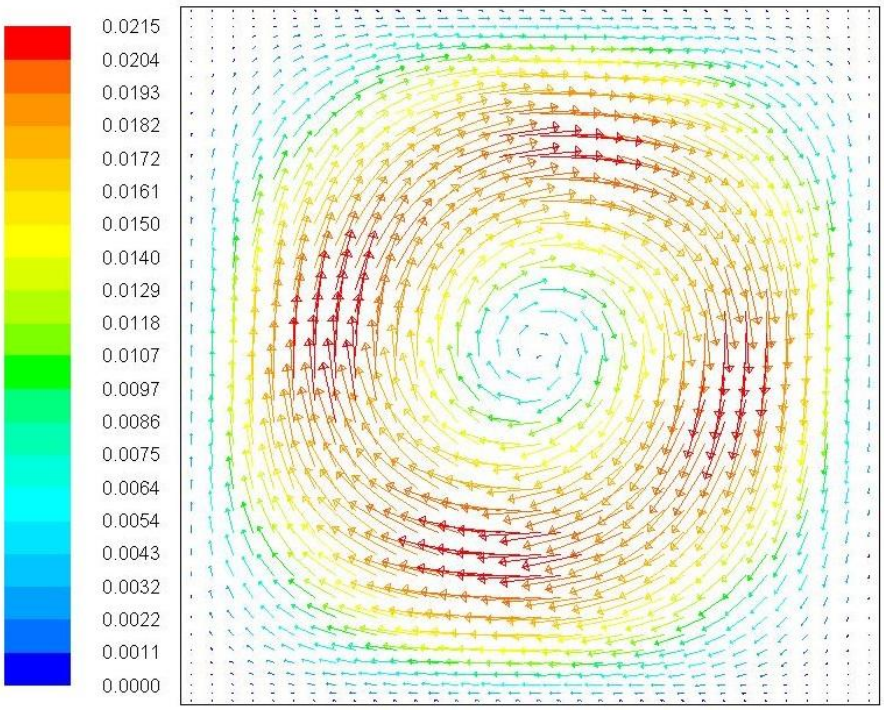


**Figure 7. Refinement 3 Mesh Velocity Vector**

## Isotherms for Different Generated Meshes

The original mesh isotherm is shown in Figure 8, the refinement 1mesh isotherm is shown in Figure 9, the refinement 2 isotherm is shown in Figure 10, and the refinement 3 isotherm is shown in Figure 11respectively. The refinement 1 mesh isotherm is showing a linear temperature distribution unlike the other scenarios as shown in Figure 9. The refinement 2 mesh isotherm looks very similar to the original mesh isotherm as shown in Figure 10. The refinement 3 mesh isotherm has similar characteristics to the original mesh isotherm, but with it being flipped left to right.

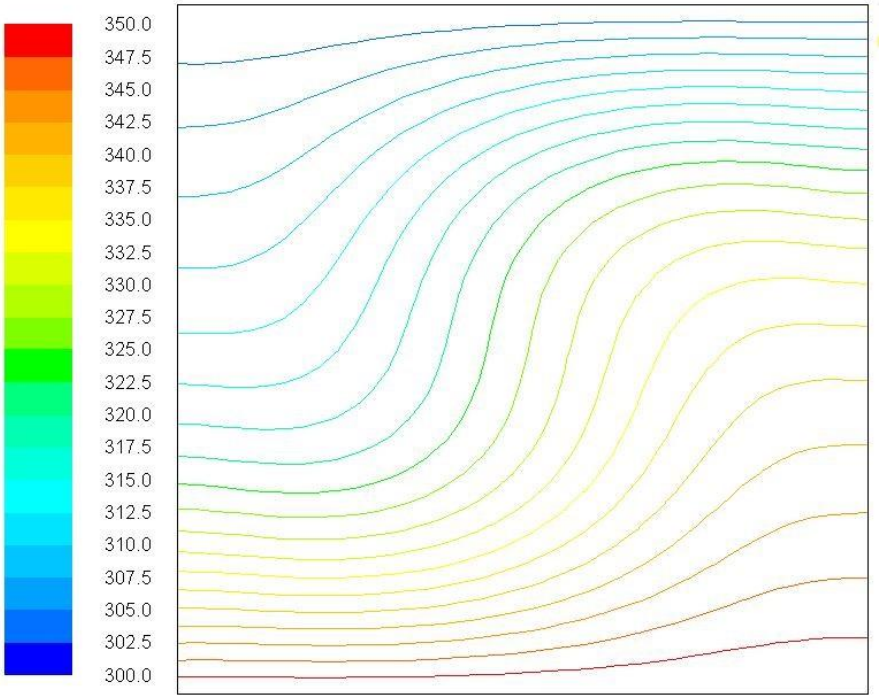


**Figure 8. Original Mesh Isotherm**


**Figure 9. Refinement 1 Mesh Isotherm**

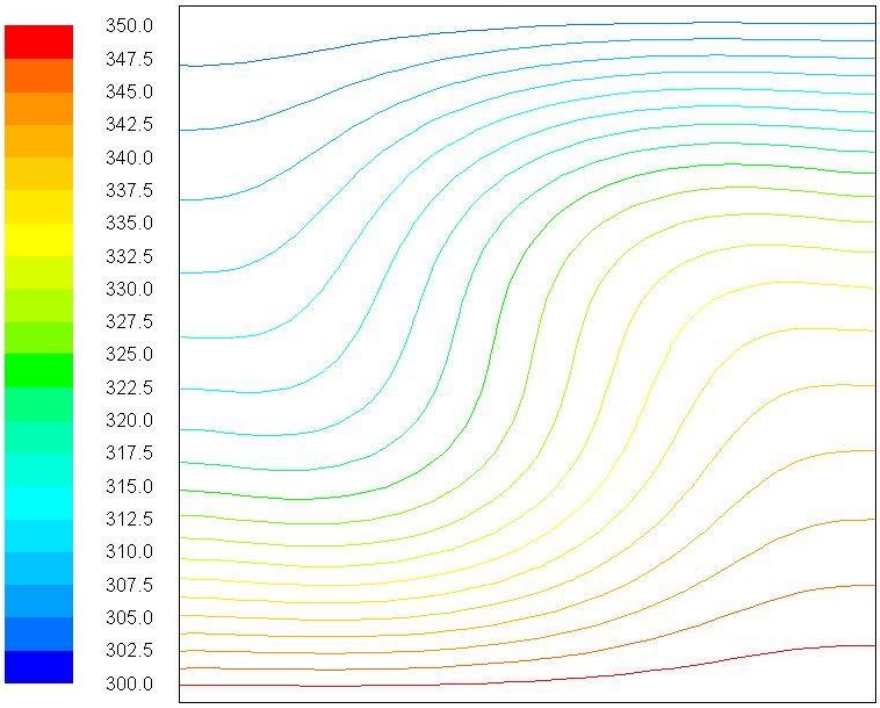


**Figure 10. Refinement 2 Mesh Isotherm**

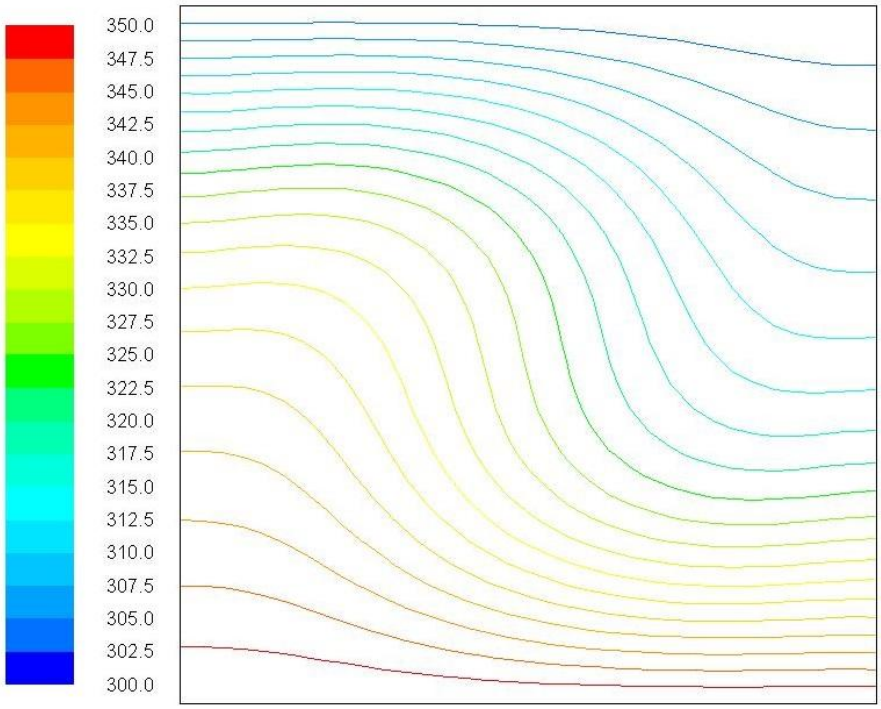


**Figure 11. Refinement 3 Mesh Isotherm**

Over the course of this mesh check it was determined that the original mesh had very similar results to the second refinement. The first refinement does not show appropriate temperature distribution, so it was deemed as inappropriate. The third refinement has results flipped left to right when compared to the other meshes. Based on these results it was determined that the original mesh and the slightly finer mesh 2 were effectively the same, so the increased mesh was unnecessary. Refinement 3 showed a different trend with less number of nodes than the original. The original mesh was determined to be appropriate based on these findings.

## Convergence Check

When the models were solved the scaled residuals were monitored until they stabilized. To ensure the model was converged the static temperature was plotted along a horizontal centerline. This plot was done for two different iterations of the model. This is shown for the natural convection cases in Figure 12 for the 1-1 case, Figure 13 for the 2-1 case, Figure 14 for the 4-1 case, Figure 15 for the 6-1 case, Figure 16 for the 8-1 case, and Figure 17 for the 10-1 case respectively. For the forced convection cases the temperature centerlines are shown in Figure 18 for the 1-1 case, Figure 19 for the 2-1 case, Figure 20 for the 4-1 case, Figure 21 for the 6-1 case, Figure 22 for the 8-1 case, and Figure 23 for the 10-1 case respectively. These plots verify that the model was fully converged.

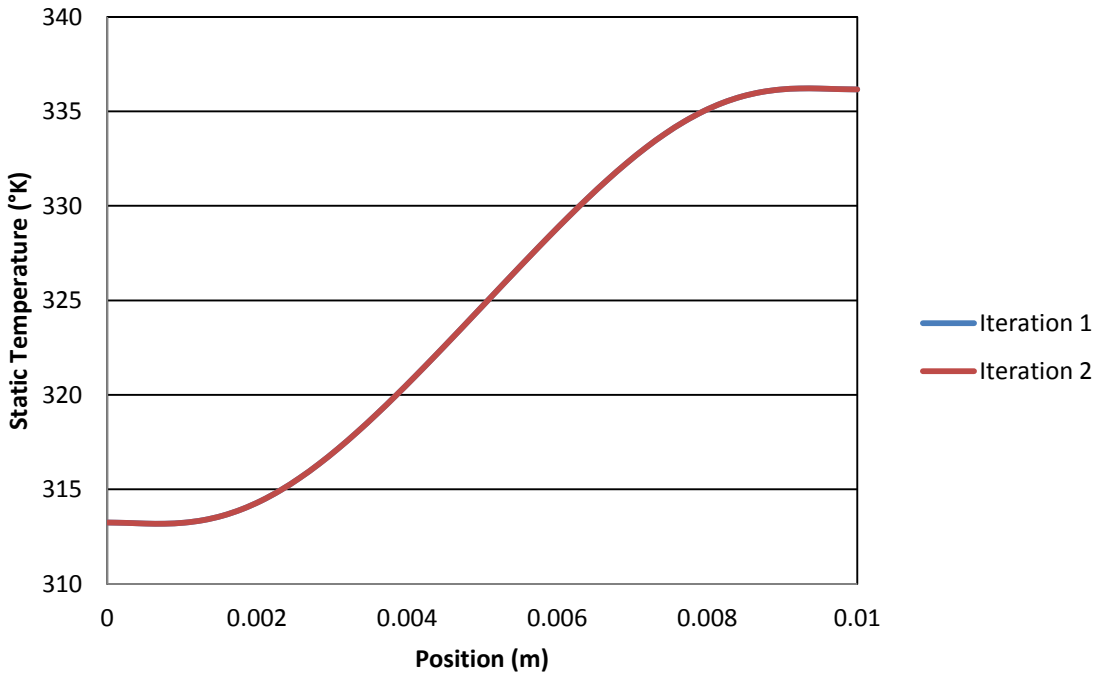


**Figure 12. Convergence for Case 1-1 in Natural Convection**

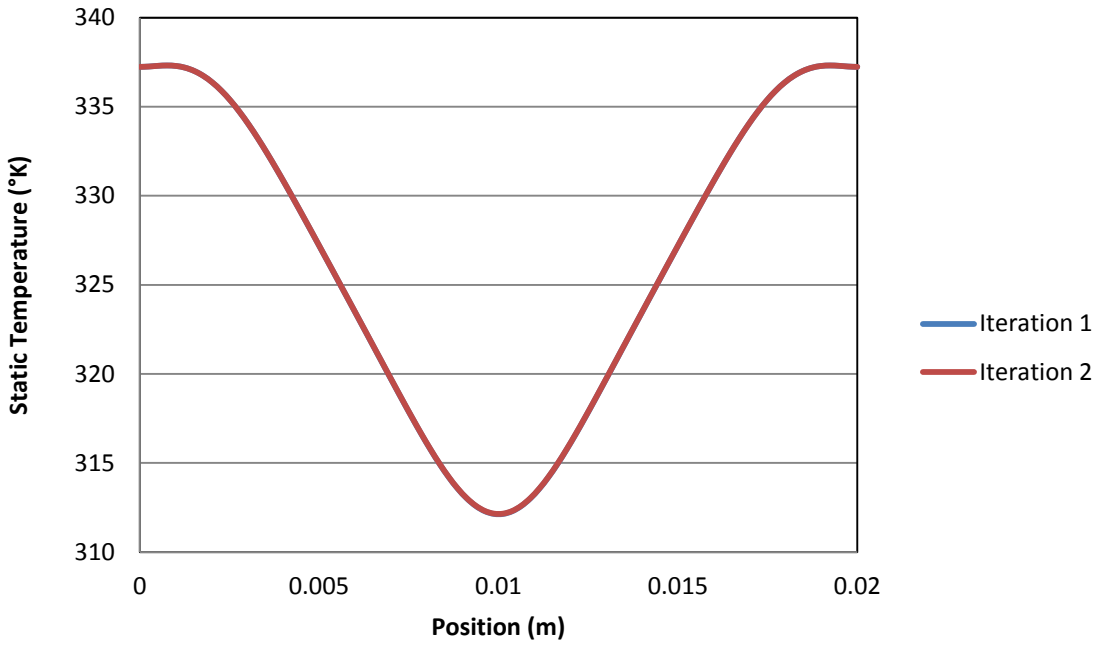


**Figure 13. Convergence for Case 2-1 in Natural Convection**

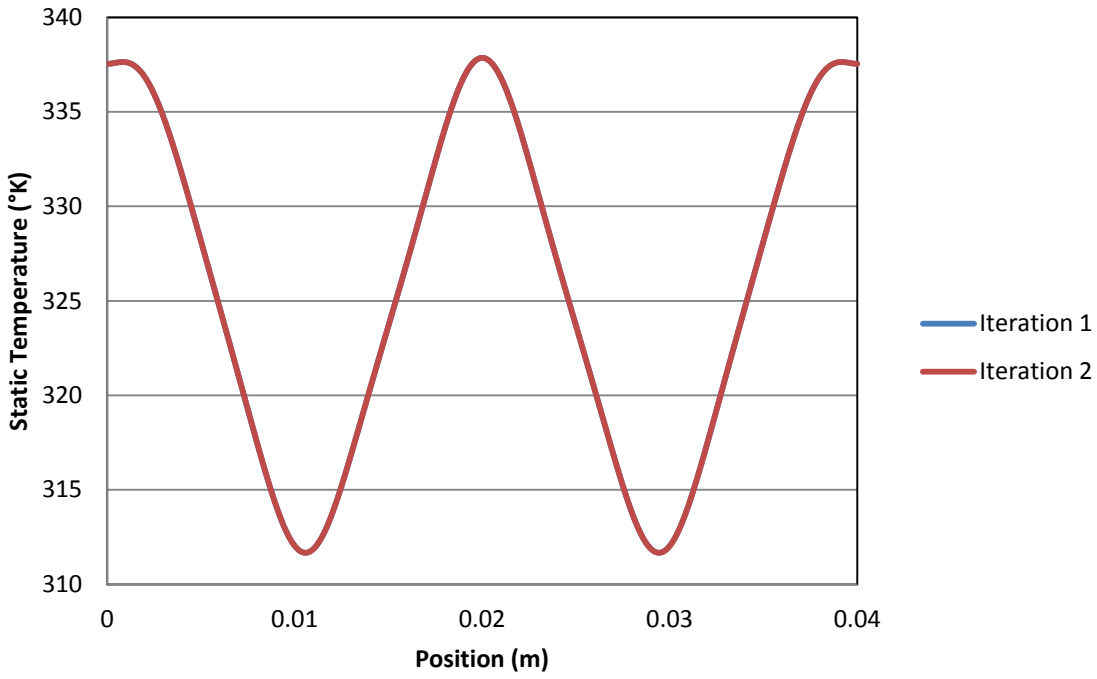


**Figure 14. Convergence for Case 4-1 in Natural Convection**

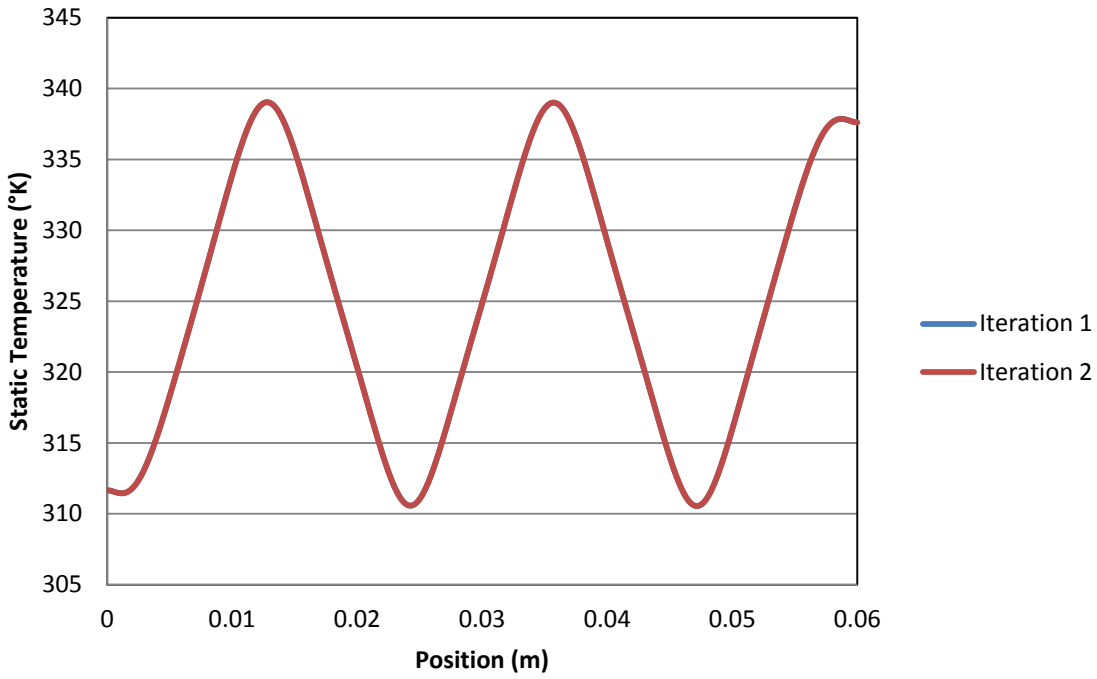


**Figure 15. Convergence for Case 6-1 in Natural Convection**

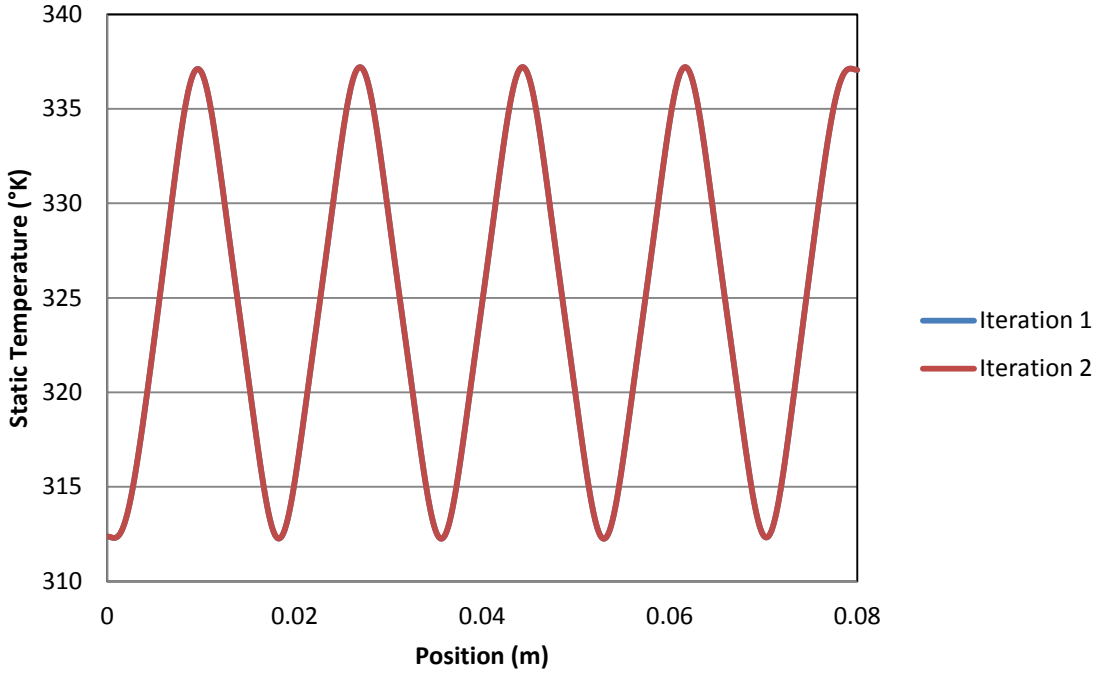


**Figure 16. Convergence for Case 8-1 in Natural Convection**

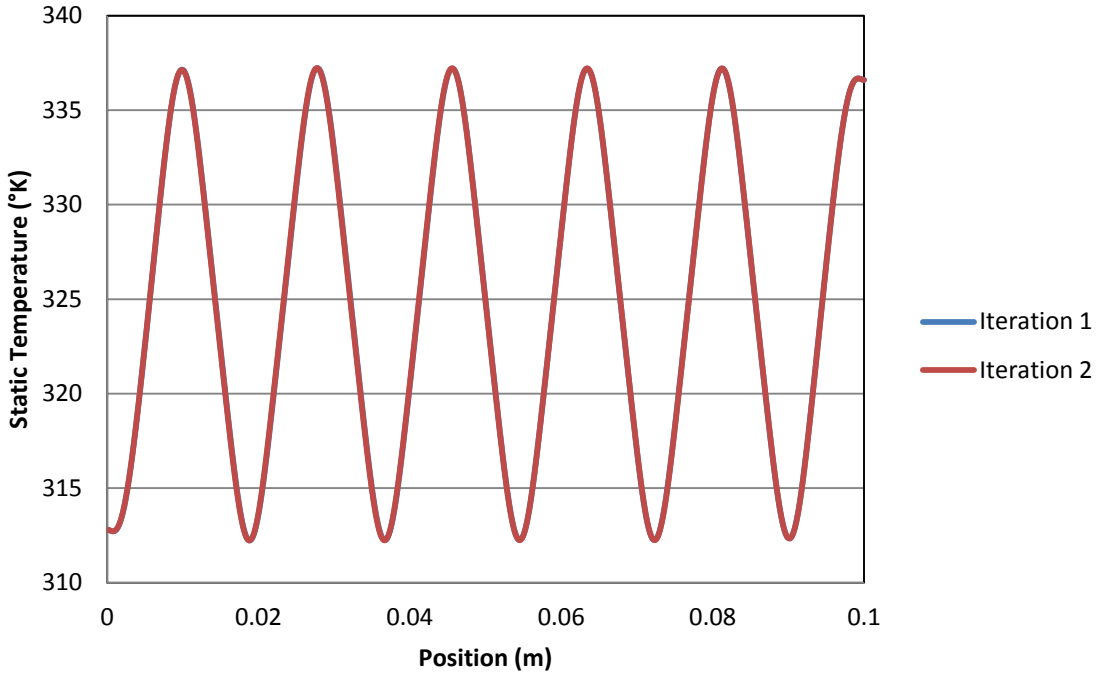


**Figure 17. Convergence for Case 10-1 in Natural Convection**

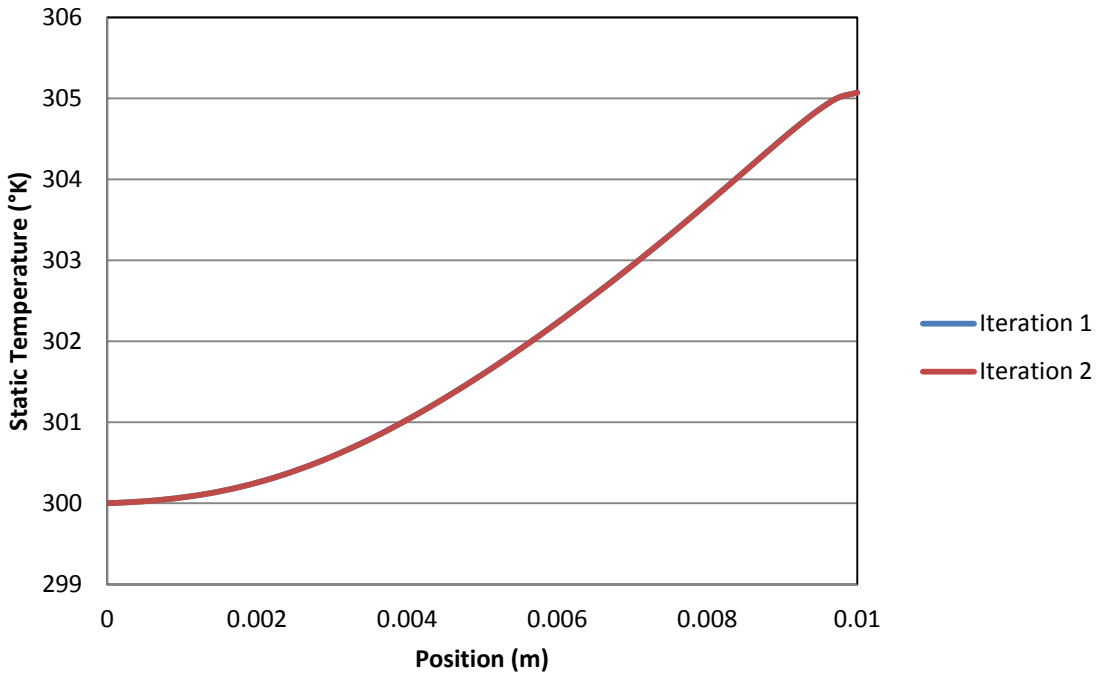


**Figure 18. Convergence for Case 1-1 in Forced Convection**

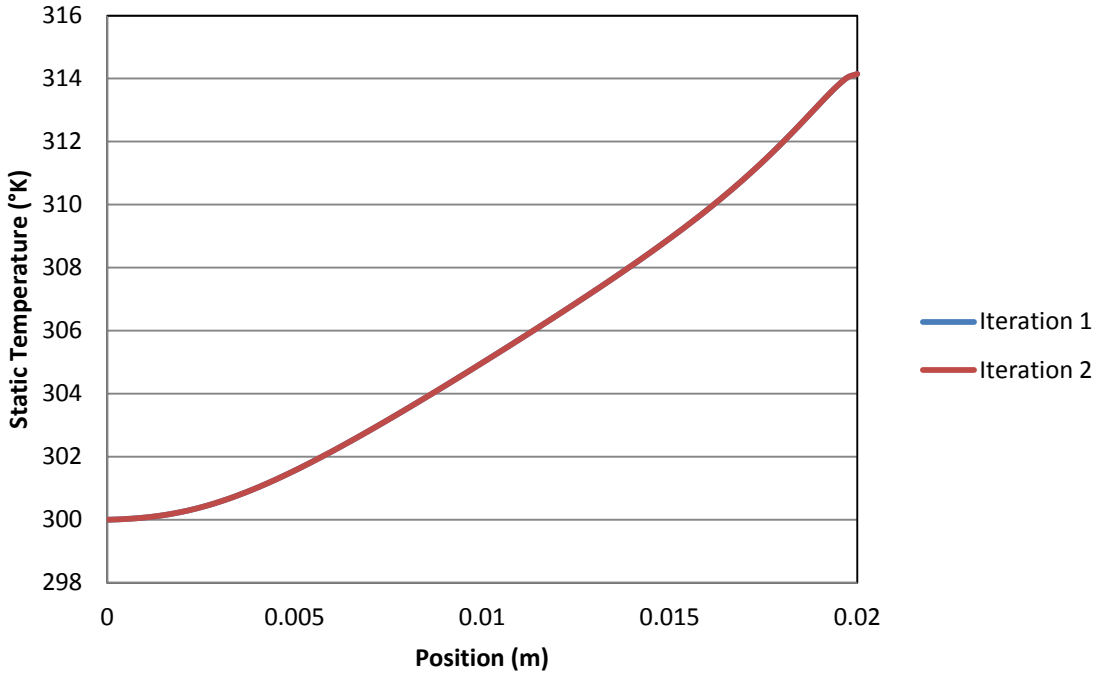


**Figure 19. Convergence for Case 2-1 in Forced Convection**

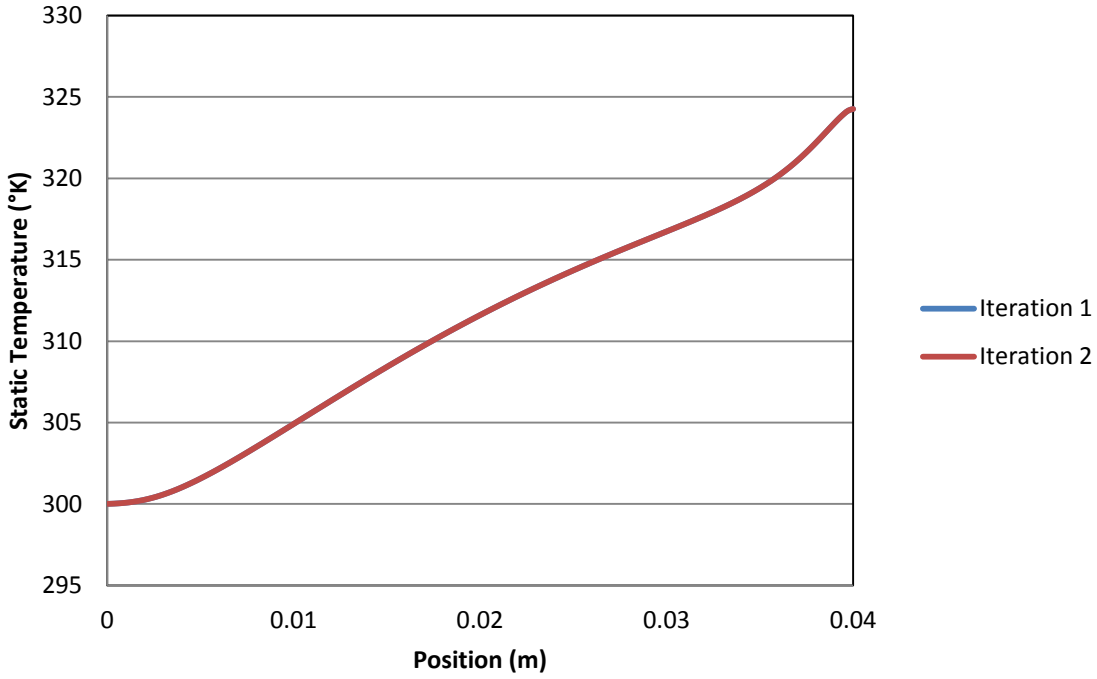


**Figure 20. Convergence for Case 4-1 in Forced Convection**

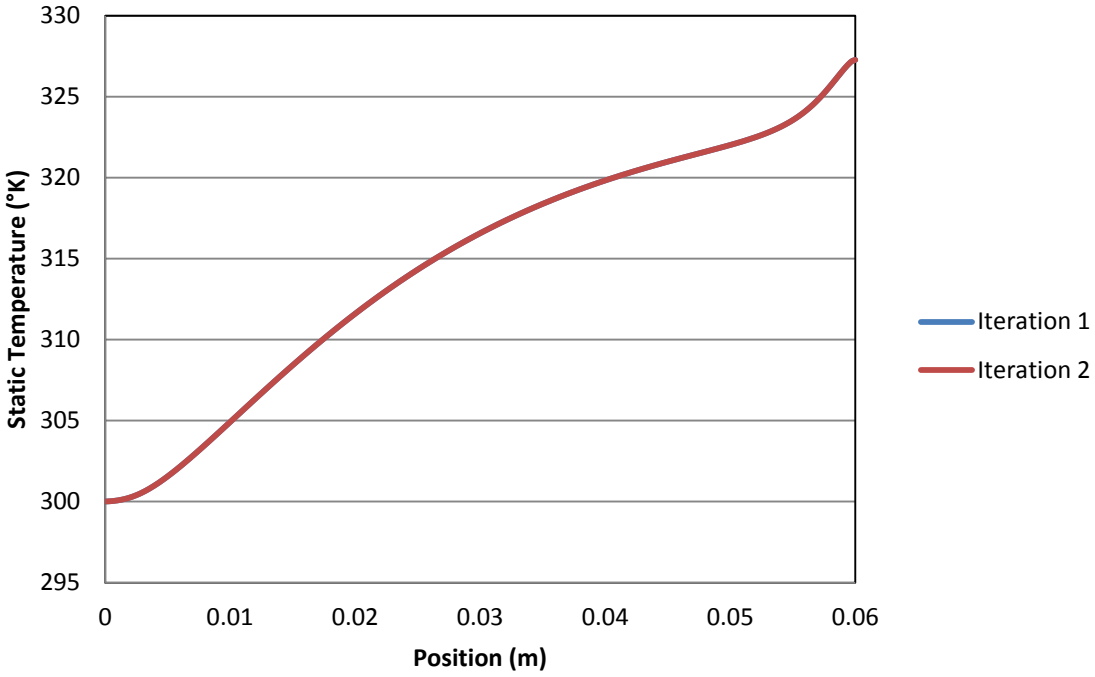


**Figure 21. Convergence for Case 6-1 in Forced Convection**

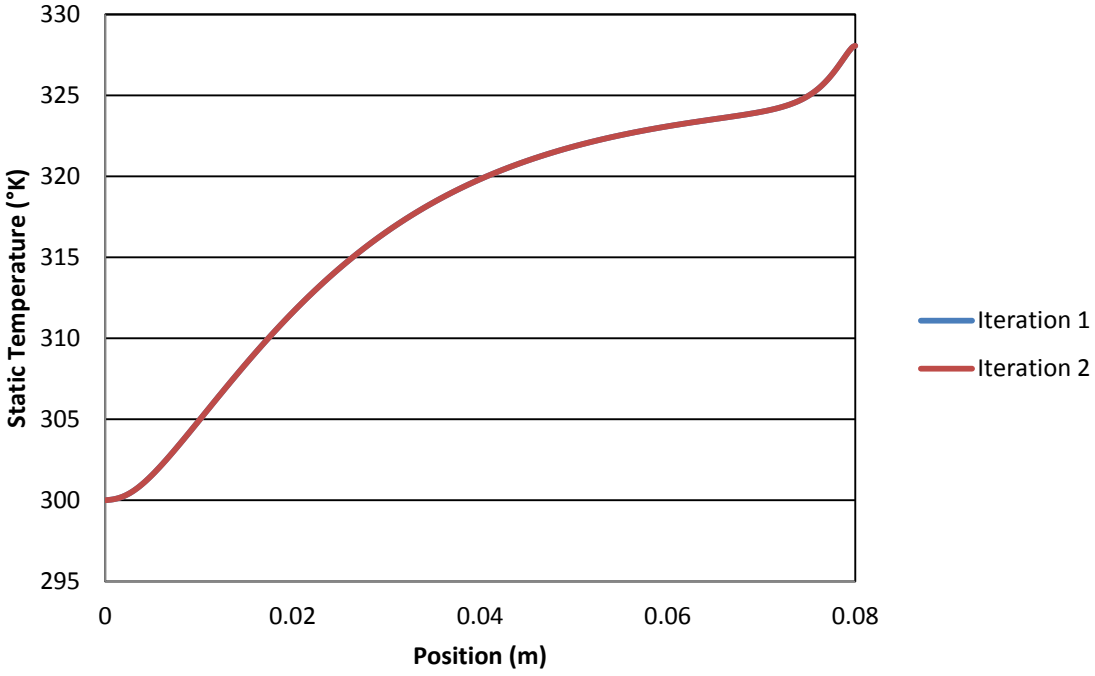


**Figure 22. Convergence for Case 8-1 in Forced Convection**

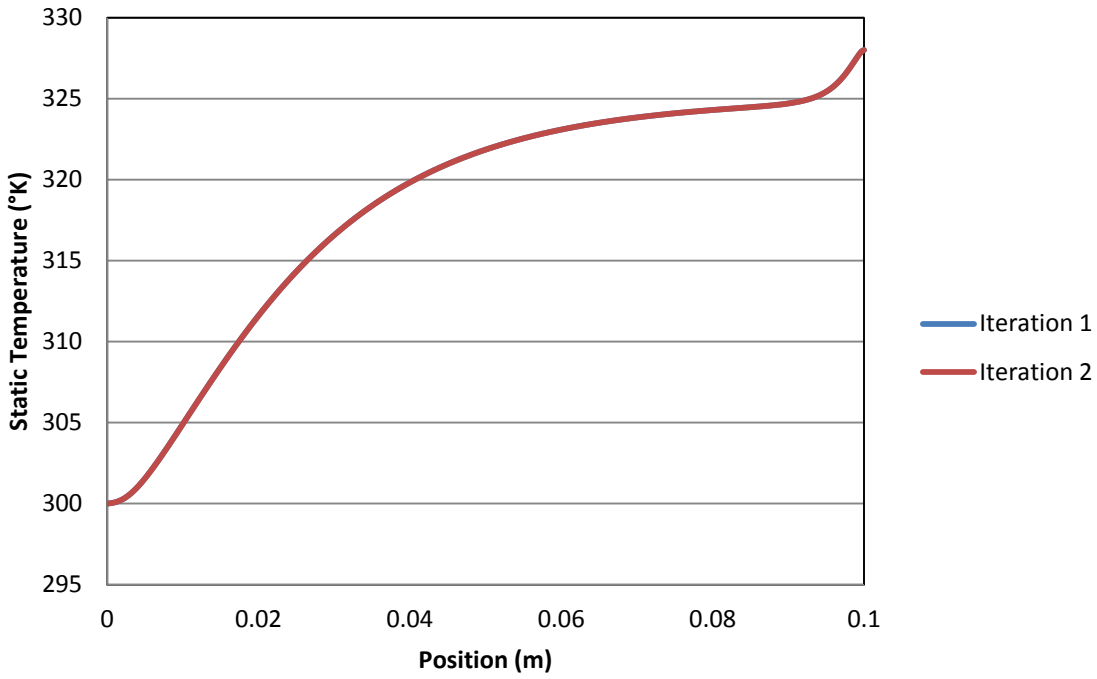


**Figure 23. Convergence for Case 10-1 in Forced Convection**

## Velocity Vector

The velocity vectors were plotted for the natural convection and forced convection of air cases. The natural convection of air cases are shown in Figure 24 for the 1-1 case, Figure 25 for the 2-1 case, Figure 26 for the 4-1 case, Figure 27 for the 6-1 case, Figure 28 for the 8-1 case, and Figure 29 for the 10-1 case respectively. The forced convection cases are shown in Figure 30 for the 1-1 case, Figure 31 for the 2-1 case, Figure 32 for the 4-1 case, Figure 33 for the 6-1 case, Figure 34 for the 8-1 case, and Figure 35 for the 10-1 case.

The natural convection cases showed a periodic air flow that was based on a repetition of the 1-1 case shown in Figure 24. The 2-1 case has 2 circular air flows, the 4-1 case has 4 airflows, the 6-1 case has 5 circular air flows, the 8-1 case has 9 circular air flows, and the 10-1 case has 11 circular air flows. This shows that as the aspect ratio increases the number of circulating flows increases.

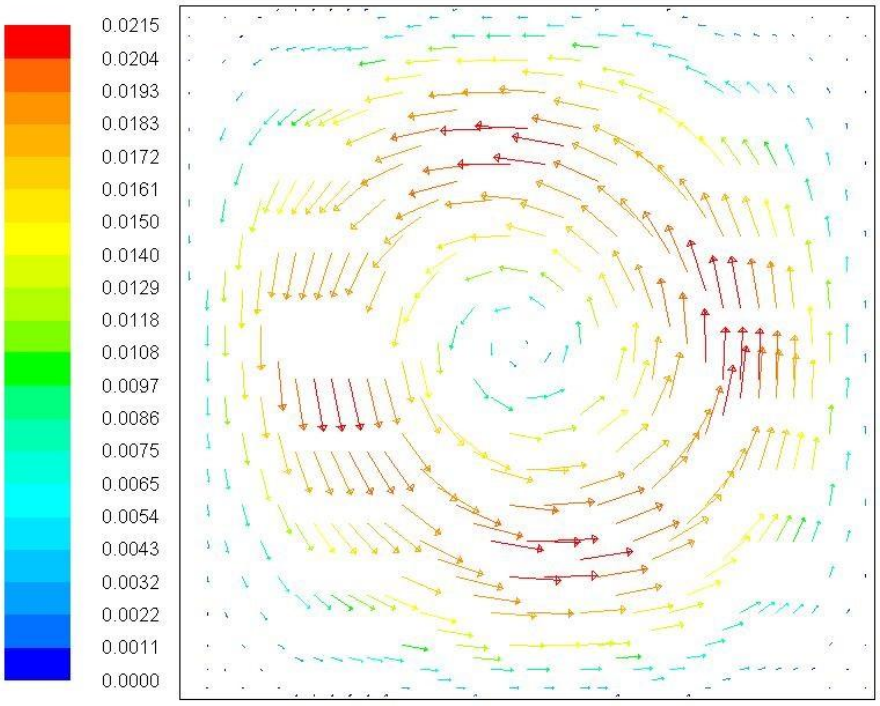


**Figure 24. Velocity Vector for Natural Convection in 1-1 Aspect Ratio Case**

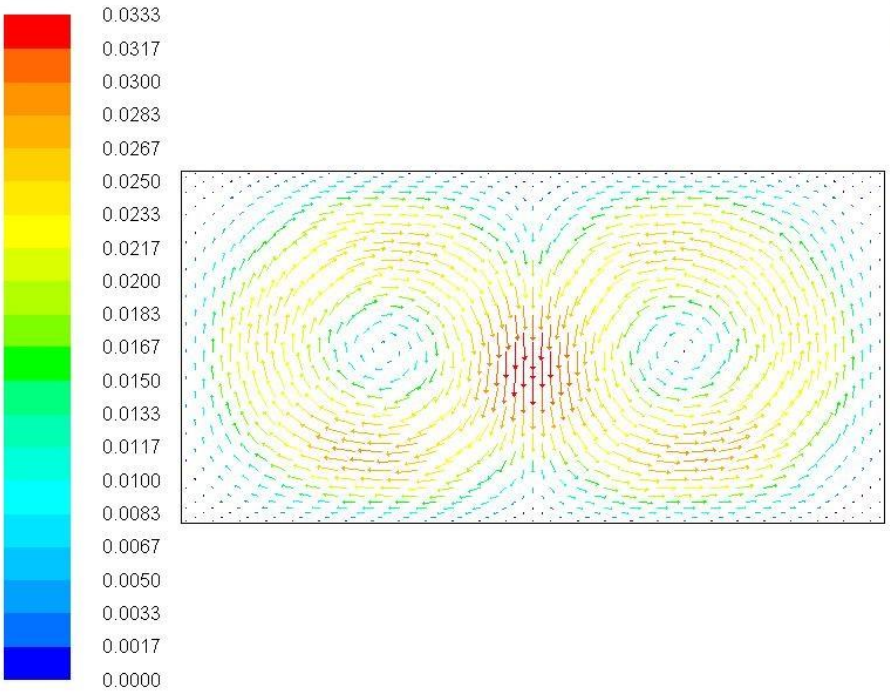


**Figure 25. Velocity Vector for Natural Convection in 2-1 Aspect Ratio Case**

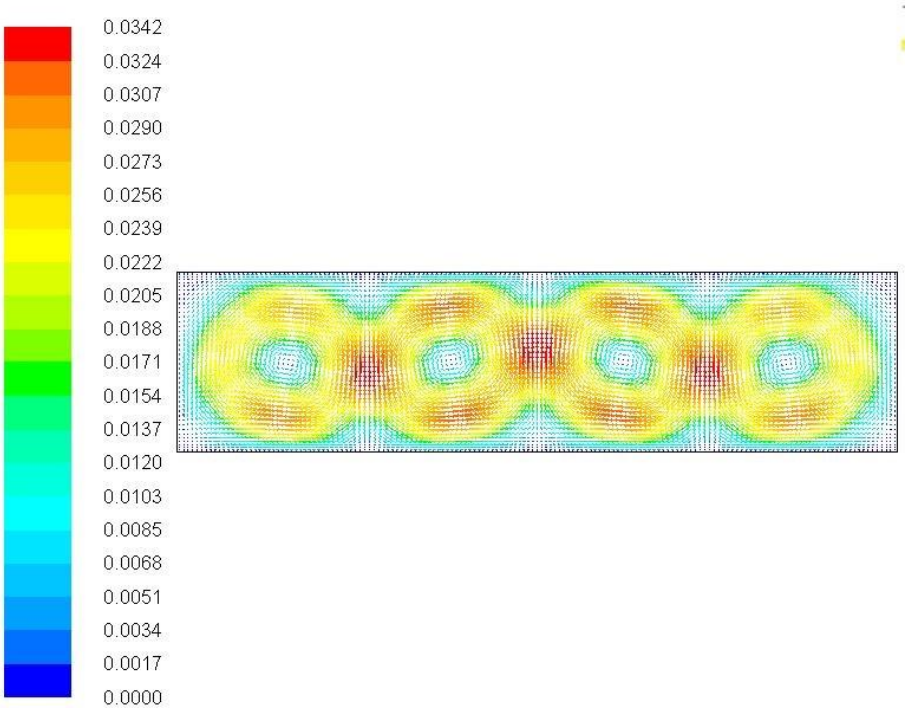


**Figure 26. Velocity Vector for Natural Convection in 4-1 Aspect Ratio Case**

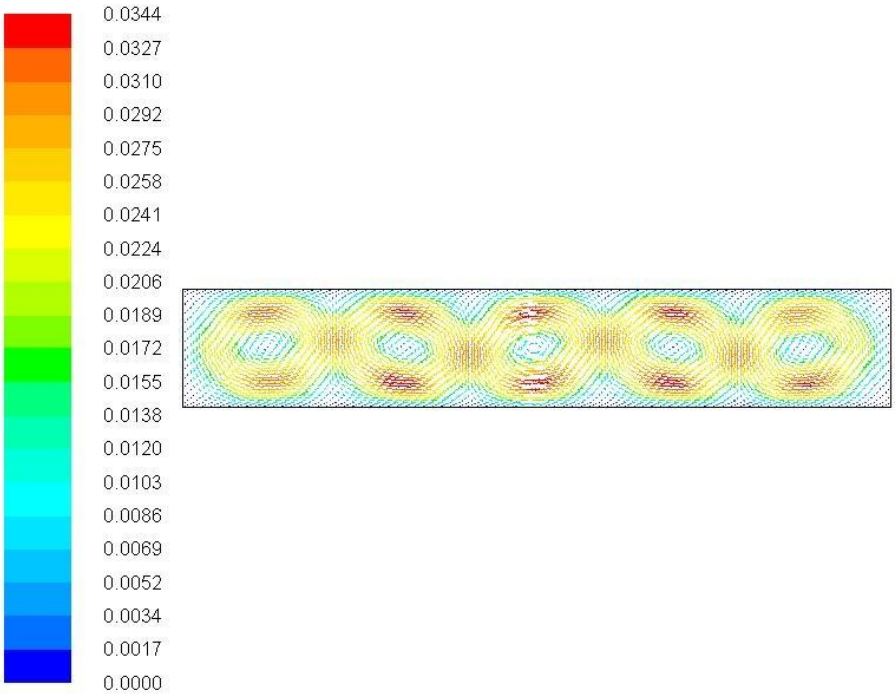


**Figure 27. Velocity Vector for Natural Convection in 6-1 Aspect Ratio Case**

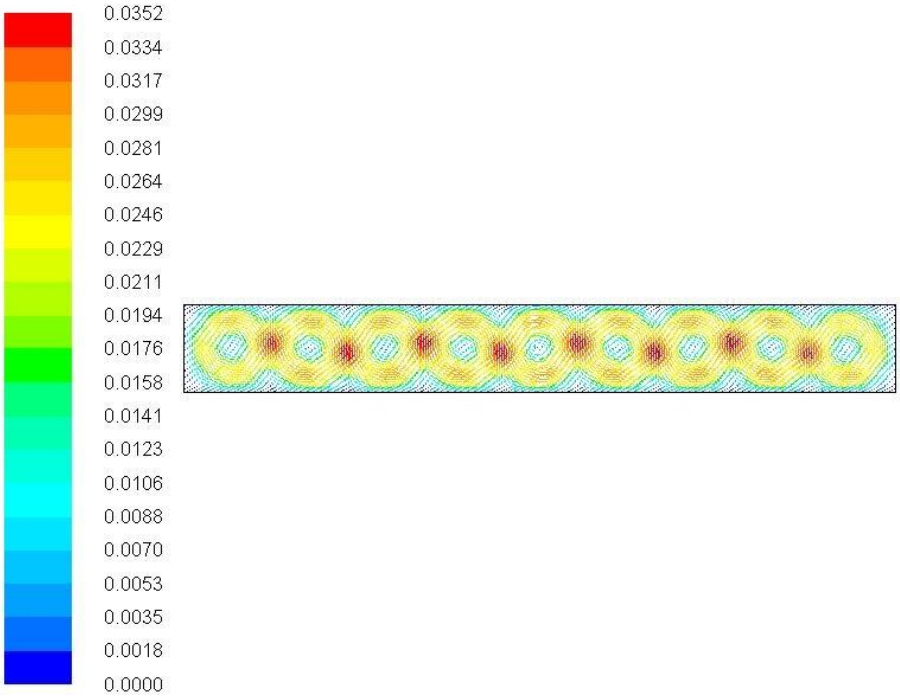


**Figure 28. Velocity Vector for Natural Convection in 8-1 Aspect Ratio Case**

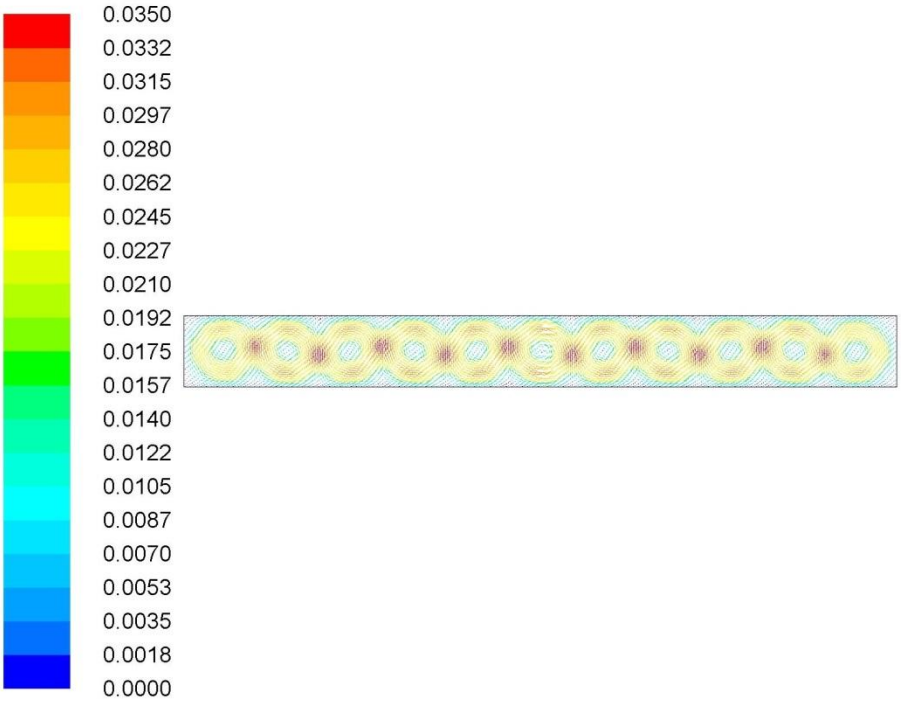


**Figure 29. Velocity Vector for Natural Convection in 10-1 Aspect Ratio Case**

The forced convection cases showed a trend of rising as the flow went to the right of the area. This resulted in the flow reversing at the bottom right corner of the area. The forced convection cases are shown in Figure 30 for the 1-1 case, Figure 31 for the 2-1 case, Figure 32 for the 4-1 case, Figure 33 for the 6-1 case, Figure 34 for the 8-1 case, and Figure 35 for the 10-1 case respectively.

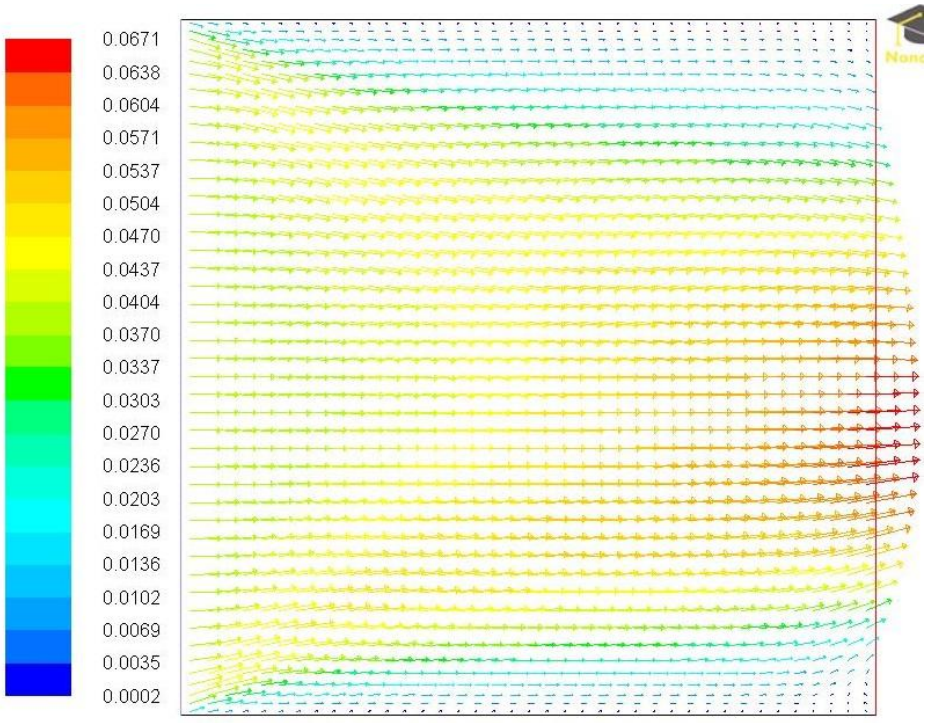


**Figure 30. Velocity Vector for Forced Convection in 1-1 Aspect Ratio Case**

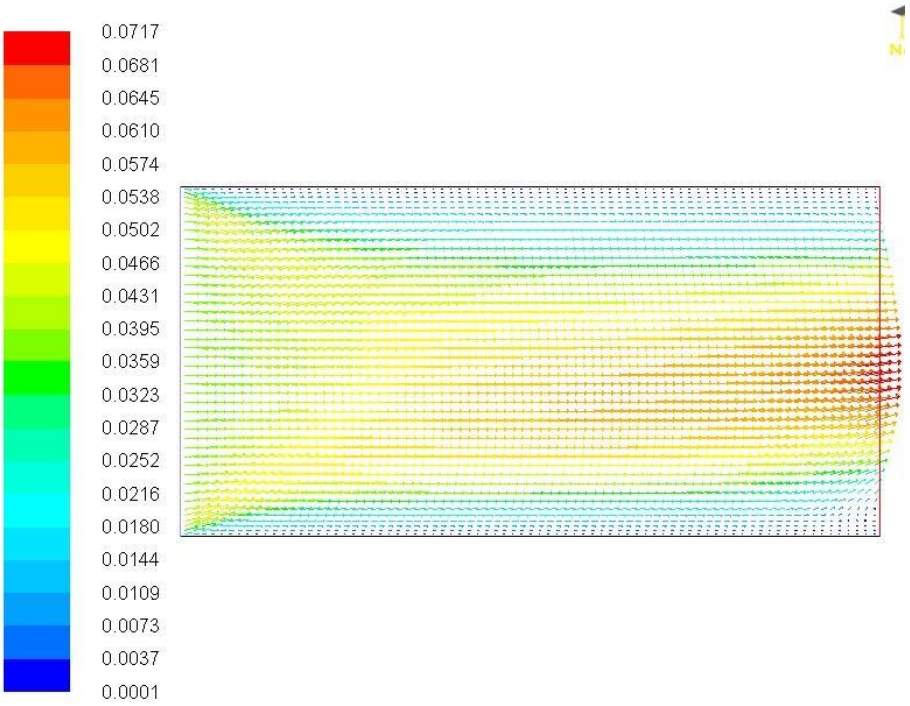


**Figure 31. Velocity Vector for Forced Convection in 2-1 Aspect Ratio Case**

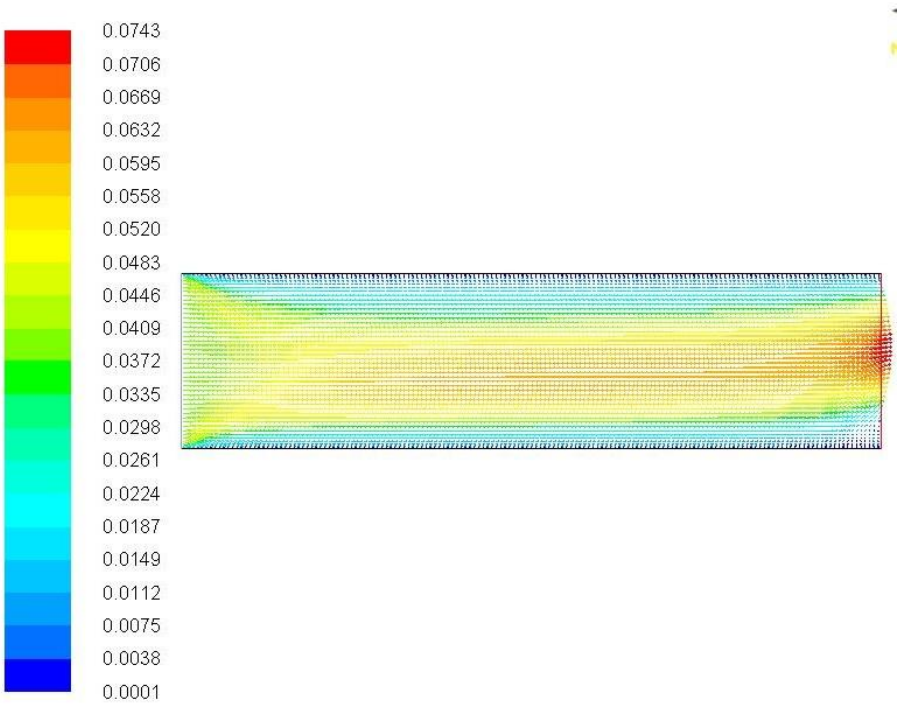


**Figure 32. Vector for Forced Convection in 4-1 Aspect Ratio Case**

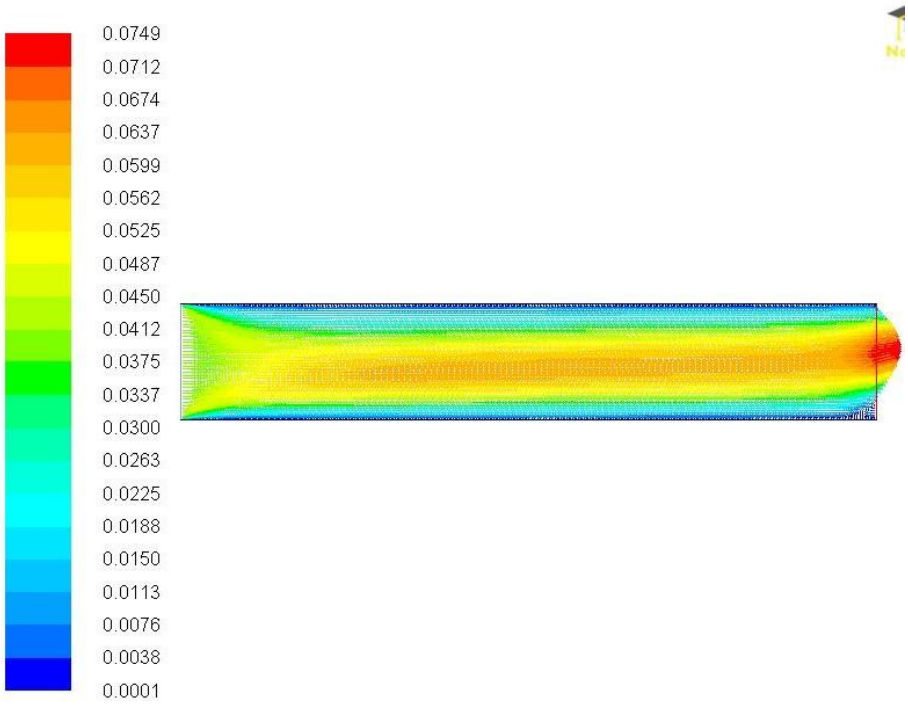


**Figure 33. Velocity Vector for Forced Convection in 6-1 Aspect Ratio Case**

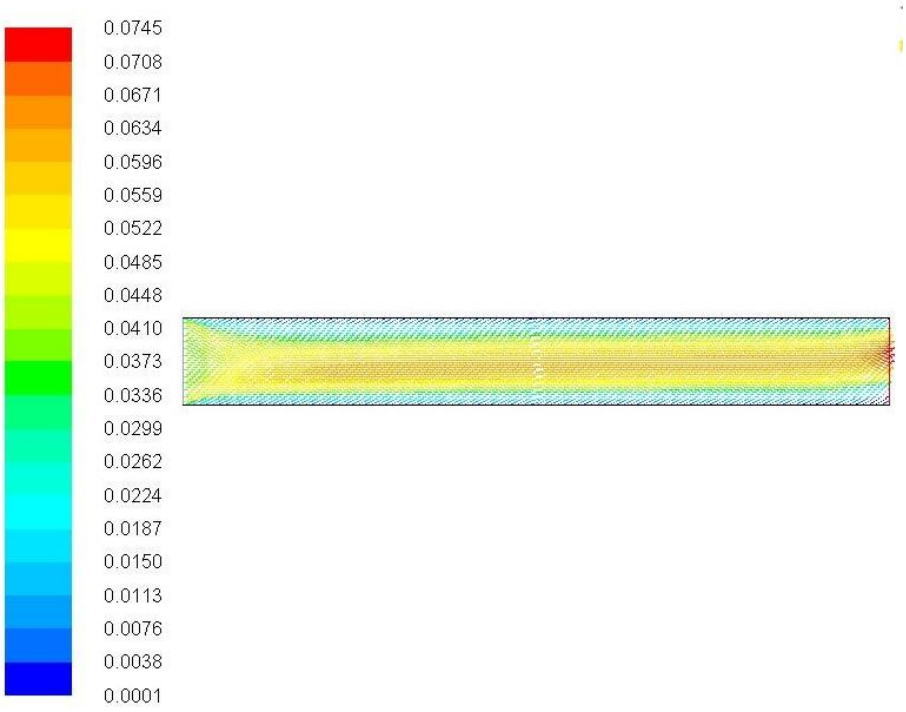


**Figure 34. Velocity Vector for Forced Convection in 8-1 Aspect Ratio Case**

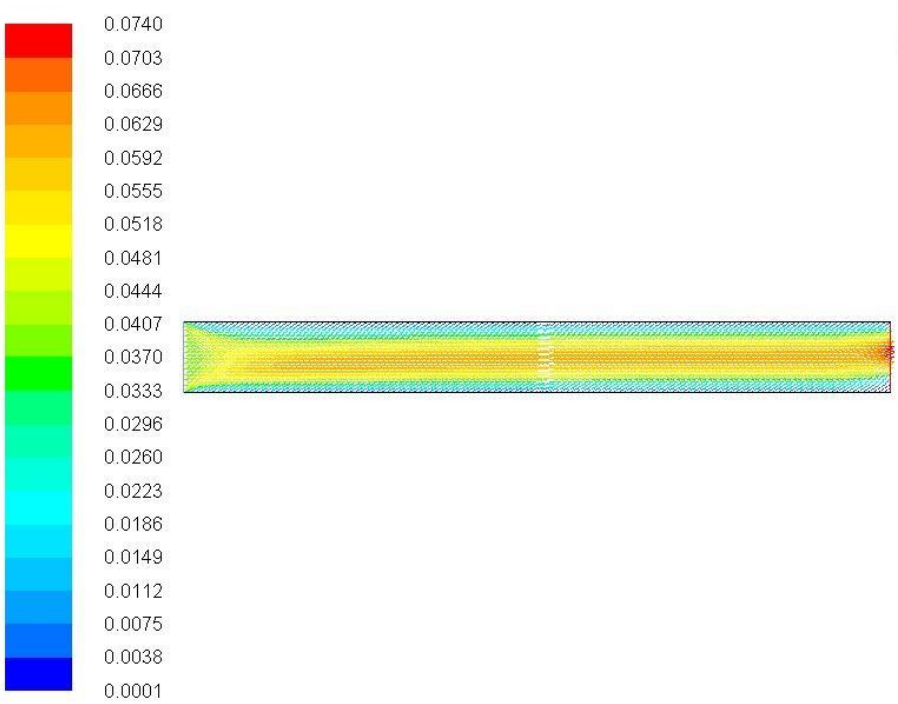


**Figure 35. Velocity Vector for Forced Convection in 10-1 Aspect Ratio Case Isotherms**

## Isotherm

The isotherm is a graphic that shows the temperature contour as lines that have a two and a half degree Kelvin temperature difference. This shows how the temperature changes within the enclosure. For natural convection the 1-1 case is shown in Figure 36, the 2-1 case is shown in Figure 37, the 4-1 case is shown in Figure 38, the 6-1 case is shown in Figure 39, the 8-1 case is shown in Figure 40, and the 10-1 case is shown in Figure 41. The natural convection cases show a similar pattern to the natural convection velocity vectors. The 1-1 case as shown in Figure 36 is repeated twice for the 2-1 case, four times for the 4-1 case, five times for the 6-1 case, nine times for the 8-1 case, and eleven times for the 10-1 case.

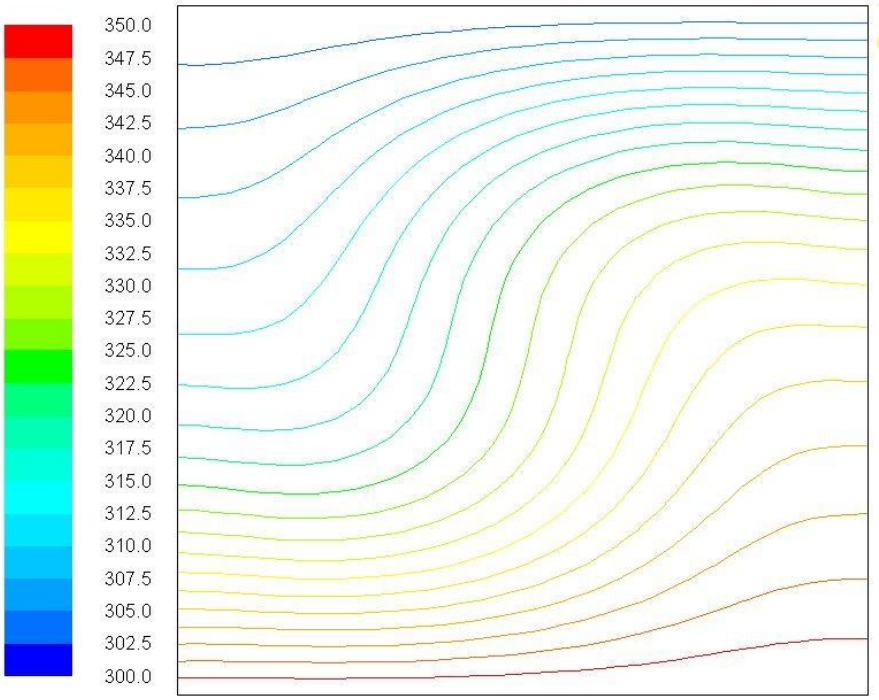


**Figure 36. Isotherm for Natural Convection in 1-1 Aspect Ratio Case**

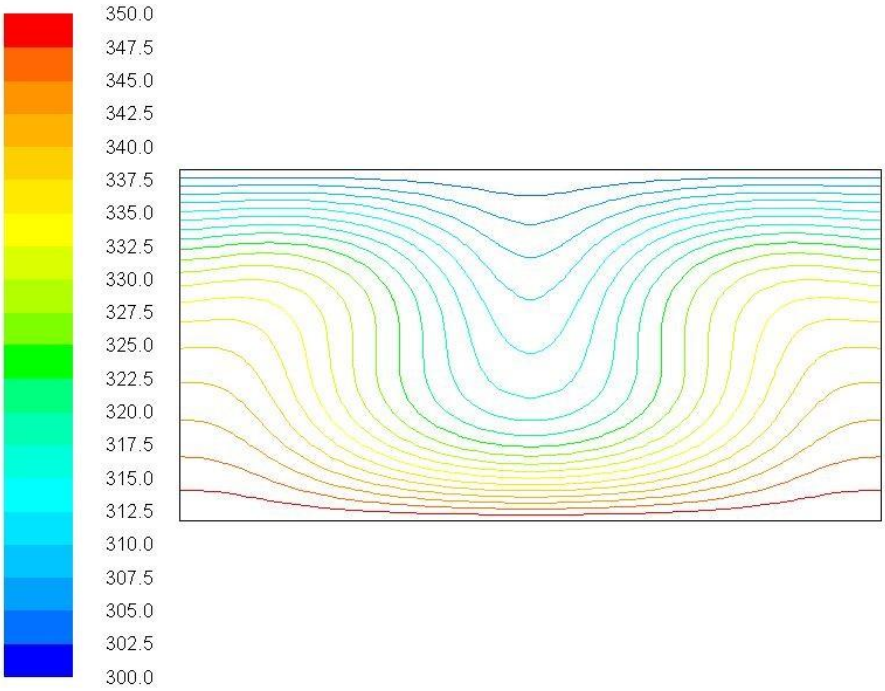


**Figure 37. Isotherm for Natural Convection in 2-1 Aspect Ratio Case**

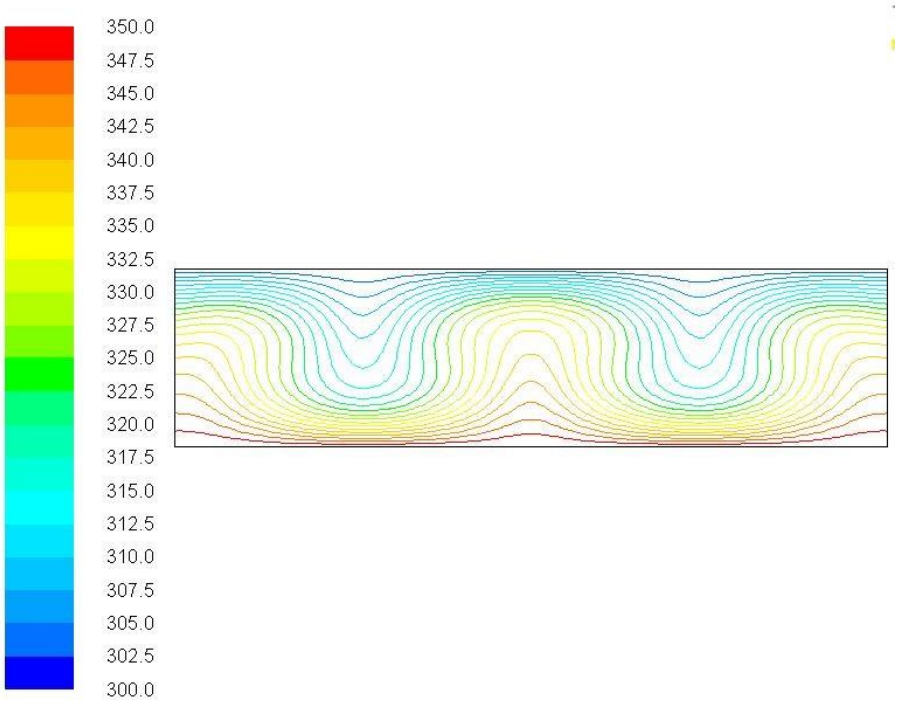


**Figure 38. Isotherm for Natural Convection in 4-1 Aspect Ratio Case**

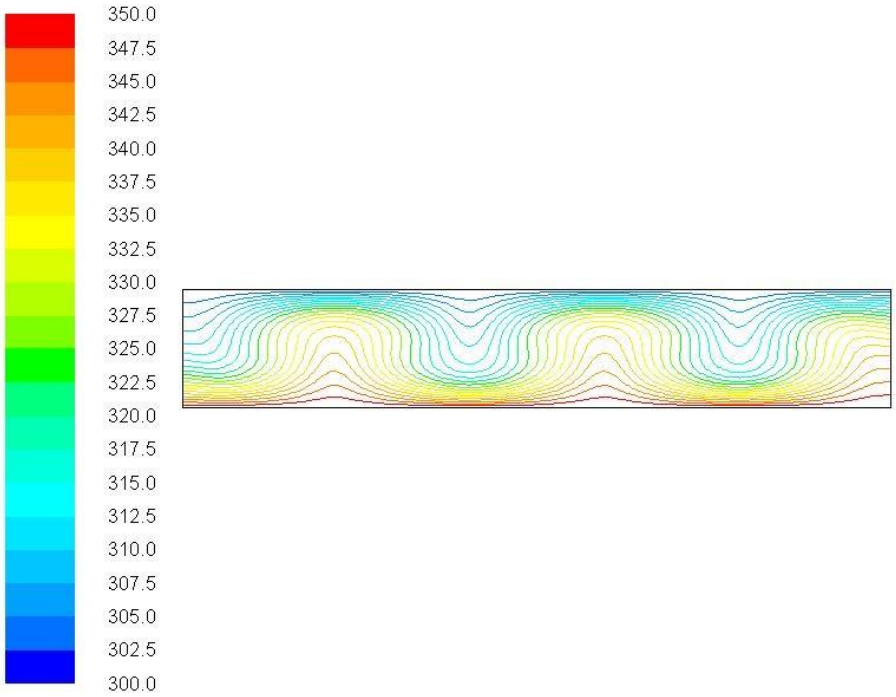


**Figure 39. Isotherm for Natural Convection in 6-1 Aspect Ratio Case**

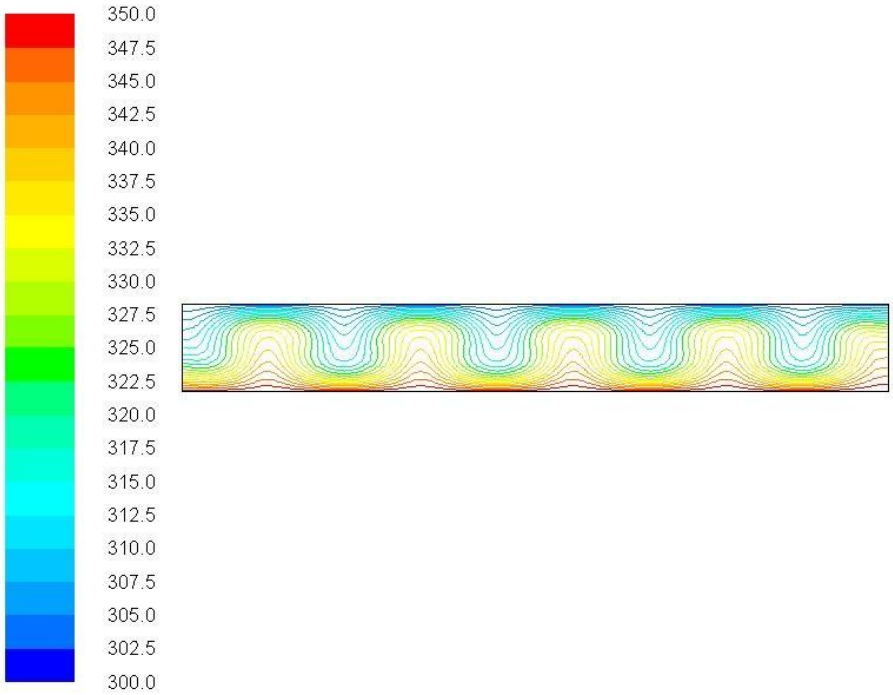


**Figure 40. Isotherm for Natural Convection in 8-1 Aspect Ratio Case**

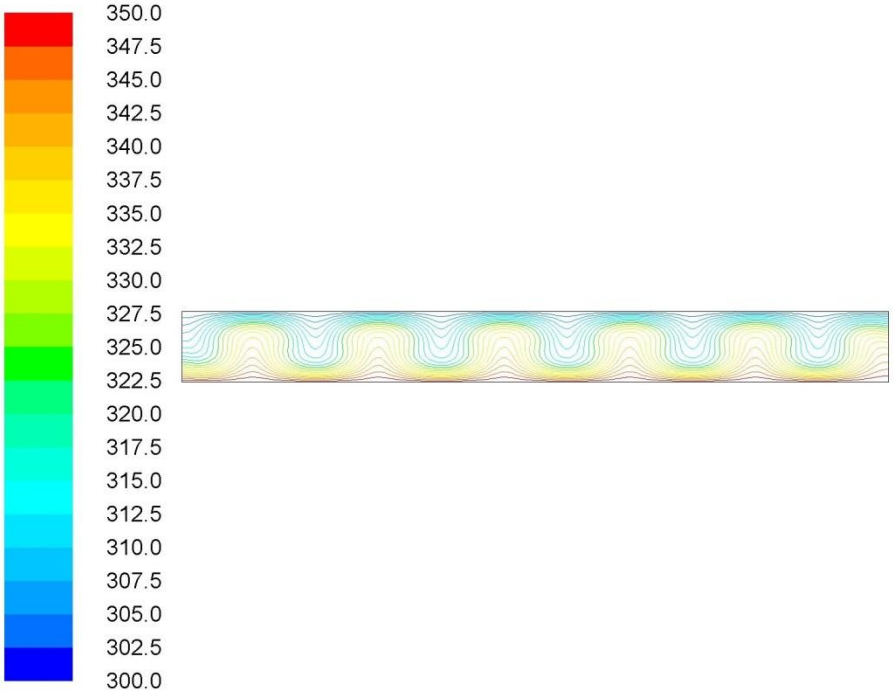


**Figure 41. Isotherm for Natural Convection in 10-1 Aspect Ratio Case**

For forced convection, the 1-1 case is shown in Figure 42, the 2-1 case is shown in Figure 43, the 4-1 case is shown in Figure 44, the 6-1 case is shown in Figure 45, the 8-1 case is shown in Figure 46, the 10-1 case is shown in Figure 47. The forced convection cases show that the temperature profile does not fully encompass the area until the 6-1 case. It also shows a trend towards rising higher as the aspect ratio increases.

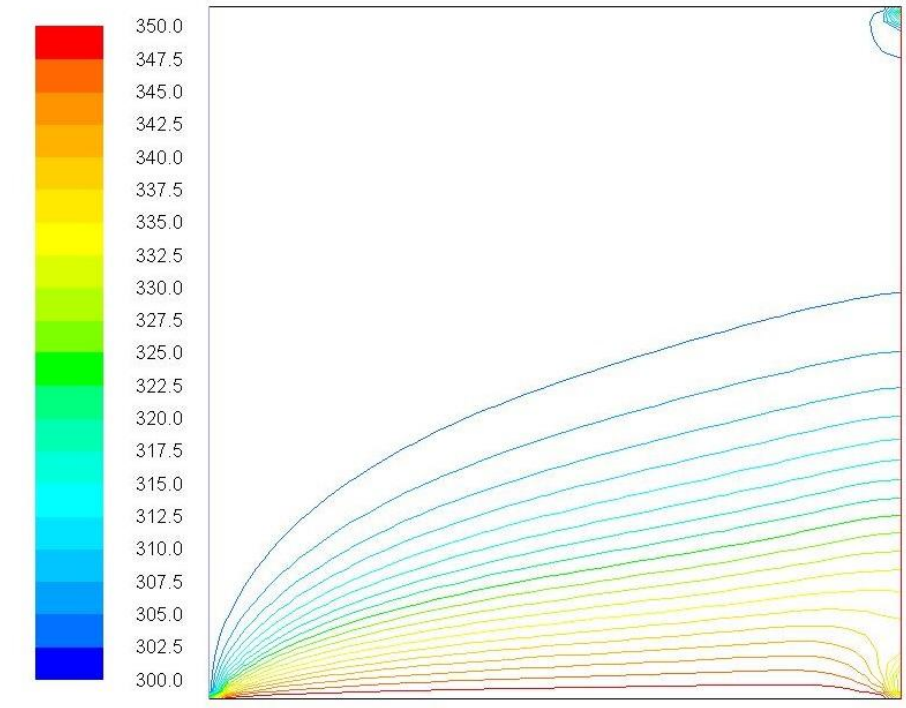


**Figure 42. Isotherm for Forced Convection in 1-1 Aspect Ratio Case**

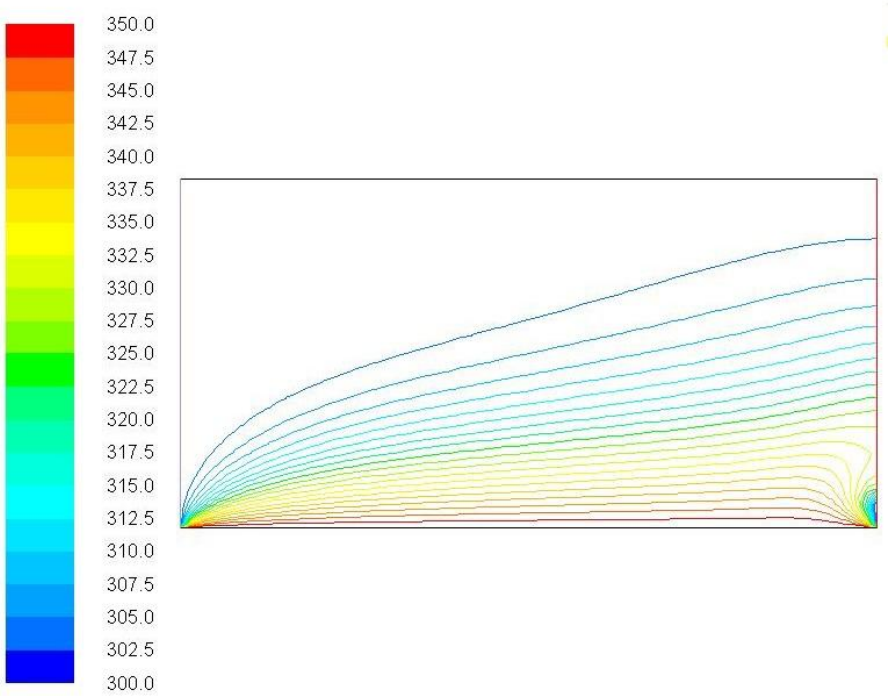


**Figure 43. Isotherm for Forced Convection in 2-1 Aspect Ratio Case**

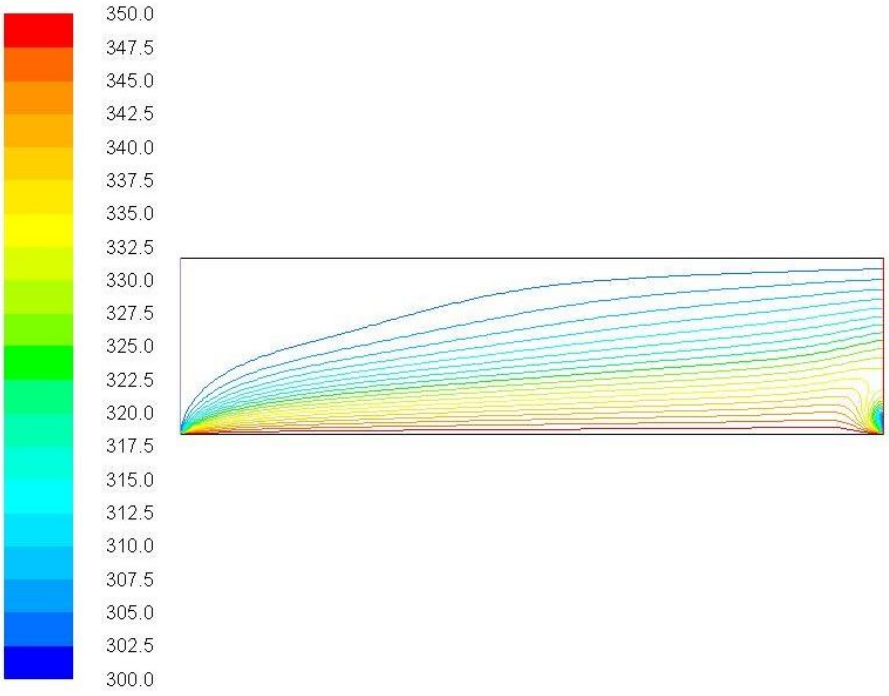


**Figure 44. Isotherm for Forced Convection in 4-1 Aspect Ratio Case**

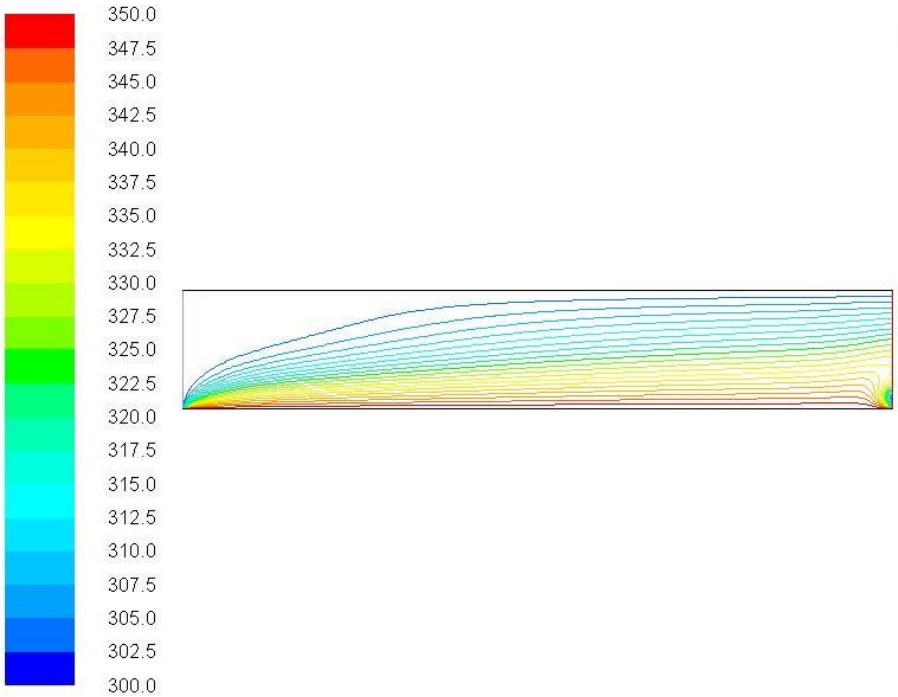


**Figure 45. Isotherm for Forced Convection in 6-1 Aspect Ratio Case**

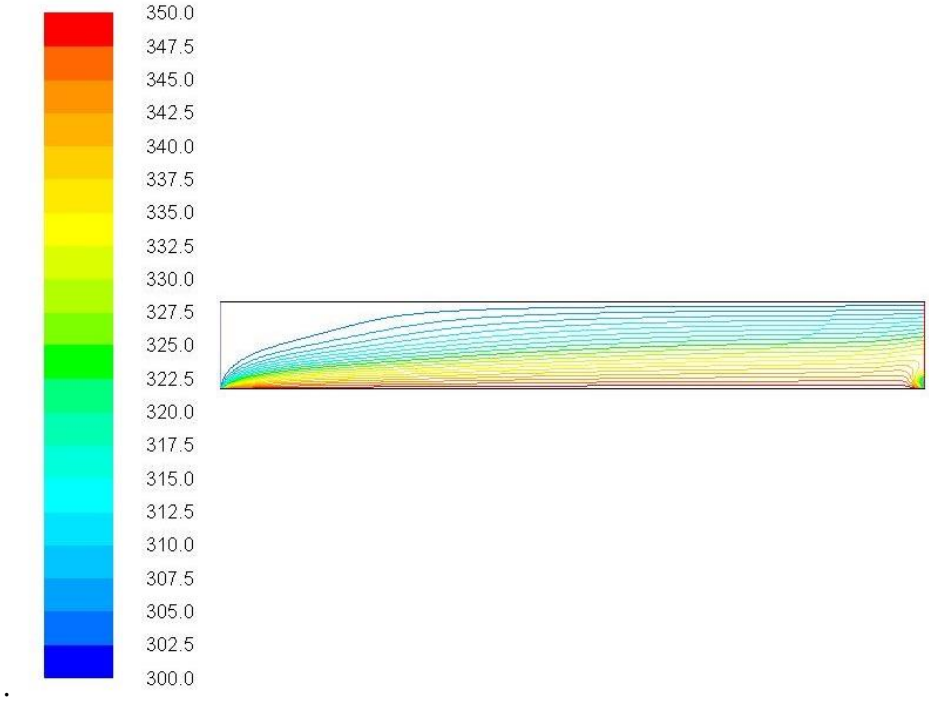


**Figure 46. Isotherm for Forced Convection in 8-1 Aspect Ratio Case**

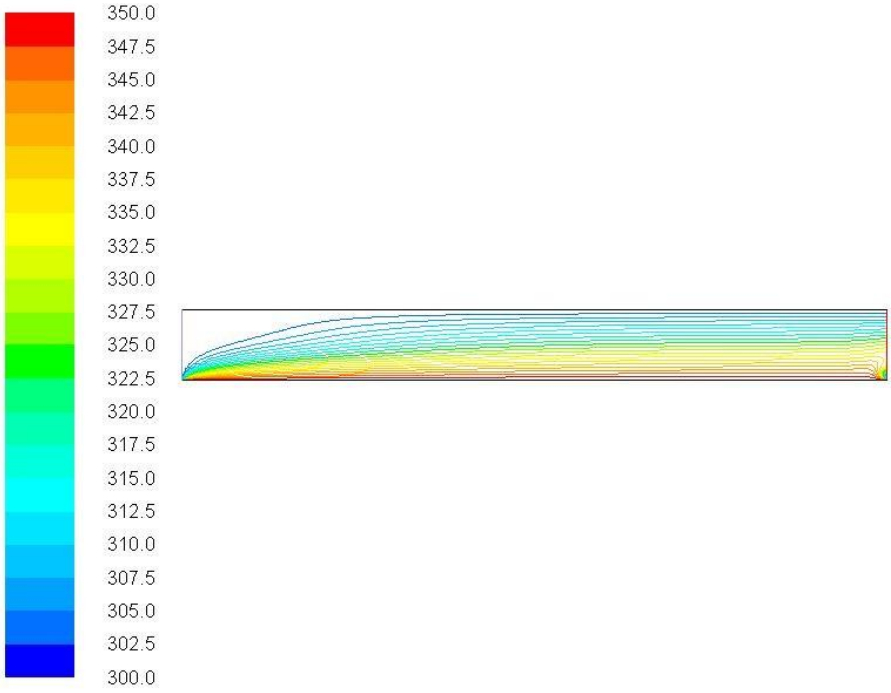


**Figure 47. Isotherm for Forced Convection in 10-1 Aspect Ratio Case**

## Surface Heat Flux

The surface heat flux is a measurement of the rate of heat transfer through a surface per unit area. This is a value that can determine if more heat can be transferred by changing the characteristics of the area of the enclosure or fluid in use. For natural convection, surface heat flux along the hot and cold walls for the 1-1 aspect ratio case is shown in Figure 48, the 2-1 aspect ratio case is shown in Figure 49, the 4-1 case is shown in Figure 50, the 6-1 case is shown in Figure 51, the 8-1 case is shown in Figure 52, and the 10-1case is shown in Figure 53 respectively. The natural convection cases show a trend of having the same pattern for both the cold wall and hot wall with similar numeric values. This is due to the conservation of energy. The pattern demonstrated by Figure 48 also repeats itself similarly to how the natural convection velocity vector can work. The heat flux from the hot wall is always positive indicating heat transfer from the wall into the fluid within the enclosure area while the cold wall heat flux is always negative indicating heat going into the wall from the fluid.

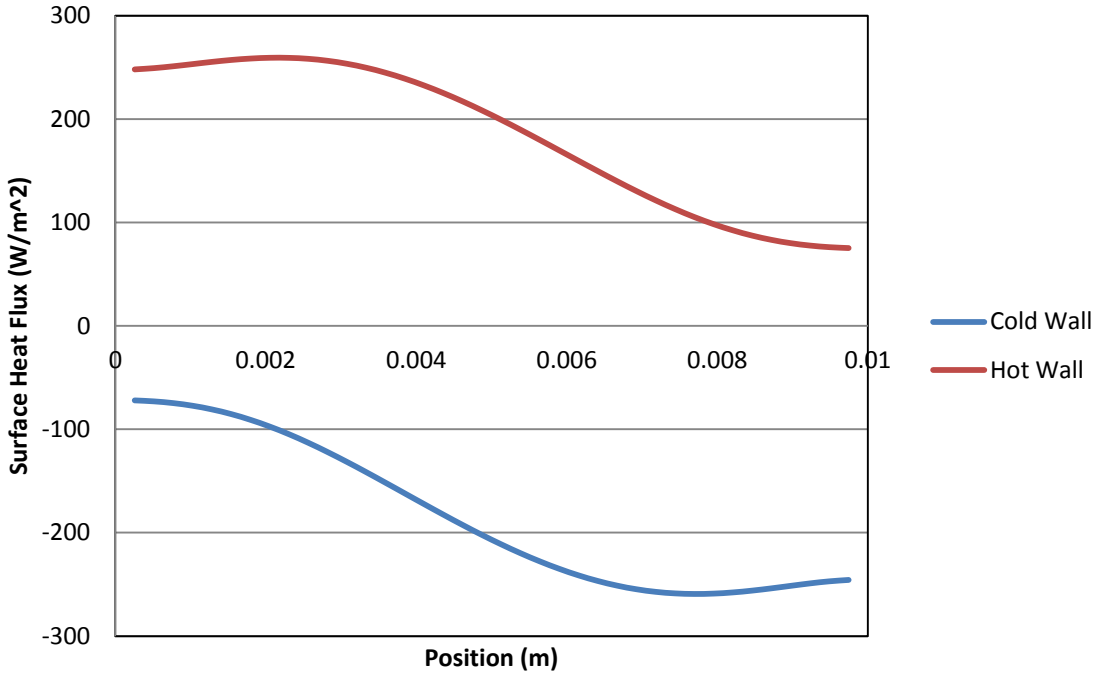


**Figure 48. Surface Heat Flux for Natural Convection along Hot and Cold Walls for 1-1 Aspect Ratio Case**

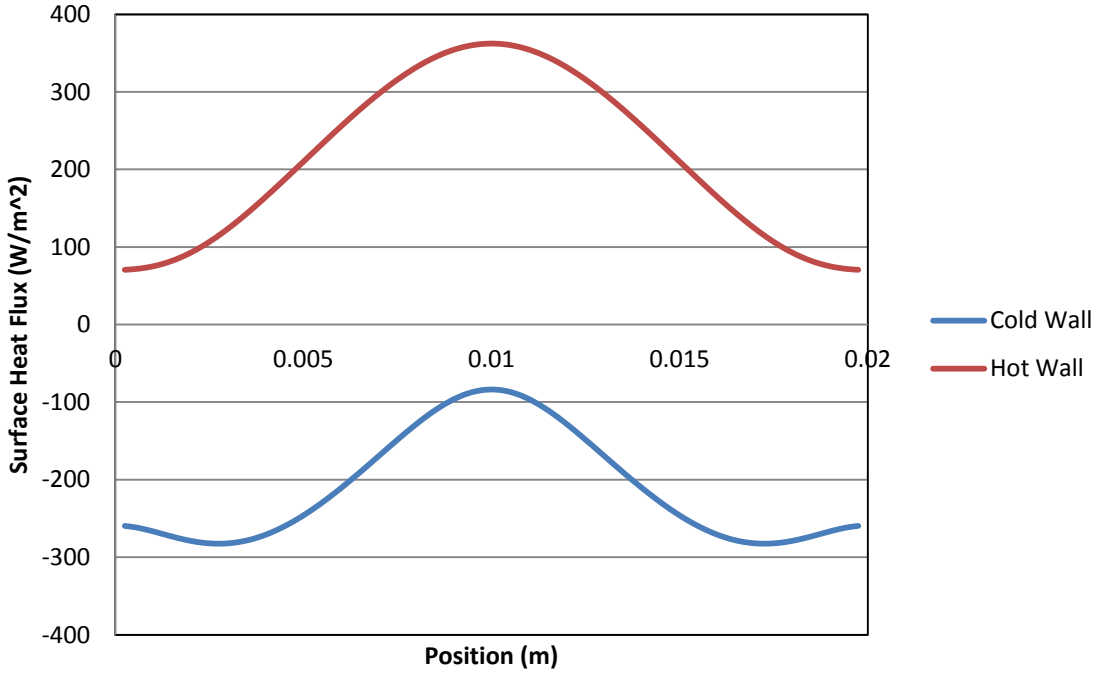


**Figure 49. Surface Heat Flux for Natural Convection along Hot and Cold Walls for 2-1 Aspect Ratio case**

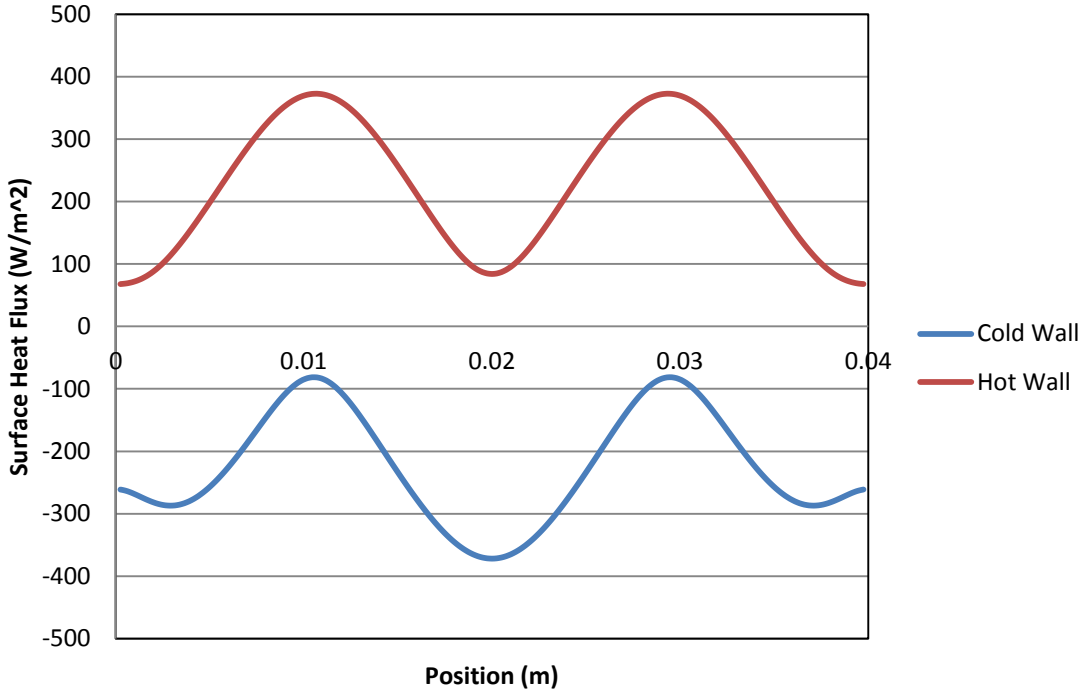


**Figure 50. Surface Heat Flux for Natural Convection along Hot and Cold Walls for 4-1 Aspect Ratio case**

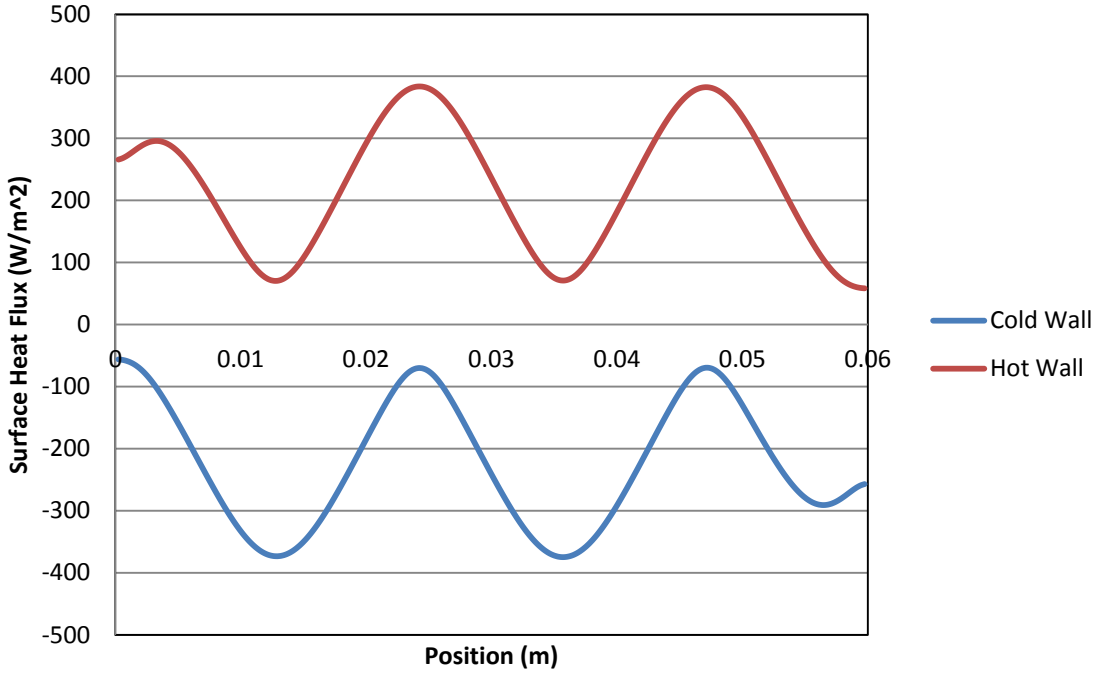


**Figure 51. Surface Heat Flux for Natural Convection along Hot and Cold Walls for 6-1 Aspect Ratio case**

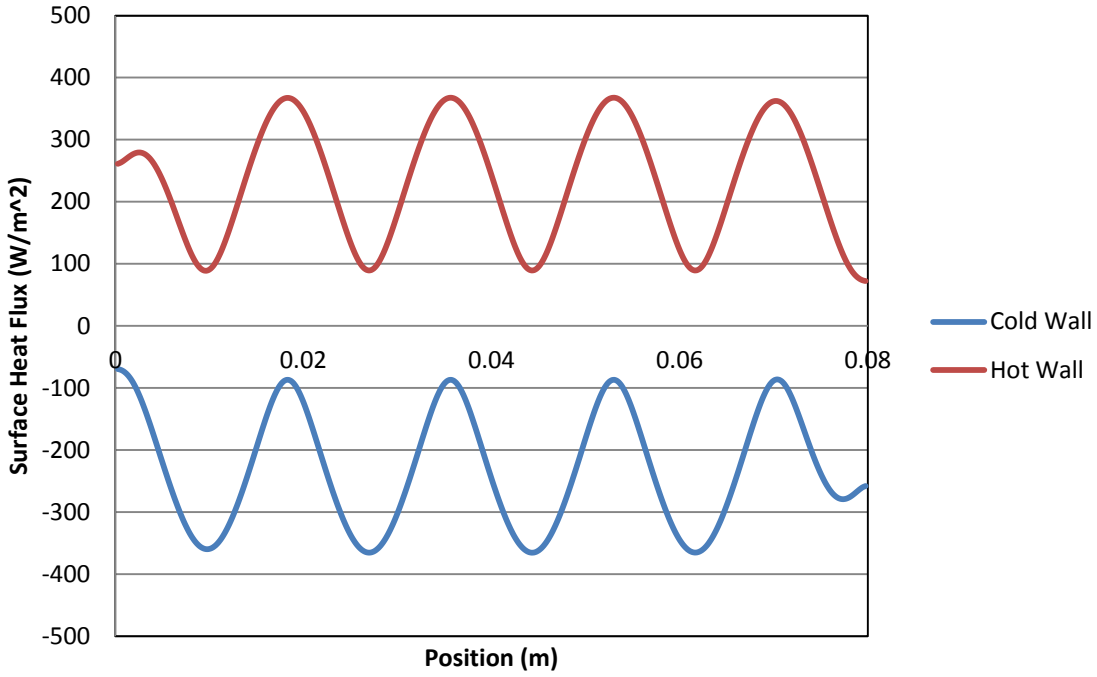


**Figure 52. Surface Heat Flux for Natural Convection along Hot and Cold Walls for 8-1 Aspect Ratio case**

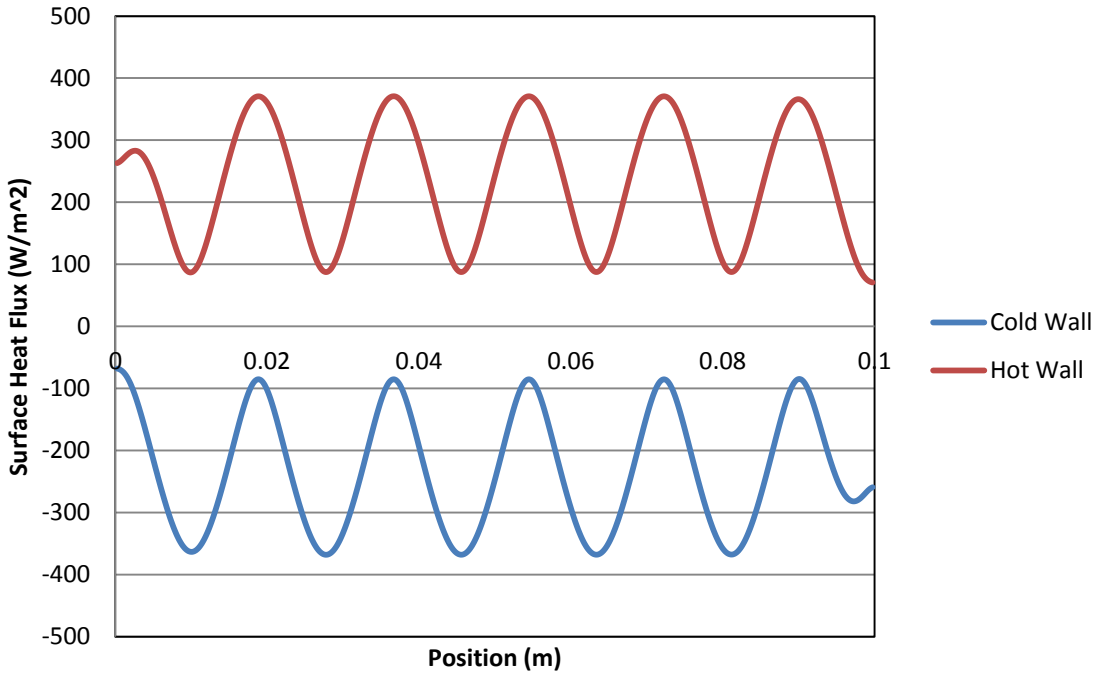


**Figure 53. Surface Heat Flux for Natural Convection along Hot and Cold Walls for 10-1 Aspect Ratio case**

For the forced convection, surface heat flux along the hot and cold walls for the 1-1 aspect ratio case is shown in Figure 54, the 2-1 case is shown in Figure 55, the 4-1 case is shown in Figure 56, the 6-1 case is shown in Figure 57, the 8-1 case is shown in Figure 58, and the 10-1case is shown in Figure 59 for the cold wall and Figure 60 for the hot wall. The forced convection surface heat flux shows trends of the cold wall having negative heat flux while the how wall has positive heat flux. There is also a characteristic of having the beginning and end of the curves to jump in heat flux dramatically. This is thought to be due to the developing air flow characteristics that exist at the beginning and end of the area.

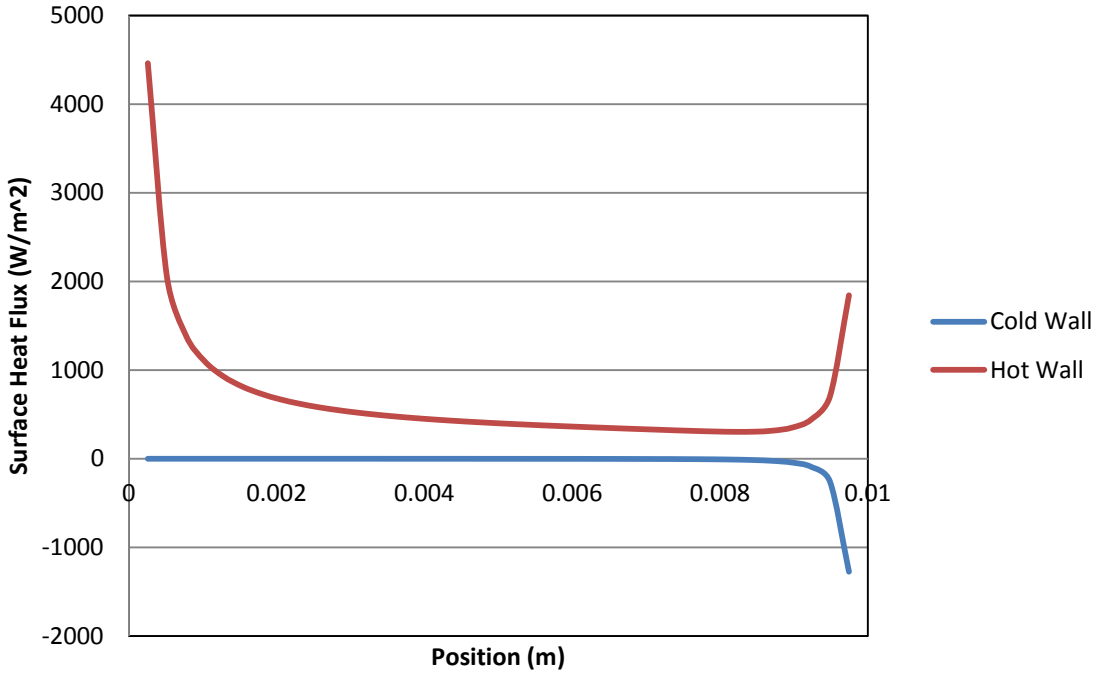


**Figure 54. Surface Heat Flux for Forced Convection along Hot and Cold Walls for 1-1 Aspect Ratio Case**

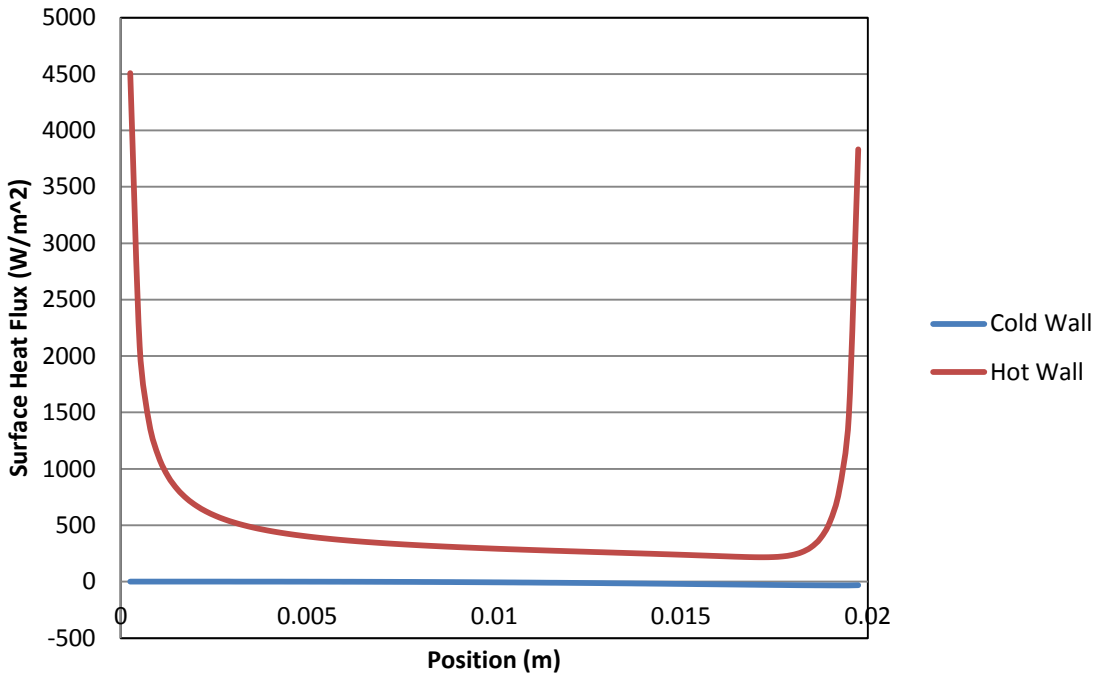


**Figure 55. Surface Heat Flux for Forced Convection along Hot and Cold Walls for 2-1 Aspect Ratio Case**

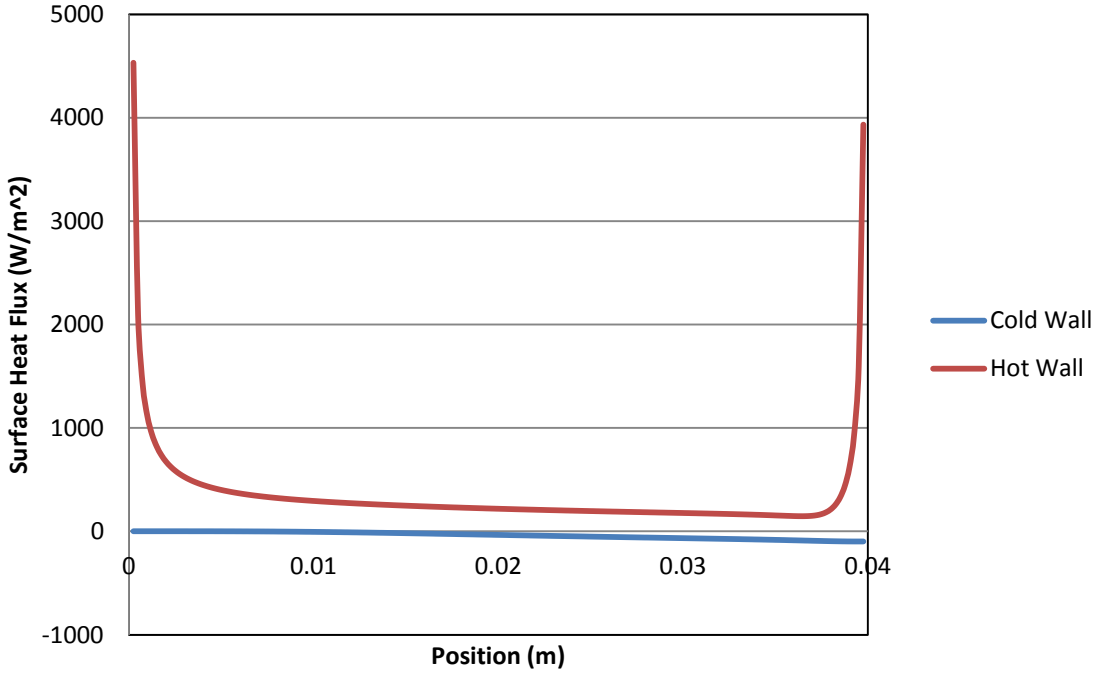


**Figure 56. Surface Heat Flux for Forced Convection along Hot and Cold Walls for 4-1 Aspect Ratio Case**

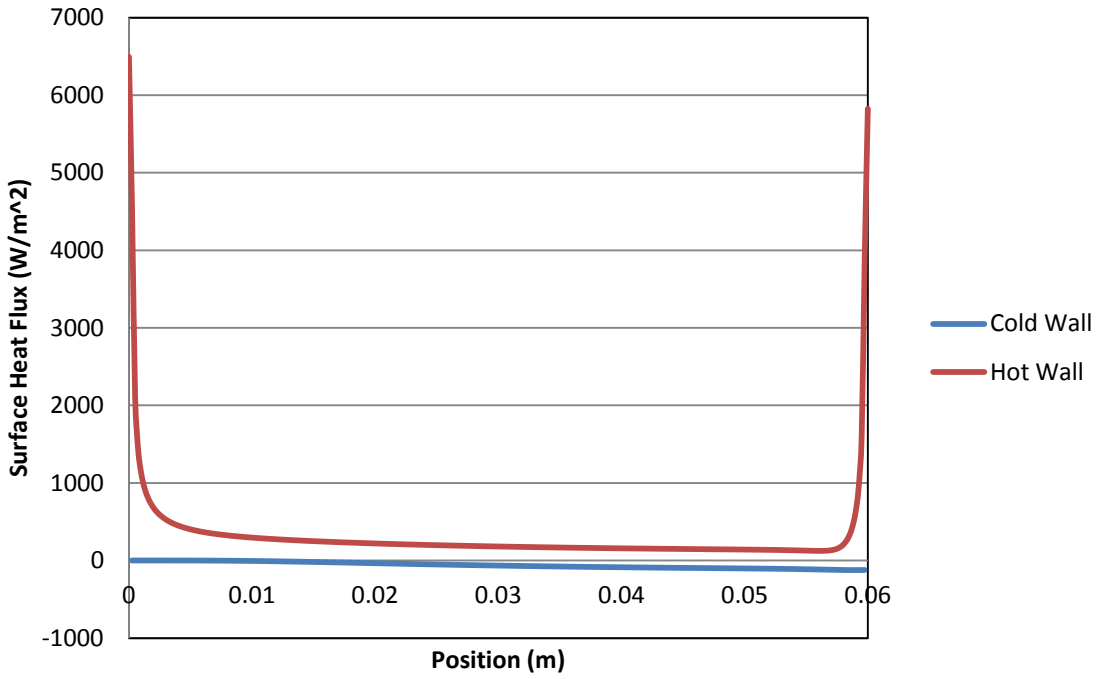


**Figure 57. Surface Heat Flux for Forced Convection along Hot and Cold Walls for 6-1 Aspect Ratio Case**

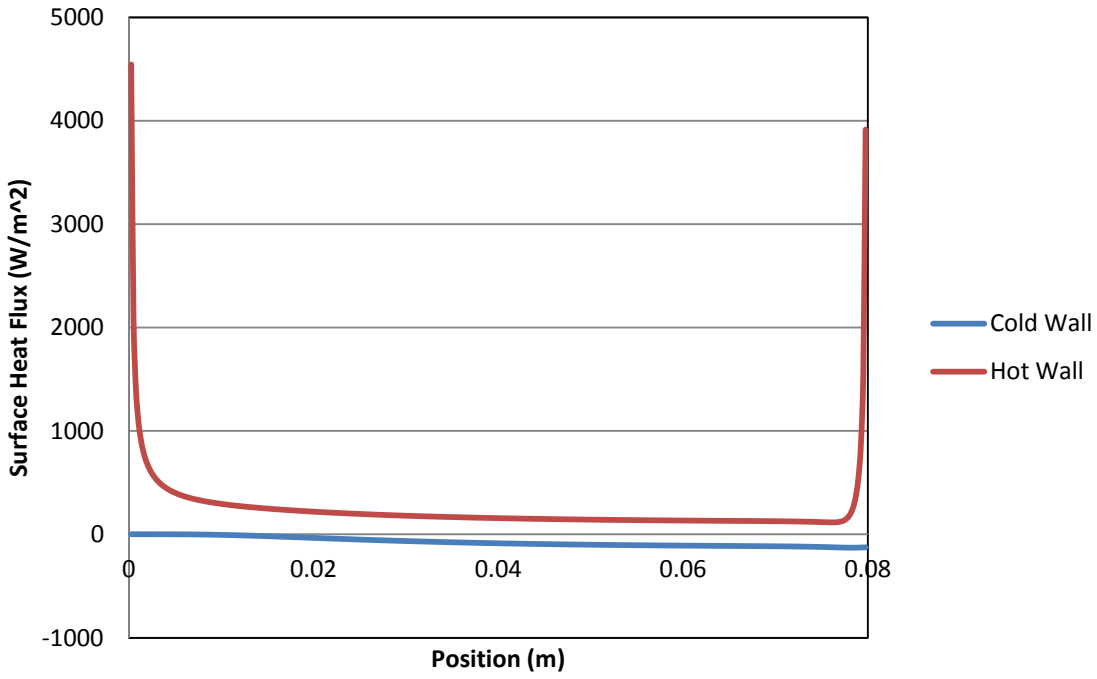


**Figure 58. Surface Heat Flux for Forced Convection along Hot and Cold Walls for 8-1 Aspect Ratio Case**

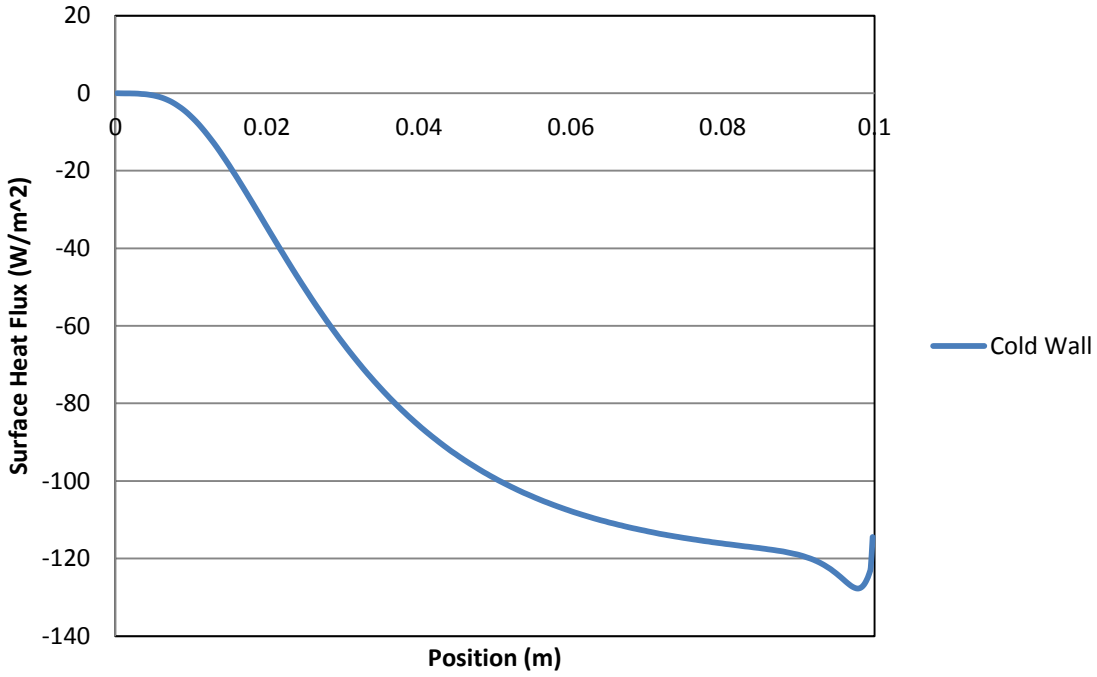


**Figure 59. Surface Heat Flux for Forced Convection along Cold Wall for 10-1 Aspect Ratio Case**

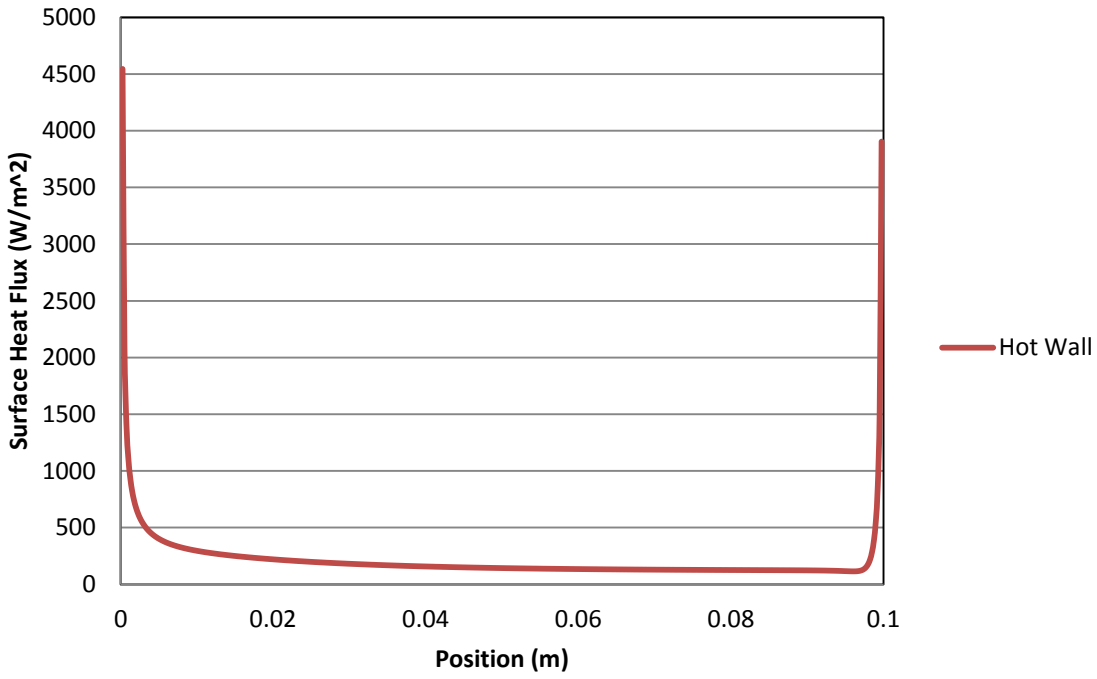


**Figure 60. Surface Heat Flux for Forced Convection along Hot Wall for 10-1 Aspect Ratio Case**

## Surface Nusselt Number

The nusselt number is a characteristic of the heat transfer whether the heat transfer is based on convection or conduction. With a nusselt number of 1 the conduction and convection are of similar magnitudes, while a large nusselt number corresponds to a more active convection. For the natural convection within the enclosure surface nusselt number along the hot and cold walls plot for the 1-1aspect ratio case is shown in Figure 61, the 2-1 aspect ratio case is shown in Figure 62, the 4-1 case is shown in Figure 63, the 6-1 case is shown in Figure 64, the 8-1 case is shown in Figure 65, and the 10-1 case is shown in Figure 66 respectively. For the forced convection of air within the enclosure surface nusselt number plot for the 1-1 aspect ratio case is shown in Figure 67, the 2-1 aspect ratio case is shown in Figure 68, the 4-1 case is shown in Figure 69, the 6-1 case is shown in Figure 70, the 8-1 case is shown in Figure 71, and the 10-1 case is shown in Figure 72 respectively.

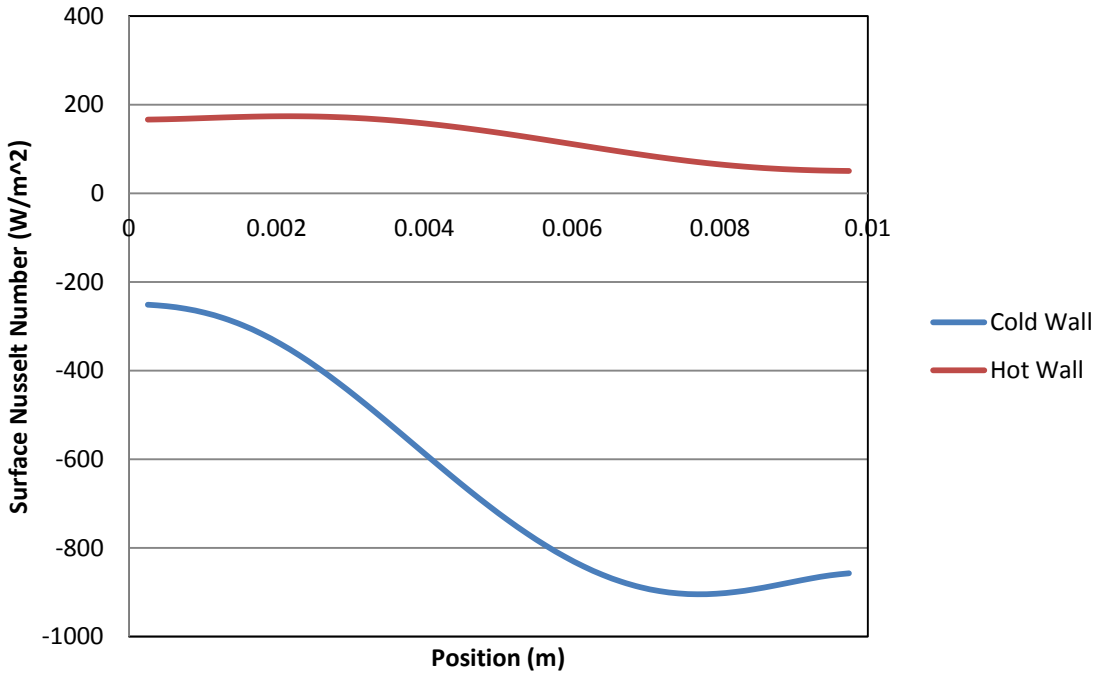


**Figure 61. Surface Nusselt Number for Natural Convection along Hot and Cold Walls for 1-1 Aspect Ratio Case**

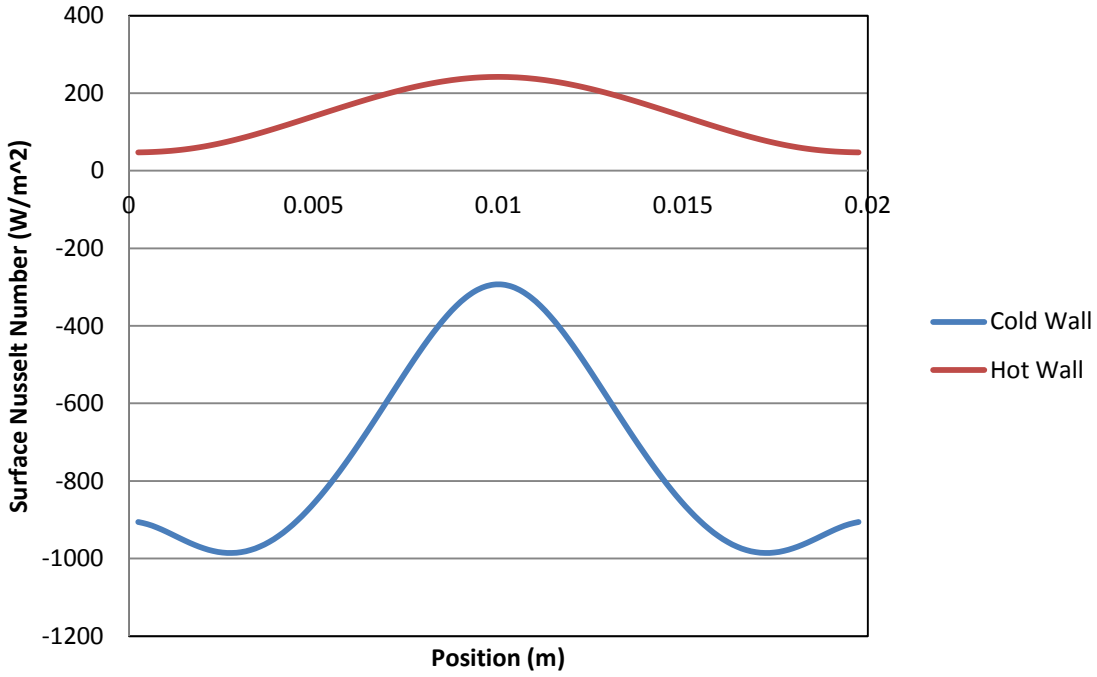


**Figure 62. Surface Nusselt Number for Natural Convection along Hot and Cold Walls for 2-1 Aspect Ratio Case**

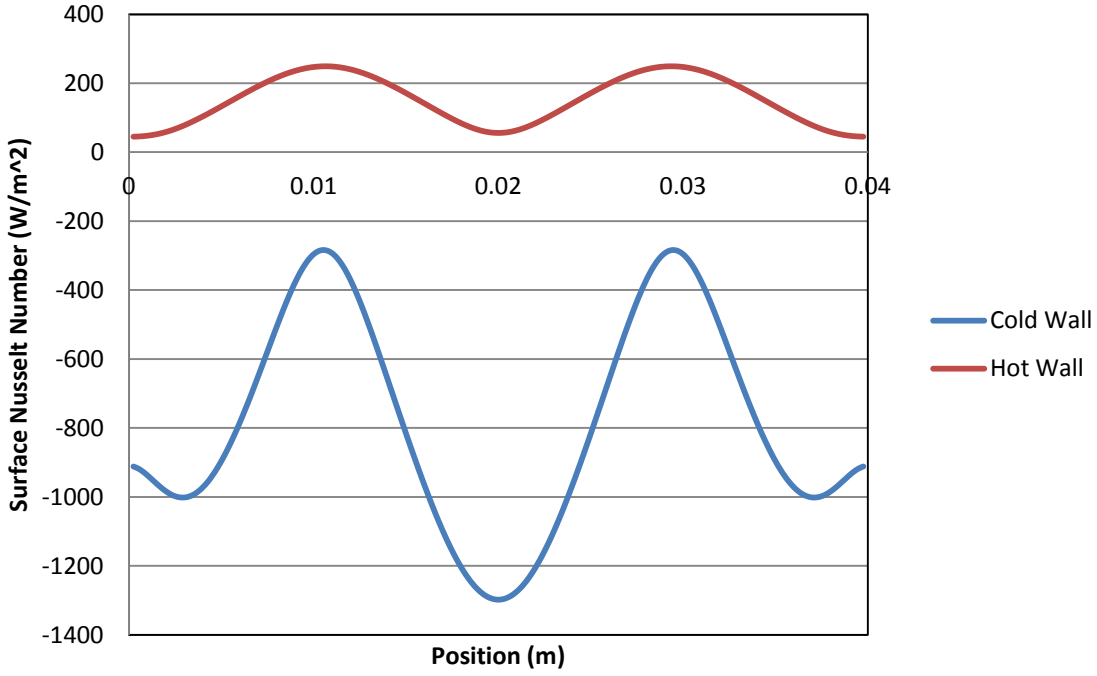


**Figure 63. Surface Nusselt Number for Natural Convection along Hot and Cold Walls for 4-1 Aspect Ratio Case**

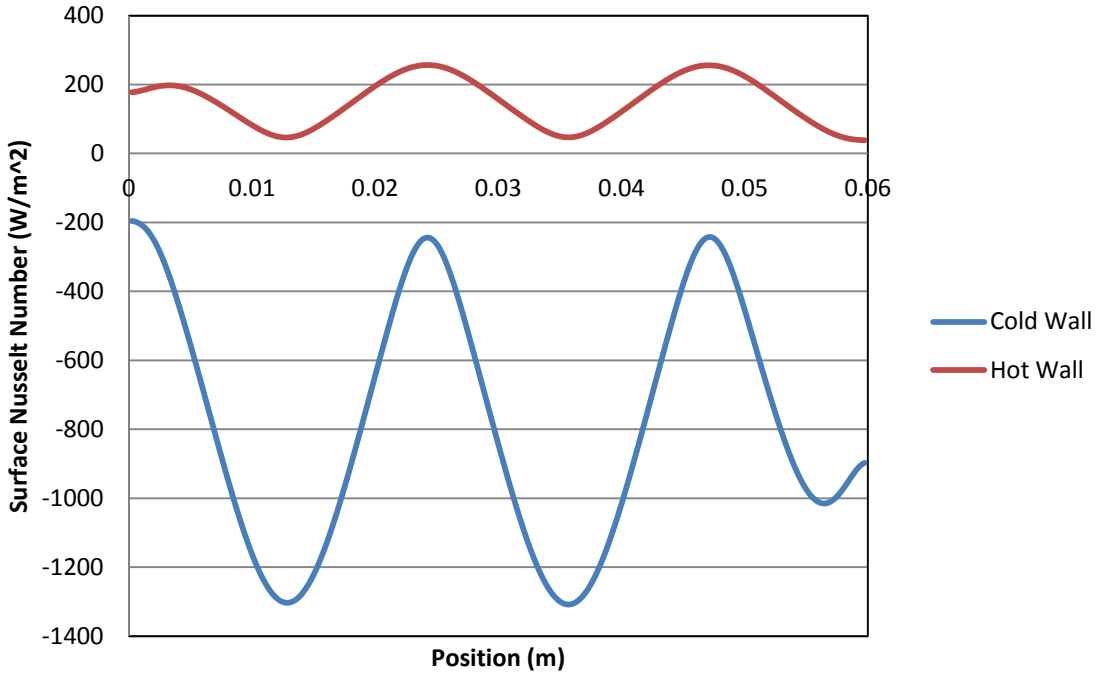


**Figure 64. Surface Nusselt Number for Natural Convection along Hot and Cold Walls for 6-1 Aspect Ratio Case**

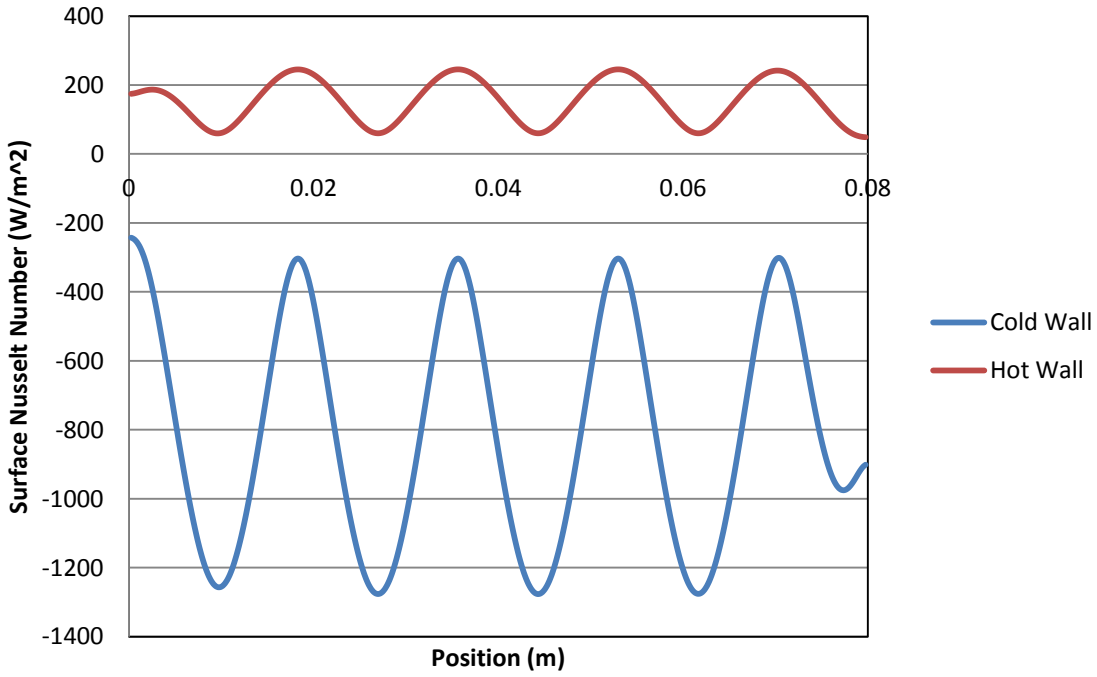


**Figure 65. Surface Nusselt Number for Natural Convection along Hot and Cold Walls for 8-1 Aspect Ratio Case**

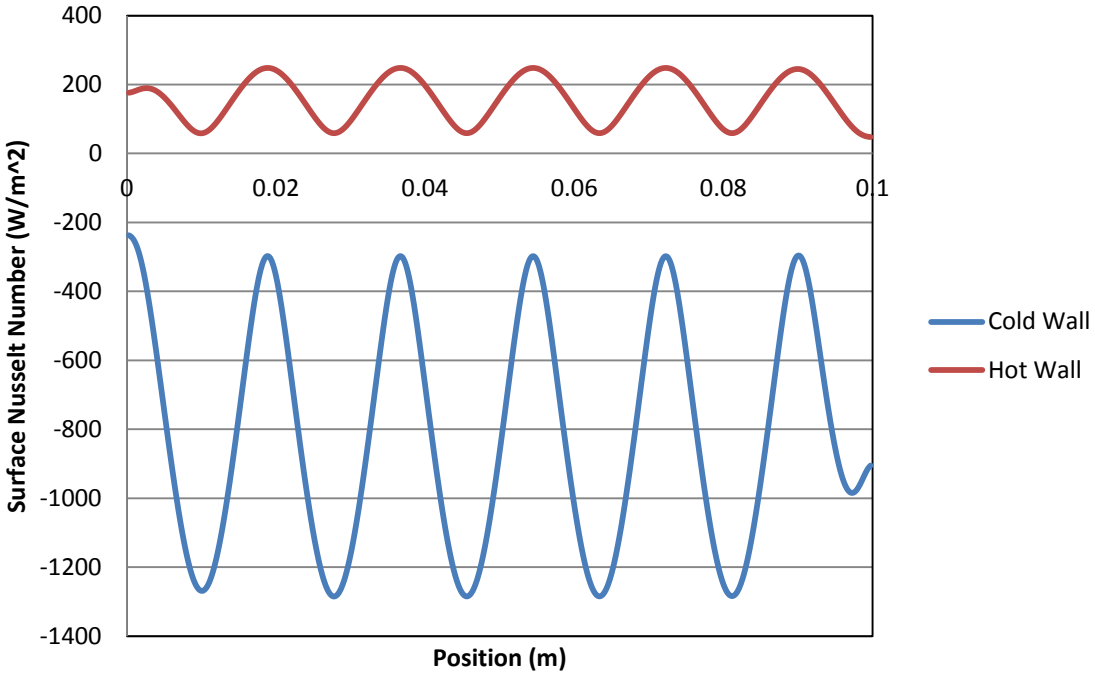


**Figure 66. Surface Nusselt Number for Natural Convection along Hot and Cold Walls for 10-1 Aspect Ratio Case**

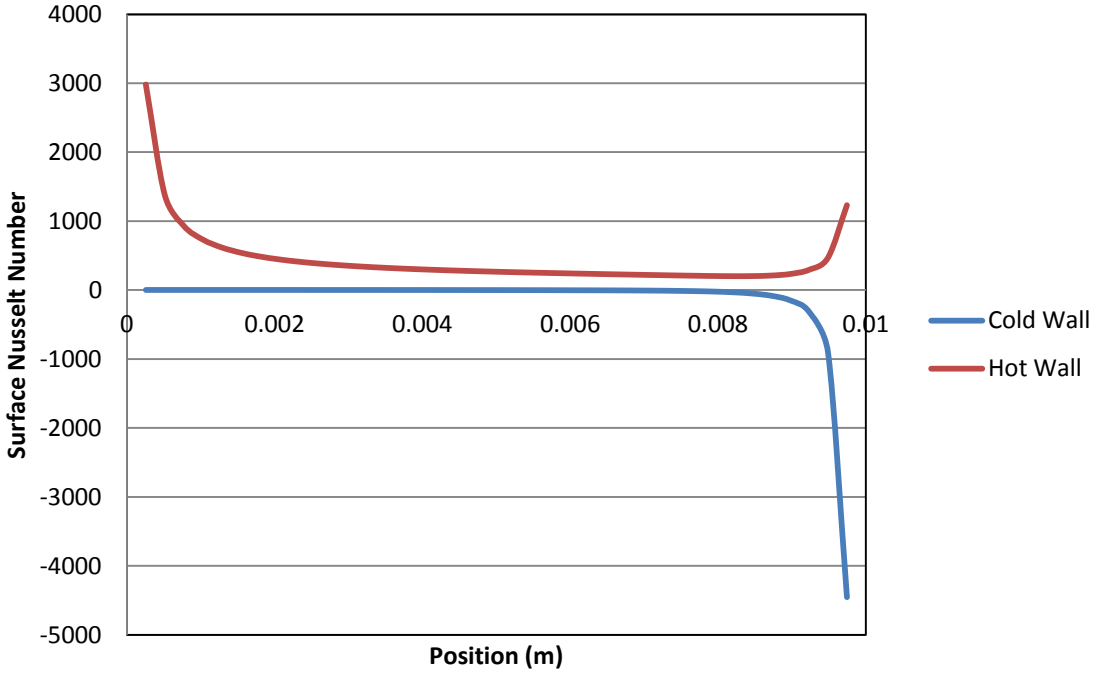


**Figure 67. Surface Nusselt Number for Forced Convection along Hot and Cold Walls for 1-1 Aspect Ratio Case**

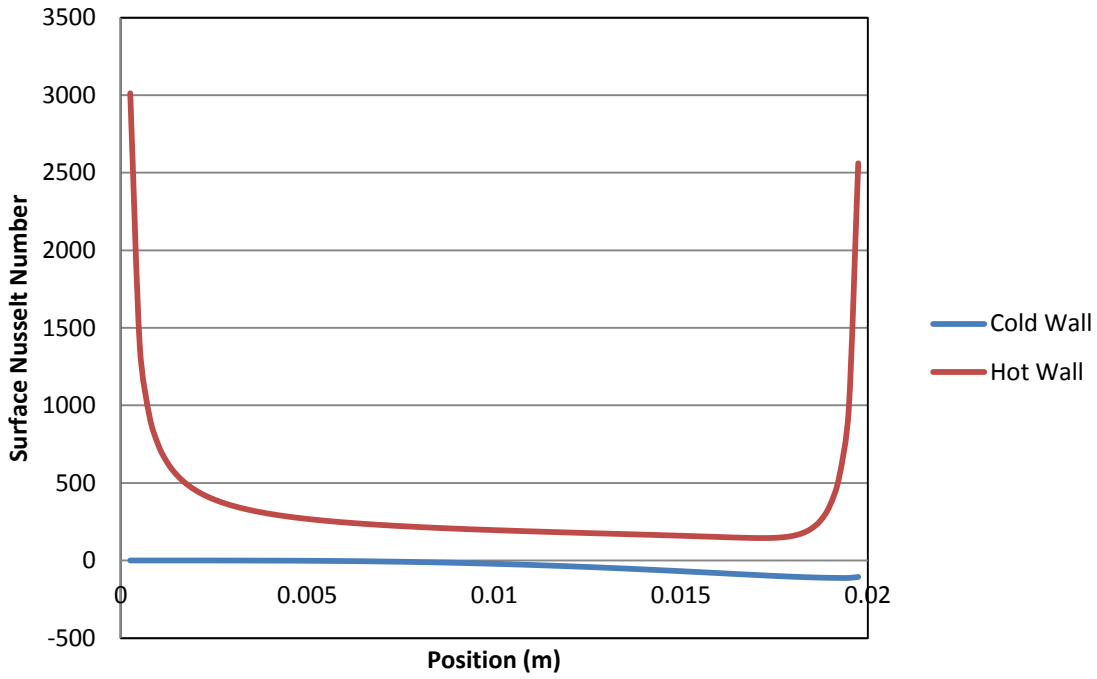


**Figure 68. Surface Nusselt Number for Forced Convection along Hot and Cold Walls for 2-1 Aspect Ratio Case**

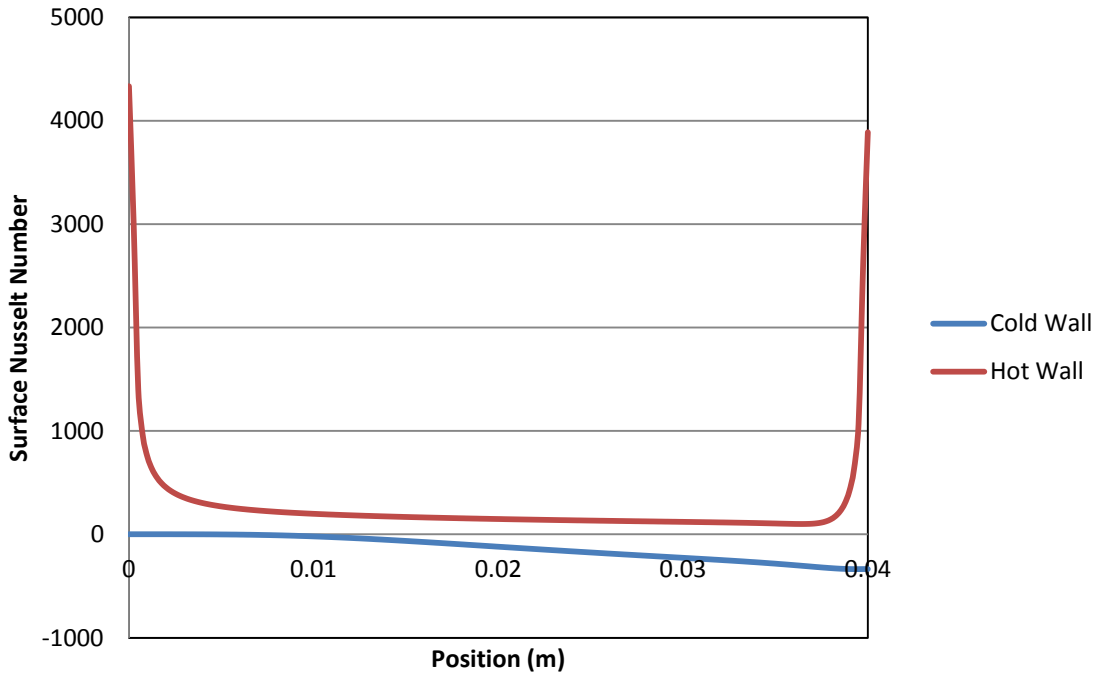


**Figure 69. Surface Nusselt Number for Forced Convection along Hot and Cold Walls for 4-1 Aspect Ratio Case**

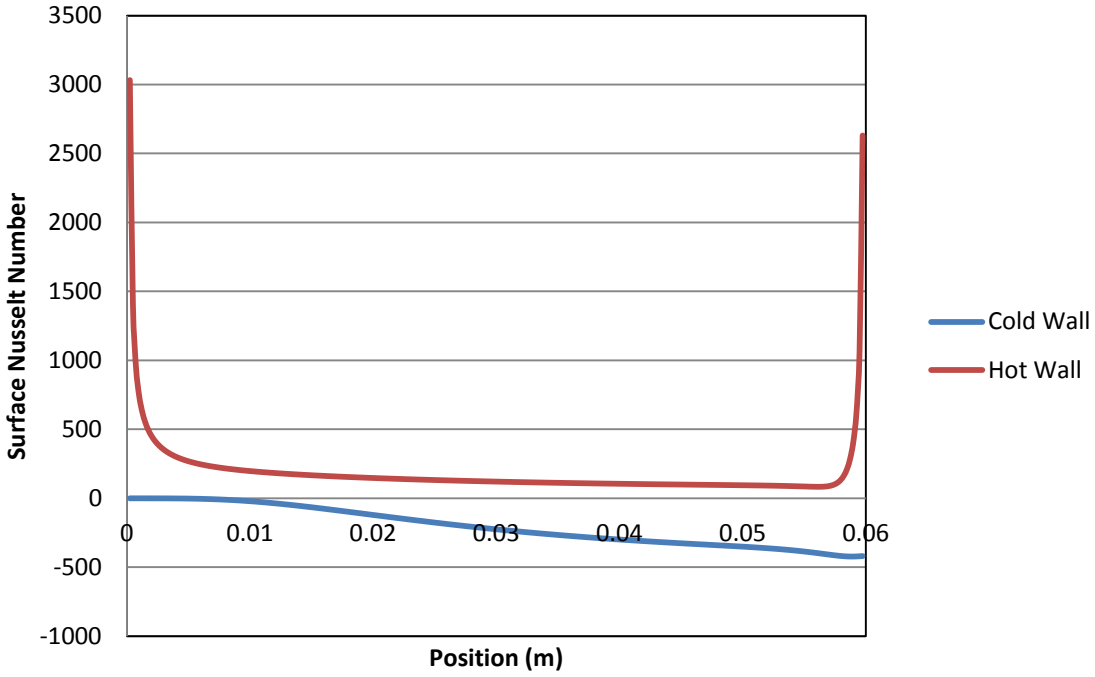


**Figure 70. Surface Nusselt Number for Forced Convection along Hot and Cold Walls for 6-1 Aspect Ratio Case**

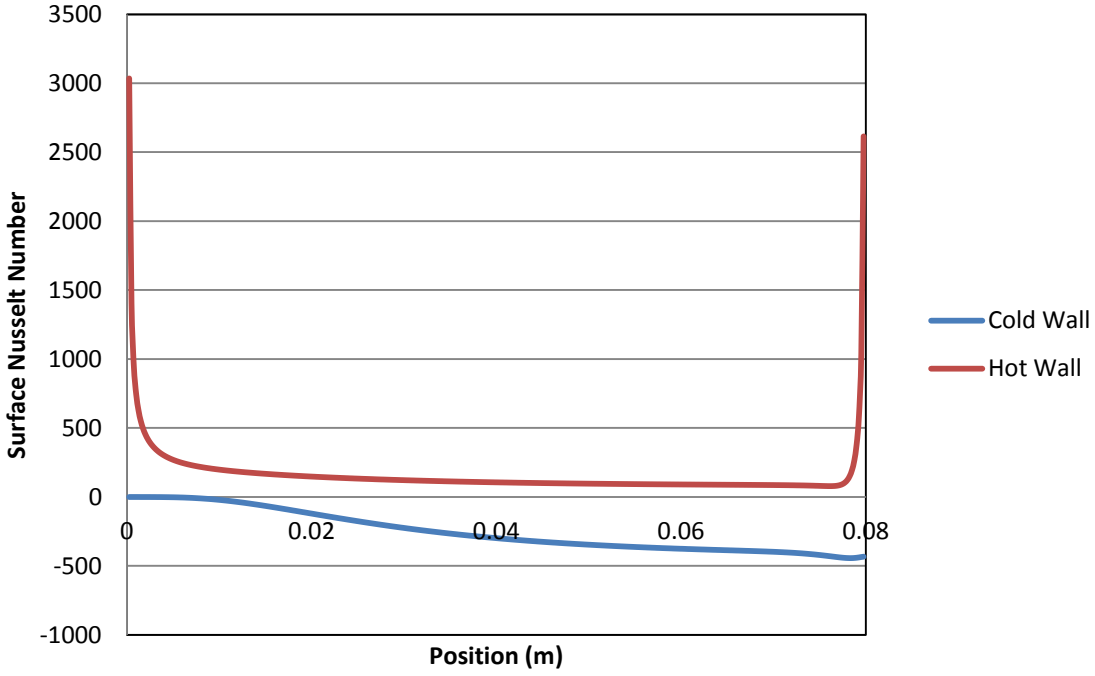


**Figure 71. Surface Nusselt Number for Forced Convection along Hot and Cold Walls for 8-1 Aspect Ratio Case**

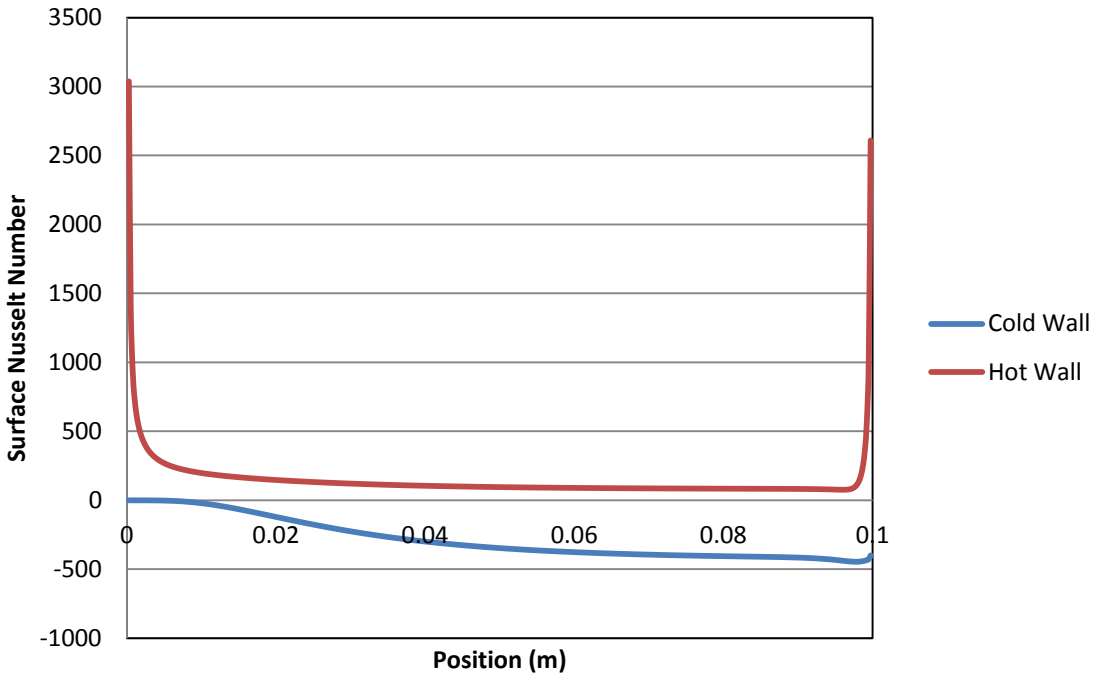


**Figure 72. Surface Nusselt Number for Forced Convection along Hot and Cold Walls for 10-1 Aspect Ratio Case**

## Natural Convection versus Forced Convection within the Enclosure

The average surface heat flux values for the natural convection of air and forced convection of air within the enclosure for 6 different aspect ratio cases were plotted together as shown in Figure 73. In the case of the natural convection heat flux, the average heat flux increases with the increase of aspect ratio. This demonstrates that within the specified aspect ratios there are increases in heat flux to the fluid of the enclosure area as a result of more circular flow regions. In the case of the forced convection heat flux, as the aspect ratio increases the average heat flux decreases. This leads to the conclusion that larger aspect ratio enclosures do not lead to an increase in heat flux for the forced convection cases.

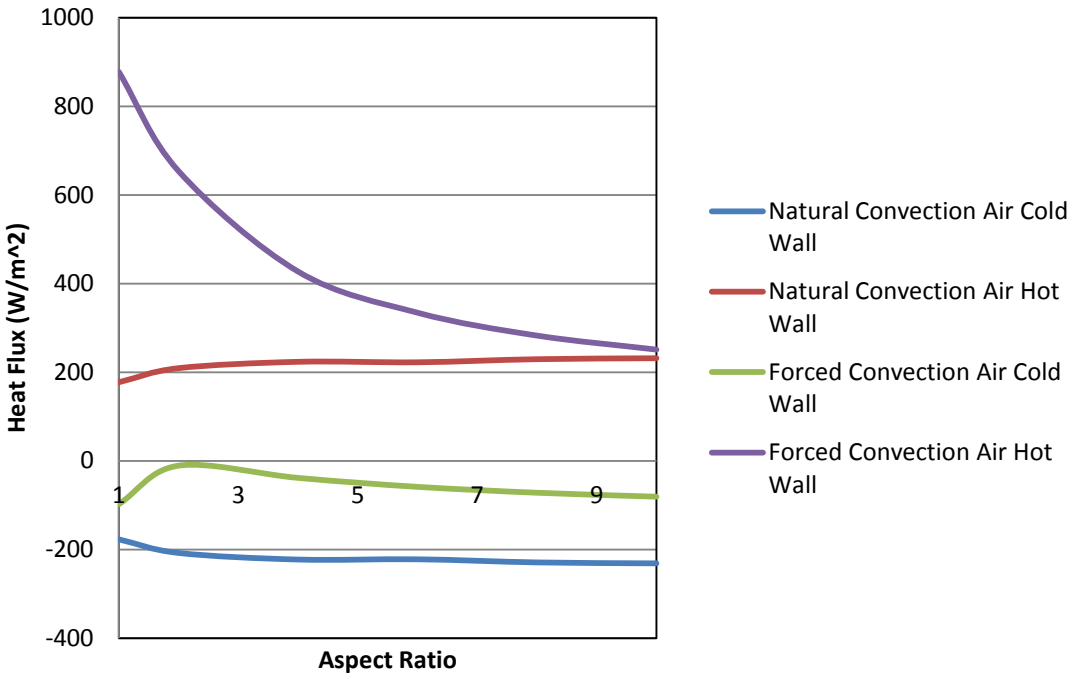


**Figure 73. Average Surface Heat Flux Compared to Aspect Ratio for Natural and Forced Convection of Air**

The average nusselt number values for the natural convection of air and forced convection of air within the enclosure of 6 different aspect ratio cases were plotted together as shown in Figure 74. The average nusselt number for the natural convection cases increase in magnitude with an increase in aspect ratio. The average nusselt number of the forced convection cases decreases with an increase in aspect ratio.

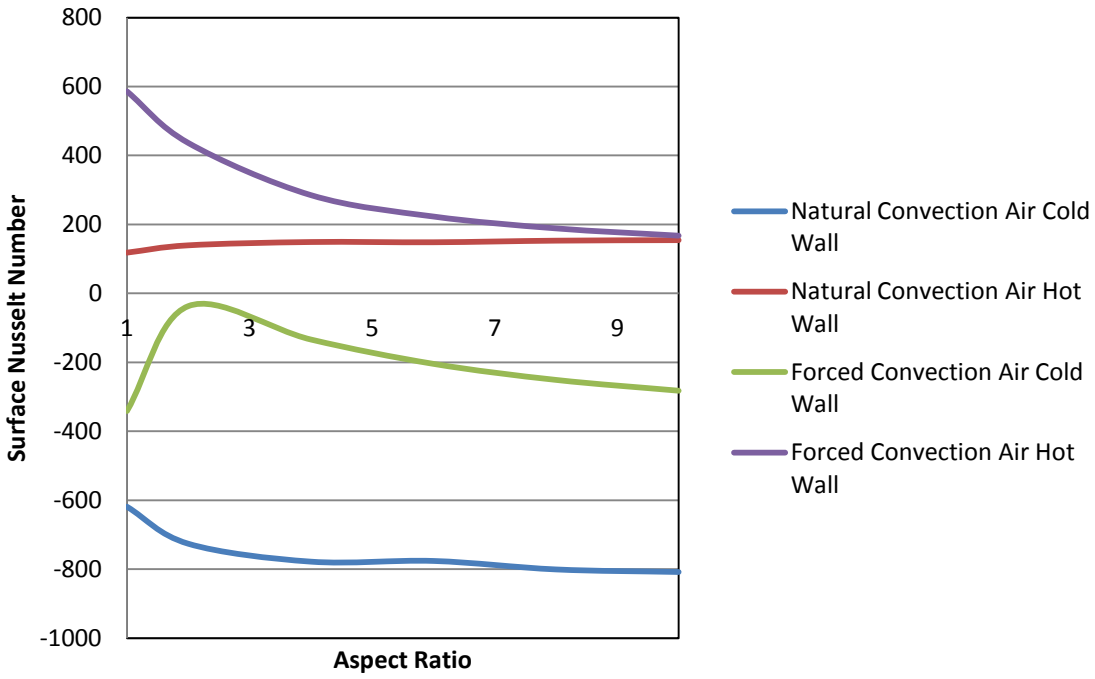


**Figure 74. Average Surface Nusselt Number Compared to Aspect Ratio for Natural and Forced Convection of Air**

## Nanofluid Particle Tracking

The particle tracking within the closed enclosure were performed and are shown in Figure 75 for the 1-1 aspect ratio case, in Figure 76 for the 2-1 aspect ratio case, in Figure 77 for the 4-1 aspect ratio case, in Figure 78 for the 6-1 aspect ratio case, in Figure 79 for the 8-1 aspect ratio case, and in Figure 80 for the 10-1 aspect ratio case. These all show that the particles can have their flow paths modeled and they show a tendency to stay on the border of the enclosure.

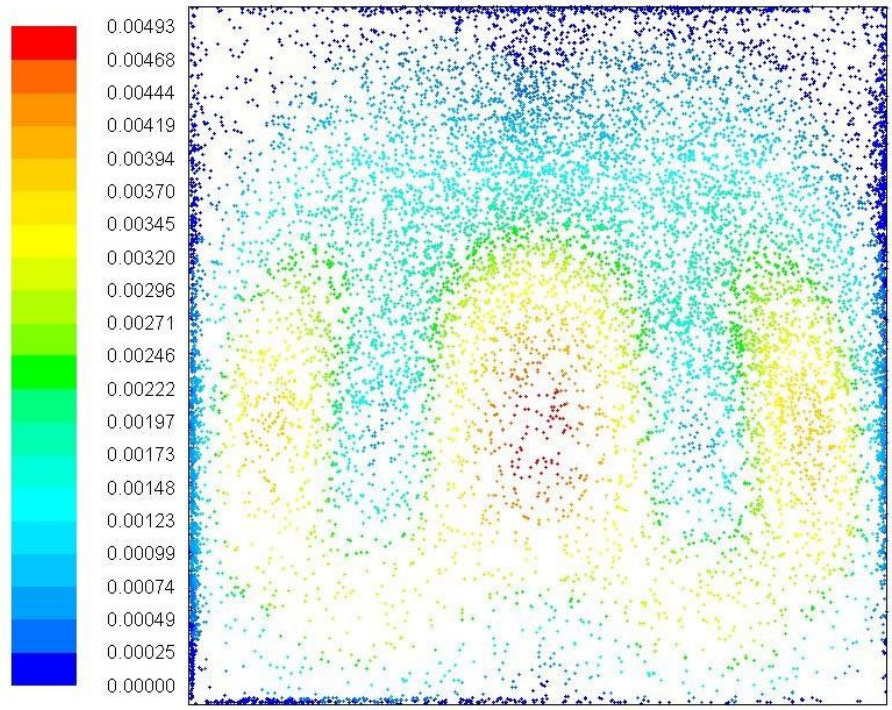


**Figure 75. Nanoparticle Tracking Within a 1-1 Aspect Ratio Enclosure**

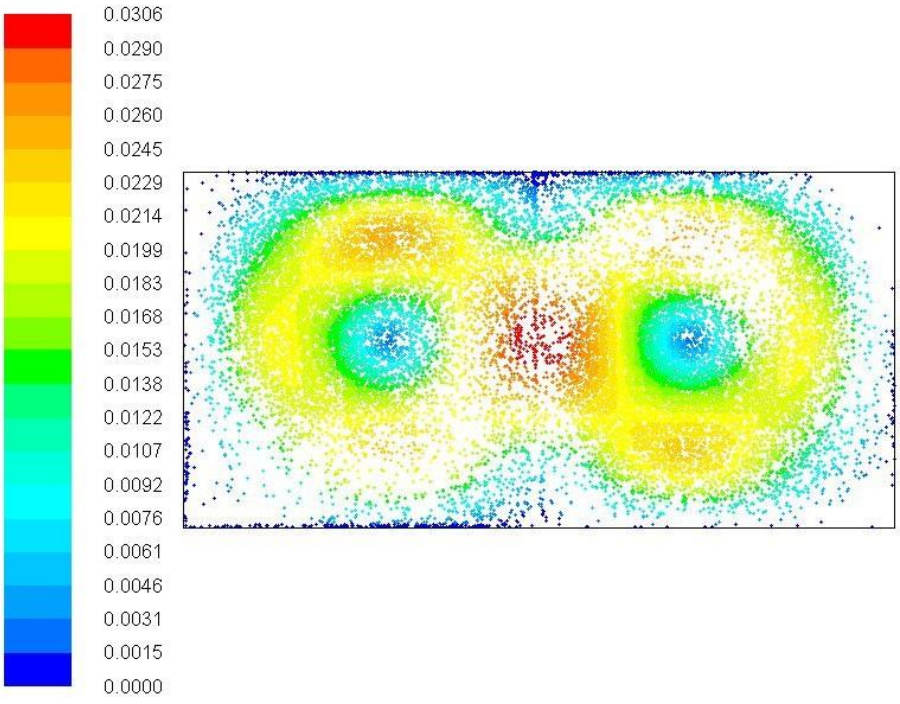


**Figure 76. Nanoparticle Tracking Within a 2-1 Aspect Ratio Enclosure**

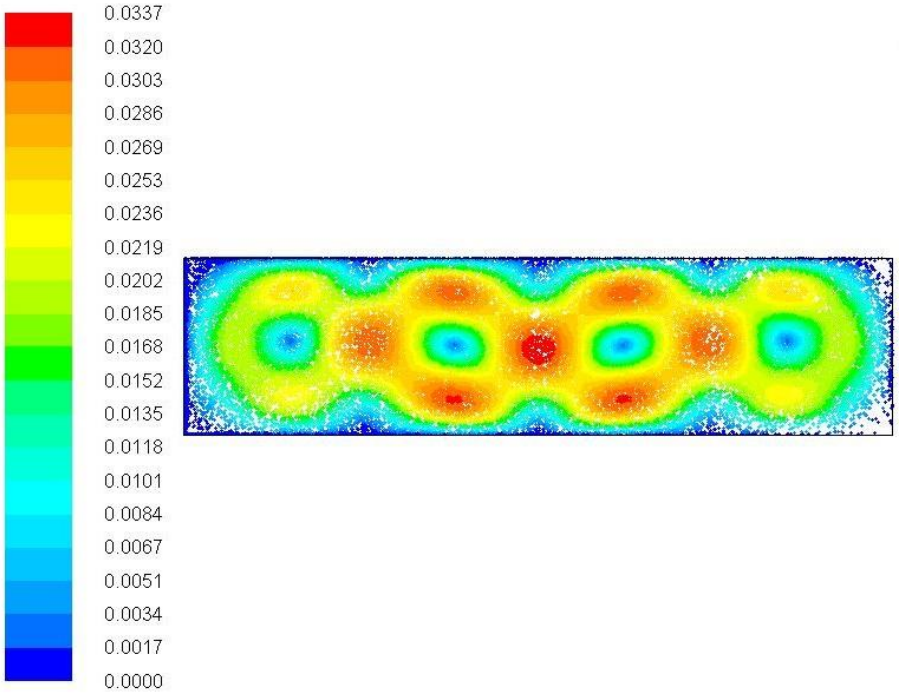


**Figure 77. Nanoparticle Tracking Within a 4-1 Aspect Ratio Enclosure**

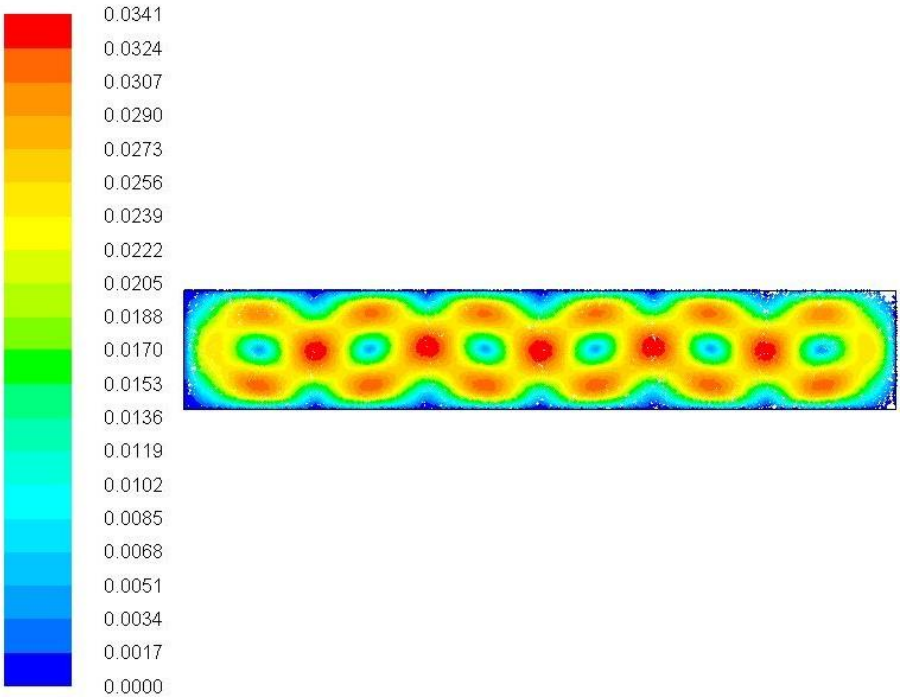


**Figure 78. Nanoparticle Tracking Within a 6-1 Aspect Ratio Enclosure**

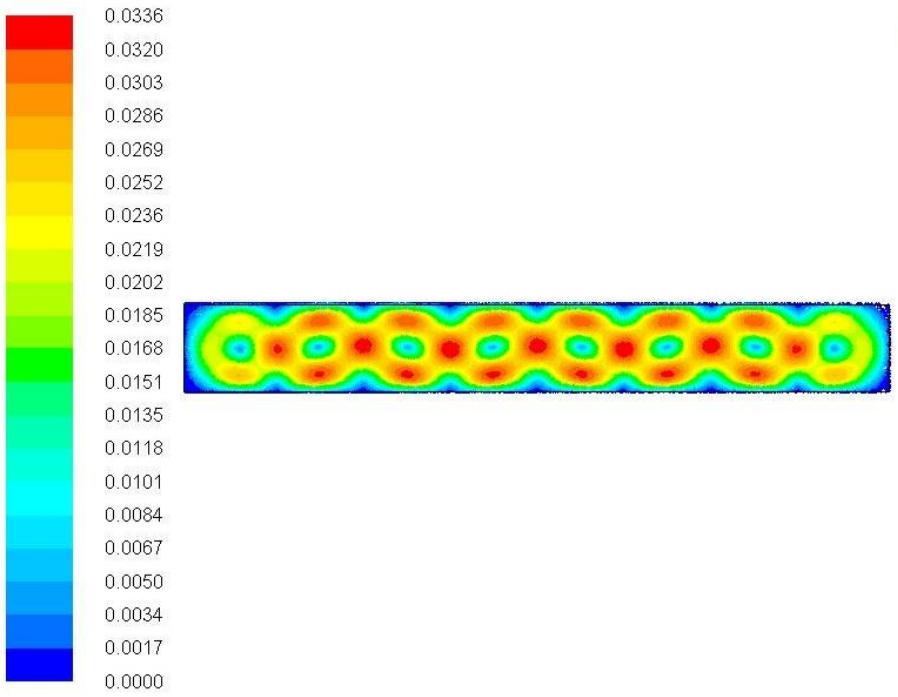


**Figure 79. Nanoparticle Tracking Within a 8-1 Aspect Ratio Enclosure**

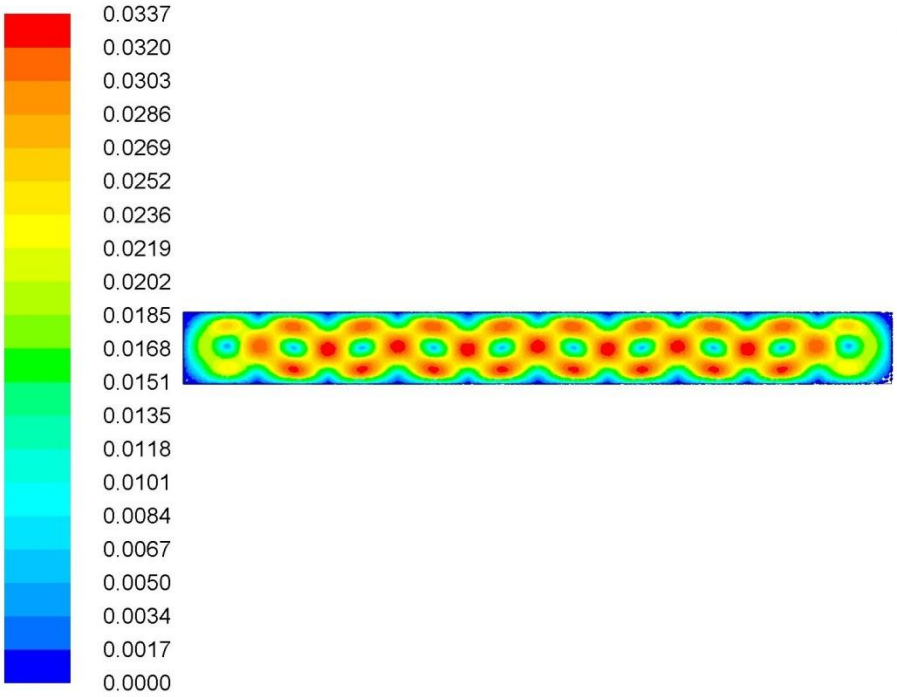


**Figure 80. Nanoparticle Tracking Within a 10-1 Aspect Ratio Enclosure**

# Chapter 5. Conclusions and Recommendations

This research has showed that there is a possibility of effectively modeling the nano fluid flows. The natural convection flows as well as forced convection flows of air within 6 different aspect ratios enclosures have been modeled and their appropriate surface heat flux and nusselt number along hot and cold walls corresponding to aspect ratio were recorded. The initial model for flow has also been developed with the nanoparticle tracking being completed. The mesh developed was found to be appropriate for the modeling purposes. The natural convection cases showed a periodic tendency as the aspect ratio increased affecting the velocity vector, isotherm, surface heat transfer, and surface nusselt number. The natural convection cases increased the magnitude of their heat transfer as well as the surface nusselt number as the aspect ratio increased. The forced convection models showed a tendency to fully develop the larger the aspect ratio that was used. Both the heat transfer and surface nusselt number decreased as the aspect ratio increased for the forced convection cases.

Future work should include developing the set of models necessary to effectively model the heat transfer of a. This developed model could then be used to work on models for erosion in fluid flow passages as well.

## References

Akbar, MK, M Rahman, SM Ghiaasiaan. 2009. Particle transport in a small square enclosure in laminar natural convection. *Journal of Aerosol Science* 40, no. 9: 747-761.

Buongiorno, J. 2006. Convective transport in nano fluids. *Journal of Heat Transfer-Transactions of the ASME* 128, no.3: 240-250.

Chen, M., & McLaughlin, J. B. 1995. A new correlation for the aerosol deposition rate in vertical ducts. *Journal of Colloid and Interface Science*, 169, 437–455.

Choi, Jeonghwan, Youngjae Kin, Anand Sivasubramaniam, Jelena Sredric, Qian Wang and Joonwon Lee. 2008. A cfd-based tool for studying temperature in rack-mounted servers. *IEEE Transactions on Computers* 57, no.8: 1129-1142.

Choi, Stephen U.S., and J.A. Eastman 1995. Enhancing thermal conductivity of fluids with nanoparticles. *ASME International Mechanical Engineering Congress & Exposition* November 12-17.

Elghobashi, S., & Truesdell, G. C. 1992. Direct simulation of particle dispersion in a decaying isotropic turbulence. *Journal of Fluid Mechanics*, 242, 655–700.

Kulkarni, Devdatta P., Praveen K. Namburu, H, Ed Bargar and Debendra K. Das. 2008. Convective heat transfer and fluid dynamic characteristics of $SiO_2$-ethylene glycol/water. *Heat Transfer Engineering* 29, no. 12:1027-1035.

Mädler, Lutz and Friedlander, Sheldon K. 2007. Transport of nanoparticles in gases: Overview and recent advances. Aerosol and Air Quality Research 7, no. 3: 304-342.

Masuda, Hidetoshi, Akira Ebata, Kazunarit Teramae, and Nobuo Hishinuma 1993. Alteration of thermal conductivity and viscosity of liquids by dispersing ultra-fine particles. Netsu Bussei 7, no.4: 227-233.

Mosavian, M. T. Hamed, S. Zeinali Heris, S. Gh. Etemad and M. Nasr Esfahany. 2010. Heat transfer enhancement by application of nano-powder. *Journal of Nanoparticle Research* 12: 2611-2619.

Ounis, H., Ahmadi, G., and McLaughlin, J. B. 1991. Dispersion and deposition of Brownian particles from point sources in a simulated turbulent channel flow. *Journal of Colloid and Interface Science*, 147, 233–250.

Sundar, L. Syam and K. V. Sharma. 2008. Numerical analysis of heat transfer and friction factor in a circular tube with $Al_2O_3$. *International Journal of Dynamics of Fluids* 4, no. 2: 121-129.

Thakurta, D. G., Chen, M., McLaughlin, J. B., & Kontomaris, K. 1998. Thermophoretic deposition of small particles in a direct numerical simulation of turbulent channel flow. *International Journal of Heat and Mass Transfer*, 41, 4167–4182.

Trisaksri, Visinee and Somchai Wongwises. 2007. Critical review of heat transfer characteristics if nano fluids. *Renewable and Sustainable Energy Reviews* 11: 512-523.

Wang, Xinwei, Xianfan Xu and Stephen U. S. Choi. 1999. Thermal conductivity of nanoparticle fluid mixture. *Journal of Thermophysics and Heat Transfer* 13, no. 4: 474-480.